To the Graduate Council:

I am submitting herewith a thesis written by Phillip L. Yeakley entitled "A Comparison of Various Computer Techniques for Calculating Wing Pressure Distributions on 3-Dimensional Aircraft". I recommend that it be accepted in partial fulfillment of the requirements for the degree of Master of Engineering, with a major in Mechanical Engineering.

S.N. Chaudhuri
S. N. Chaudhuri, Major Professor

We have read this thesis
and recommend its acceptance:

Accepted for the Council:

L Evans Roth
Vice Chancellor
Graduate Studies and Research

A COMPARISON OF VARIOUS COMPUTER TECHNIQUES FOR CALCULATING WING PRESSURE DISTRIBUTIONS ON 3-DIMENSIONAL AIRCRAFT

A Thesis

Presented for the

Master of Engineering

Degree

The University of Tennessee, Knoxville

Phillip L. Yeakley

August 1980

ACKNOWLEDGMENTS

The author wishes to express his appreciation to his major professor, Dr. S. N. Chaudhuri, University of Tennessee Space Institute, for his invaluable assistance in approaching the problem. The author also wishes to thank Mrs. Joanne M. Yeakley for typing the draft manuscript, and for her support throughout the graduate program. Special thanks are also due to the many men and women of the Arnold Engineering Development Center who made the experimental data and computer facilities available for this study.

ABSTRACT

The prediction of wing pressure distributions on 3-dimensional aircraft configurations is a problem of great interest and importance in the development of new aircraft designs. Many techniques have been developed utilizing high speed digital computers to address this problem. These techniques differ greatly in their degree of sophistication, computer resources required, inputs and quality of results. This study examines three computer codes for predicting pressure distributions and evaluates their performance on a generalized 3-dimensional aircraft configuration relative to pressure distributions measured in a wind tunnel. In addition, the three computer codes are compared to one another in terms of computer resources required. Of the three computer codes utilized, two are considered "off the shelf" programs representing the state of the art in numerical fluid mechanics. The third program was written for this study and is more typical of some of the more specialized techniques.

An examination of the data generated using these programs indicates that all give good results at low Mach numbers, but that the performance of each is impaired to varying degrees by increasing Mach number. It is also observed that dramatic savings in computer resources result through the use of a more specialized program. It is therefore held that by carefully evaluating the needs of a particular problem and selecting a computer program to match these needs, a significant

saving in time and computer resources can be obtained while maintaining the quality of the results.

TABLE OF CONTENTS

LIST OF FIGURES

FIGURE PAGE

LIST OF SYMBOLS

a Local speed of sound.

a_o Approximate lift slope for an infinite sheared wing with finite thickness.

AR Wing aspect ratio.

C Local wing chord length.

C_L Estimated wing section lift coefficient.

C_m Section pitching moment coefficient about the section leading edge.

C_P Wing surface pressure coefficient.

$F_0 \rightarrow F_4$ Coefficients computed to describe the approximate airfoil shape.

$f(X/C)$ Approximate airfoil shape function.

$f'(X/C)$ Interpolated airfoil shape function.

H The number of interpolation stations along the wing chord, forward and aft of the point of maximum airfoil thickness.

I, J, K Coordinates in the domain of the transformed space.

ℓ Weighting factors for the airfoil coordinate interpolation.

M Free stream Mach number.

N Number of points along the wing chord at which pressure coefficients are to be computed.

q Magnitude of the velocity vector.

$q(X)$ Source strength distribution along the wing chord.

R_{LE} Wing leading edge radius.

R_{BODY} Fuselage radius.

S_1, S_2, S_3 Functions dependent on the airfoil shape, which account for differences from the thin wing results due to wing thickness.

$\Delta_1, \Delta_2, \Delta_3$ Shape functions used to determine the S_1, S_2 and S_3 functions at selected points.

t/c Airfoil thickness ratio.

u, v, w Velocity components at a point in space in the x, y and z directions respectively.

U, V, W The contravarient components of the velocity vector in the transformed domain I, J, K.

V_c Velocity induced normal to the fuselage by the presence of the fuselage.

V_N Component of V_x normal to the wing surface.

V_n Component of V_0 normal to the fuselage centerline.

V_0 Free stream velocity.

V_p Component of V_0 parallel to the fuselage centerline.

V_T Component of V_x tangent to the wing surface.

V_x Component of V_0 parallel to the wing chord.

V_z Component of V_0 normal to the wing chord.

X Airfoil coordinate along the chord line in the x-direction.

Y Wing span location measured from the wing center in the y-direction.

Z Airfoil coordinate normal to the wing plane in the z-direction.

x, y, z Physical space coordinates.

α	Wind tunnel model angle of attack, degrees.
α_g	Geometric angle of attack for computed data, degrees.
α_e	Effective angle of attack of wing alone, radians.
α_e'	Effective angle of attack for wing and fuselage, radians.
α^*	Effective angle of attack due to the fuselage alone, radians.
β	Subsonic compressibility factor, $\sqrt{1-M^2}$.
γ	Ratio of specific heats.
$\gamma(x)$	Vortex strength distribution along the wing chord.
$\Delta\alpha_{FUSE}$	Increment in angle of attack due to the fuselage, radians.
ε	Angle between the airfoil chord line and the tangent to the airfoil surface at a point.
h	Complex plane where $h = x + zi$.
h^*	Transformed complex plane h , where $h^* = x^* + z^* i$.
θ	Airfoil trailing edge half angle, input to the program in degrees but converted to radians for use.
θ_i	Parameter used to define the X/C locations at which pressure coefficients are to be computed.
$\prod$	Symbol indicating the product of a series of terms.
ρ	Air density at any point in space.
$\sum$	Symbol indicating the summation of a series of terms.
Φ	Transonic velocity potential function.
ϕ	Local wing sweep angle, radians.
$\phi_{c/2}$	Sweep angle of the 50% chord line, radians.
ϕ_e	Wing effective angle of sweep, radians.
$*$	Superscript indicating a parameter in the h^*-plane.

CHAPTER I

INTRODUCTION

I.1 Statement of the Problem

In recent years the development of new aircraft configurations has become increasingly dependent on the ability to predict the air pressure distributions on the aircraft at various flight conditions. At the same time, the rapid advances in high speed digital computer technology has given the aircraft designer precisely the tools needed to address this problem. As a result, many techniques have been developed using the computer to predict the pressure distribution on 3-dimensional isolated wings and wing-body combinations. These techniques vary greatly in terms of the type of aircraft geometries they may evaluate, the flight conditions they can accept, the input information necessary to approach a specific problem, the computer resources required to reach a solution, and ultimately in the quality of the results obtained. This study examines three computer prediction techniques and compares their results for a specific problem with results obtained experimentally by measuring pressure distributions in a wind tunnel. Also examined are the resources required to reach these results.

I.2 Selection of Computer Codes

Three computer codes are selected for use in this study, having a variety of features and techniques. The first of these is a program written for this study based on a technique detailed by A. Jagadesh Prasad (1) of the India Institute of Science. This program is typical of the more specialized codes, dealing best with a specific class of problems. This program is called the "Subsonic Wing Pressure Prediction Code" and is referred to as SWPP or SWPP-Code throughout this study. The second program selected is called the BOPPE-Code developed by Charles W. Boppe (2) of Grumman Aerospace Corporation. This program is very general in the type of geometries and flight conditions it can evaluate and solves a set of simplified flow equations using an iterative numerical approach. The final program selected is FLOW-27 developed by Antony Jameson of Courant Institute of Mathematical Science and D. A. Caughey of Cornell University (3,4). This program is also very general in the type of geometries and flight conditions it can evaluate, and solves the full transonic potential flow equations using an iterative numerical approach. Both the BOPPE-Code and FLOW-27 are considered "off the shelf" programs and are selected in part due to their availability to the author. A more detailed description of each of these programs is presented in Chapter III.

I.3 Aircraft Geometry Selection

The selection of an aircraft configuration for evaluation in this study was based on the requirement that the configuration had to meet two conditions. First, the configuration had to be such that each of the three computer codes used could accurately represent the geometry. Secondly, existing wind tunnel data had to be available for the configuration. Although none of the candidate configurations met both of these requirements in every detail, the selected configuration was considered more than adequate for the problem at hand. The configuration chosen was a generalized transonic aircraft, and a detailed description of the wind tunnel model is presented in Chapter II.

CHAPTER II

EXPERIMENTAL APPARATUS AND PROCEDURES

II.1 Wind Tunnel

The experimental data used in this study was collected in the Aerodynamic Wind Tunnel (4T) of the Arnold Engineering Development Center (AEDC) by R. A. Paulk and J. F. Herman (5). This tunnel is a closed-loop, continuous flow, variable density tunnel, in which the Mach number can be varied from 0.1 to 1.3 and can be set at 1.6 and 2.0 by placing nozzle inserts over the permanent sonic nozzle. The stagnation pressure can be varied from 300 to 3700 psfa at all Mach numbers. The test section is 4 foot square and 12.5 feet long with perforated variable porosity (0.5 to 10% open) walls. It is completely enclosed in a plenum chamber from which the air can be evacuated allowing part of the tunnel airflow to be removed through the perforated walls of the test section.

The model support system consists of a pitch sector and sting attachment capable of positioning the model at angles of attack from -7 to 28 degrees. A roll mechanism in the pitch sector permits the model to be rolled from -180 to 180 degrees about the sting centerline. Aircraft pitch and yaw attitudes are then obtained through a combination of pitch and roll attitudes. The tunnel test section and model support system are shown schematically in Figure 1.

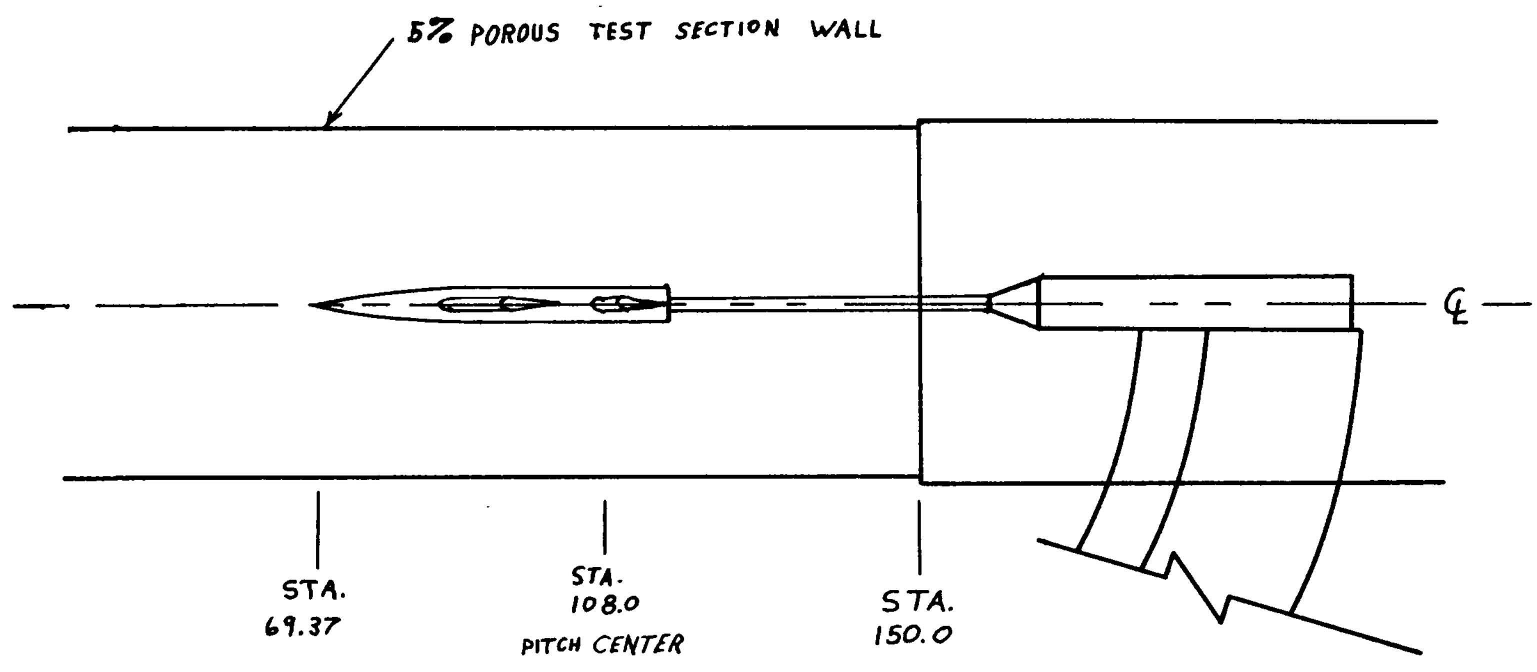

Fig. 1 Wind Tunnel and Model Support System

II.2 Test Article and Model Instrumentation

The wind tunnel model used to obtain the experimental data in this study was the AEDC transonic wall interference model, a generalized transonic aircraft consisting of a wing, body and horizontal tail. The fuselage was of circular cross section with a 4.65 caliber tangent ogive nose and a 9.38 caliber cylindrical afterbody. The wing and horizontal tail were mounted to the fuselage along the fuselage centerline and were swept back 30 degrees. All lifting surfaces were NACA-0012 airfoil sections, with no taper, twist or camber and having no dihedral angle or incidence angle relative to the fuselage. Details of the model are shown in Figure 2.

The model was sting mounted in the tunnel, and instrumented with a six-component main balance and 92 surface pressure orifices. Of these pressures, 41 were located on the fuselage of horizontal tail and are not used in this study. The remaining 51 pressures were distributed streamwise along the wing as shown in Figure 2 at span stations of 40, 65 and 90%. At each span station 17 pressures were distributed with 13 on the wing upper surface and 4 on the wing lower surface. A typical airfoil section is shown in Figure 3, along with the location of the pressure orifices along the wing chord.

The data used for this study was collected at Mach numbers of 0.5, 0.7 and 0.9 at a constant total pressure of 1000 psfa, corresponding to unit Reynolds numbers of from 1.4 to 2.0 million per foot. The model angle of attack was varied from -6 to 12 degrees

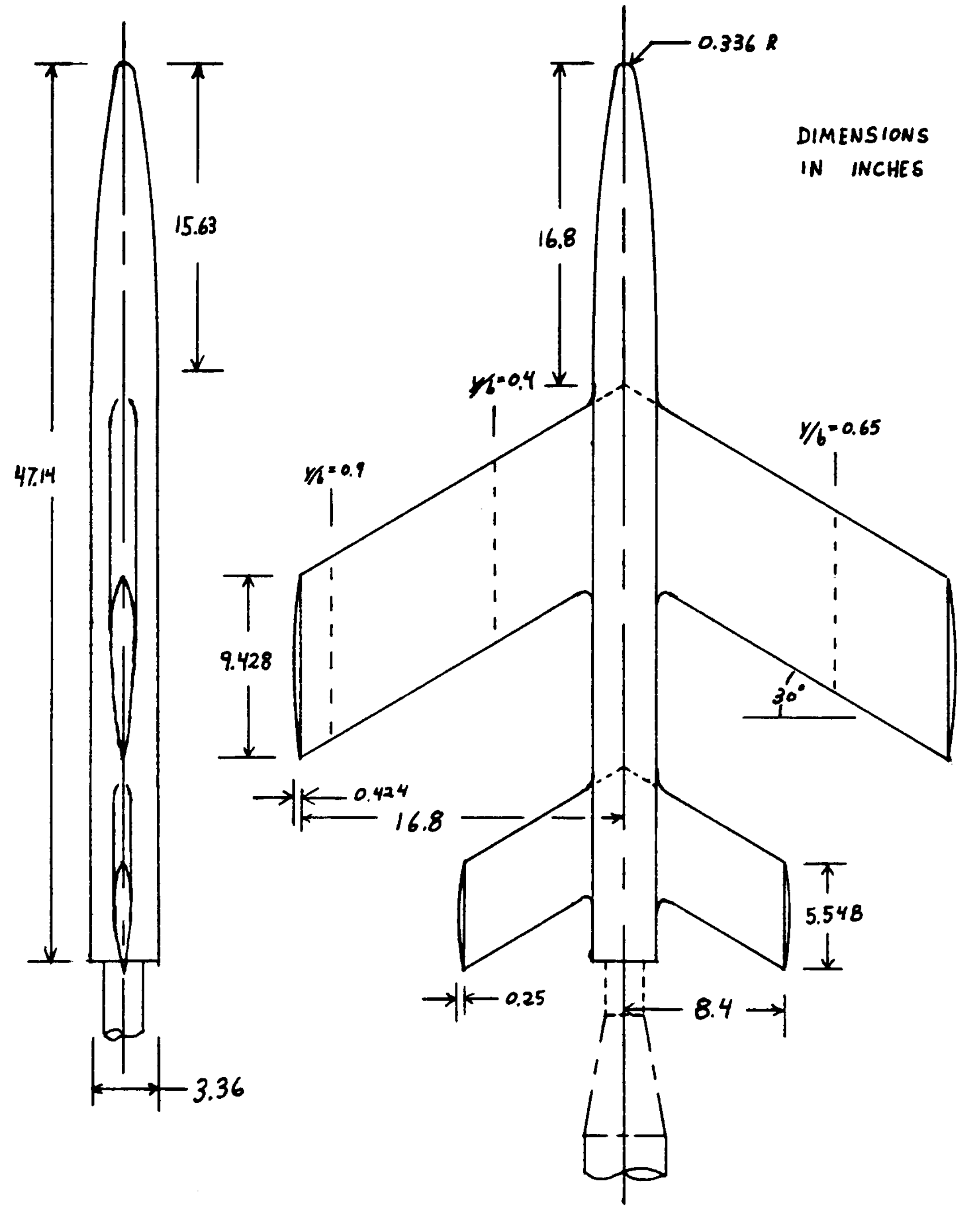

Fig. 2 Details of Wind Tunnel Model Geometry

NACA - 0012

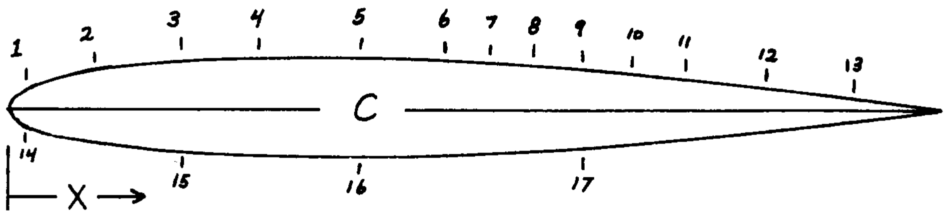

Orifice Number	X/C
1	0.02
2	0.10
3	0.20
4	0.30
5	0.40
6	0.45
7	0.50
8	0.55
9	0.60
10	0.65
11	0.70
12	0.80
13	0.90
14	0.02
15	0.20
16	0.40
17	0.60

Fig. 3 Location of Pressure Orifices Along the Wing Chord of the Wind Tunnel Model

in 2 degree increments using a pitch-pause method to allow the pressures to reach a steady-state value before recording the data. These data were collected in support of the AEDC Transonic Adaptive Wall Study in which the wind tunnel wall porosities were varied in an effort to minimize the wall interference on the model. Although no wall interference corrections were made to this data, it was shown by R. L. Parker and W. L. Sickles (8) that the wall interference had been minimized through the use of these adaptive wall techniques and that the data could be considered interference free.

CHAPTER III

COMPUTATIONAL TECHNIQUES

III.1 Description of FLOW-27

The program FLOW-27 developed by Jameson and Caughey (3,4) is typical of the sophisticated numerical techniques being developed and used to evaluate aircraft pressure distributions, and is considered to represent the "state of the art". For a given aircraft geometry, this code numerically solves the full transonic potential flow equations about the aircraft.

As presented by Jameson and Caughey (3), using a cartesian coordinate system where u, v and w are the velocity components in the x, y and z directions, the transonic potential equation is equivalent to the continuity equation

$$\frac{\partial}{\partial x}(\rho u) + \frac{\partial}{\partial y}(\rho v) + \frac{\partial}{\partial z}(\rho w) = 0 \qquad (1)$$

with the derivitive of the density ρ related to the speed of sound and the magnitude of the velocity by the energy equation for a calorically perfect gas

$$\frac{\partial \rho}{\partial q} = -\frac{\rho}{a^2} q \qquad (2)$$

and the requirement that the velocity vector be the gradient of some scalar function Φ. By introducing the quantity $Q = \frac{1}{2} q^2$, equation 1 can be written as

$$a^2\left(\frac{\partial u}{\partial x}+\frac{\partial v}{\partial y}+\frac{\partial w}{\partial z}\right)-\left(u\frac{\partial Q}{\partial x}+v\frac{\partial Q}{\partial y}+w\frac{\partial Q}{\partial z}\right)=0 \qquad (3)$$

Applying an arbitrary (non-singular) coordinate transformation to the coordinate system I, J, K, equation 3 becomes

$$a^2\left(\frac{\partial U}{\partial I}+\frac{\partial V}{\partial J}+\frac{\partial W}{\partial K}\right)-\left(U\frac{\partial Q}{\partial I}+V\frac{\partial Q}{\partial J}+W\frac{\partial Q}{\partial K}\right)=0 \qquad (4)$$

where U, V, and W are the contravarient components of the velocity vector in the new coordinate system, multiplied by the determinate of the Jacobian of this transformation.

The numerical solution of equation 4 is based on its equivalence to the usual quasilinear form of the potential equation, for which reliable numerical schemes have been developed. A finite difference approximation to equation 4 is constructed using central differences everywhere. Using a central differences scheme, the equation becomes unstable in locally supersonic regions. To stabilize the equation in these regions, an artificial viscosity is then added in conservative form, effectively giving an upwind bias. The difference equations developed in this manner are then solved using an iterative line relaxation technique.

The use of this technique requires only a local description of the mapping function. As a result the solution process is essentially decoupled from the generation of the grid network. Thus the finite difference grid can be constructed in any convenient manner, and all that is subsequently needed are the coordinates of the mesh points. As such, the grid network is generated by mapping the physical space into a rectangular prism in which the wing lies on one surface of the prism, the fuselage on another surface, the vertical plane of symmetry on another as shown in Figure 4. A uniform rectangular mesh in this domain is then mapped back into the physical domain to give the cartesian coordinates of the grid points.

This program is designed to be used on isolated wings and wing-body combinations of quite general geometries and at a wide range of flight conditions. However, for this study the aircraft geometry as evaluated by FLOW-27 is not identical to the aircraft geometry as tested in the wind tunnel. Although the differences are not thought to affect the results, it is important that these differences be clearly identified. First and foremost, the wind tunnel model has a horizontal tail which is not included in the computer analysis. Also, the wing tips of the model are slightly faired while the wing tips in the computer analysis are squared off. Two additional variations are that for the computer program the model is free flying (not supported by a sting), and no wind tunnel walls are modeled in the far flowfield. A comparison of the wind tunnel geometry and that used in this program is shown in Figure 5. Aside from these differences, the model geometry is accurately represented, and it is felt that the differences mentioned should not greatly affect the wing pressure distributions between 40 and 90% span.

The program inputs required for a solution are the aircraft geometry and flight conditions as well as certain program control

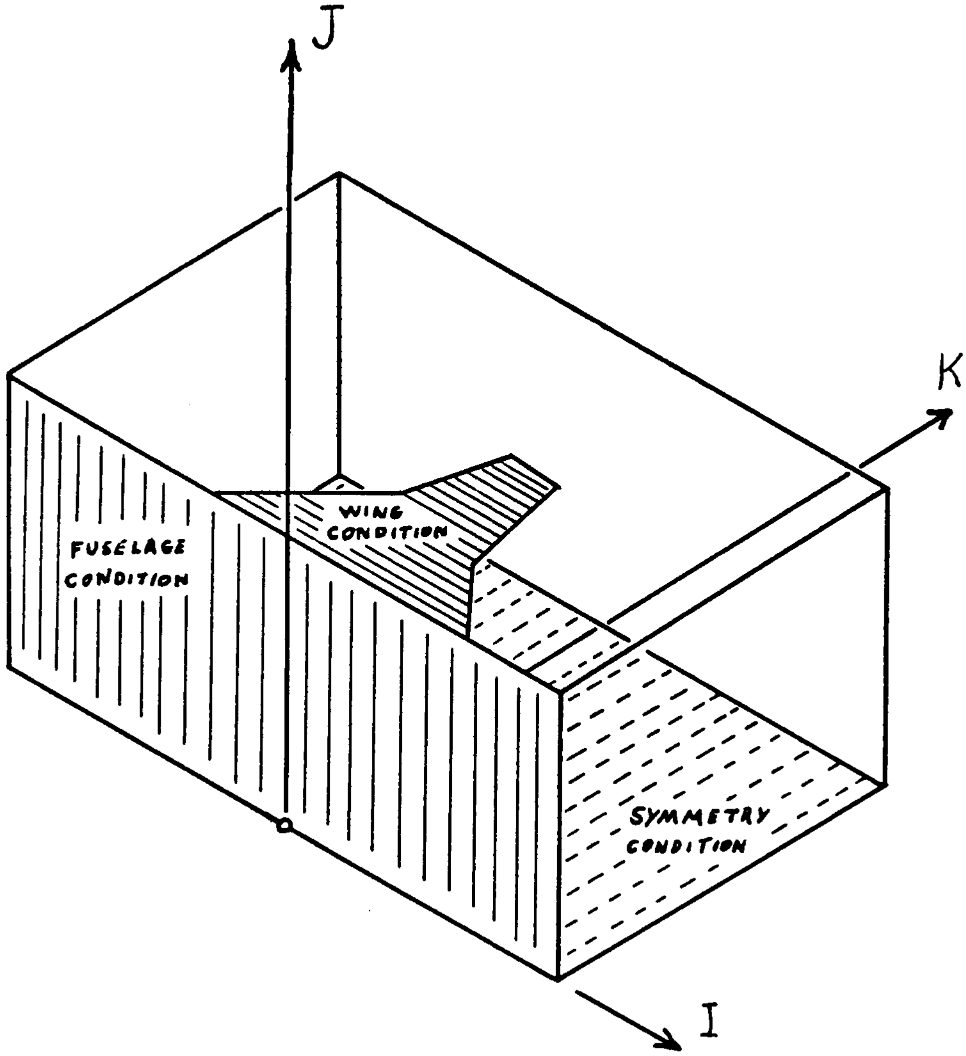

Fig. 4 Transformed Computational Domain for FLOW-27

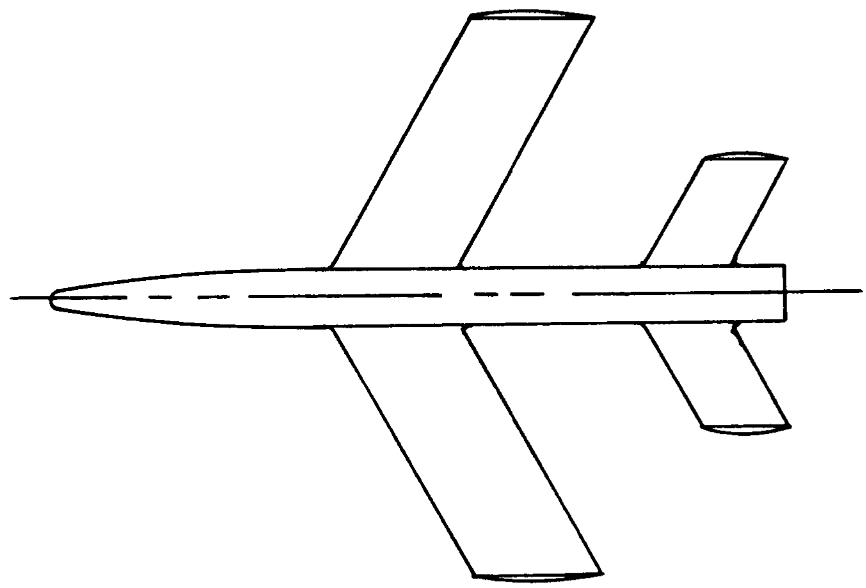

TEST GEOMETRY

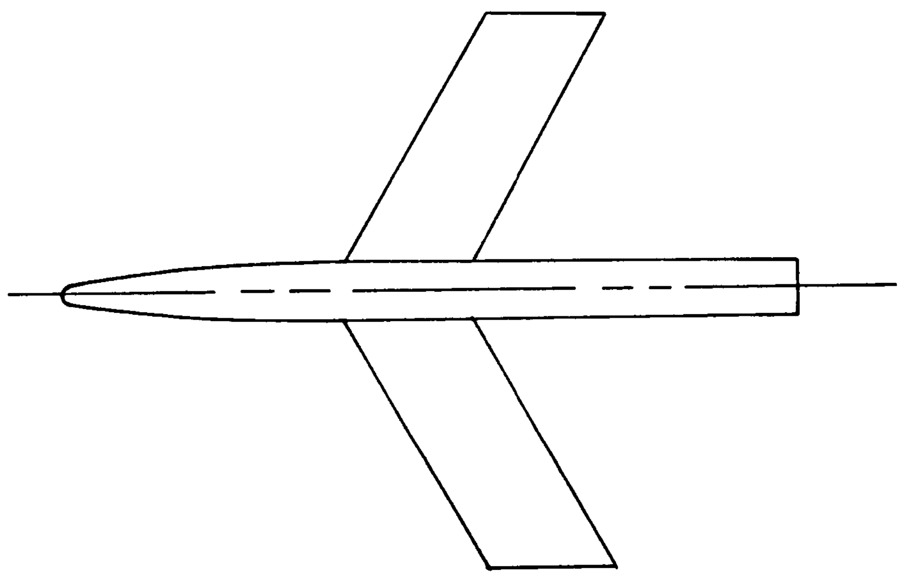

FLOW-27 GEOMETRY

Fig. 5 Comparison of Wind Tunnel and FLOW-27 Aircraft Geometry variables. The geometry of the fuselage is given by fuselage cross-sections at various positions along the body. The wing geometry is given in terms of its location on the fuselage, airfoil coordenates at various spanwise locations, wing sweep, twist, taper, camber, dihedral and incidence angle relative to the fuselage. The flight conditions are given in terms of Mach number, angle of attack and angle of sideslip. The control variables are parameters such as the convergence criterion, maximum number of iterations per step and output control parameters.

III.2 Description of BOPPE-Code

The BOPPE-Code developed by Boppe (2) is similar in nature to FLOW-27 in that both are sophisticated numerical solutions which solve their respective equations on a grid network using an iterative technique. For a particular problem the BOPPE-Code numerically solves the transonic small disturbance flow equation, modified to include three additional terms from the full potential flow equation. This equation is written as

$$\left[1-M^2-(\gamma+1)M^2\frac{\partial\phi}{\partial x}-\frac{\gamma+1}{2}M^2\left(\frac{\partial\phi}{\partial x}\right)^2\right]\frac{\partial}{\partial x}\left(\frac{\partial\phi}{\partial x}\right)-2M^2\frac{\partial\phi}{\partial y}\frac{\partial}{\partial y}\left(\frac{\partial\phi}{\partial x}\right)$$

$$+\left[1-(\gamma-1)M^2\frac{\partial\phi}{\partial x}\right]\frac{\partial}{\partial y}\left(\frac{\partial\phi}{\partial y}\right)+\frac{\partial}{\partial z}\left(\frac{\partial\phi}{\partial z}\right)=0 \qquad (5)$$

The terms $2M^2\frac{\partial\phi}{\partial y}\frac{\partial}{\partial y}\left(\frac{\partial\phi}{\partial x}\right)$ and $(\gamma-1)M^2\frac{\partial\phi}{\partial x}\frac{\partial}{\partial y}\left(\frac{\partial\phi}{\partial y}\right)$ are known as the cross-flow terms and are included to permit shock waves which are highly swept to be treated more accurately. A third term included from the full potential equation is $\frac{\gamma+1}{2} M^2 \left(\frac{\partial \phi}{\partial x}\right)^2 \frac{\partial}{\partial x}\left(\frac{\partial \phi}{\partial x}\right)$. This term is a second order term in the streamwise direction which results in a more accurate determination of the local velocity. This local velocity is critical in transonic solutions because the type of the potential equation changes from elliptical to hyperbolic in locally supersonic regions. A grid network is established about the aircraft using a fine grid spacing near the aircraft where large gradients occur, and a coarse grid spacing throughout the remaining flowfield. The coarse grid consists of 51, 26 and 31 grid lines in the x, y and z directions respectively as shown in Figure 6. For the coarse grid the coordinates have been stretched such that the whole physical space is covered to account for the far field effects, while requiring that approximately half of the grid lines fall on the aircraft. The fine grid is made up of a fuselage grid of 70, 20 and 39 grid lines in the x, y and z directions which enclose the fuselage, and a grid of 100 by 34 grid lines in the x and z directions at each y location at which a coarse grid line intersects the wing, Figures 7 and 8. On this grid network a finite difference approximation to the modified equation is constructed in non-conservative form. The use of non-conservative differences rather than conservative differences works to good advantage in that non-conservative differences introduce more artificial viscosity into the flow and result in better agreement with observed phenomenon. Central differences are used in subsonic regions, while upwind differences are used in supersonic regions to stabilize

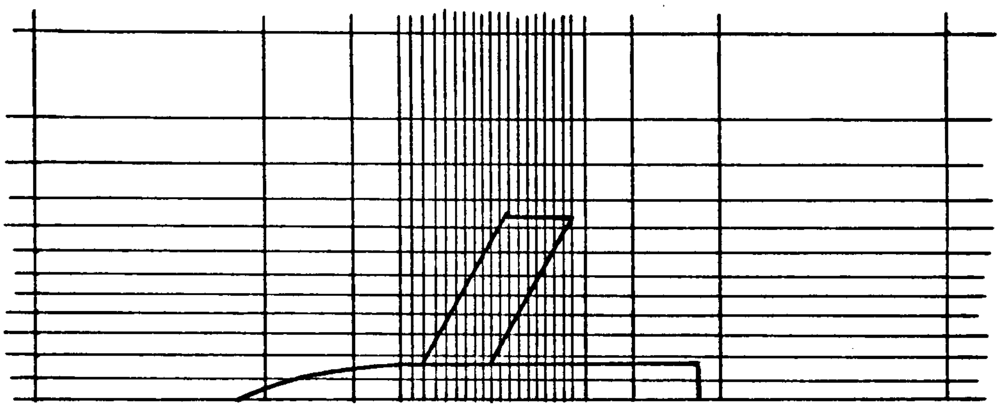

Fig. 6 BOPPE-Code Coarse Grid

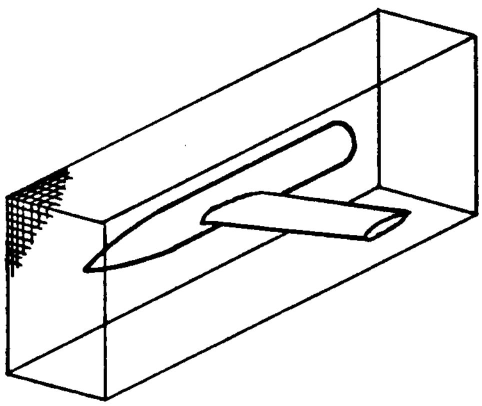

Fig. 7 BOPPE-Code Fuselage Fine Grid

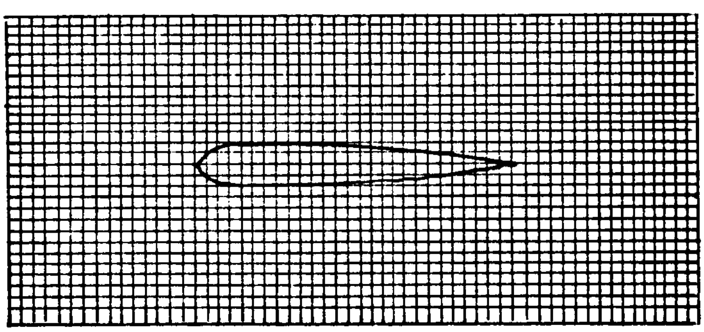

Fig. 8 BOPPE-Code Wing Fine Grid

the solution. These difference equations are then solved using a line relaxation technique which is iterated to reach a solution. The coarse grid covering the flowfield is solved first, and used as a starting point for the fine grid solution.

The BOPPE-Code, as with FLOW-27, is designed for use on isolated wings and wing-body combinations. Here again there are certain differences between the aircraft geometry as represented to the program and the configuration tested in the wind tunnel. The most significant difference is the absence of the horizontal tail in the computer description of the geometry. The wing tip geometry as represented to the program was squared off parallel to the free stream direction, while the model incorporated small tip fairings, and the tangent ogive nose of the model has a hemispherical tip, while the nose as represented to the program extends the ogive nose to a sharp point. In addition to these variations in the aircraft geometry, the model support system and wind tunnel walls are not included in the flowfield. These differences are shown in Figure 9. Aside from these geometry differences, the wind tunnel model is accurately represented to the program.

The program inputs required are the aircraft geometry, flight conditions and program control variables. The geometry is given in terms of fuselage cross-sections along the body, wing planform given as wing leading and trailing edge locations at various spanwise stations, wing location on the fuselage, and airfoil coordinates and wing twist angle at various spanwise locations. The flight conditions

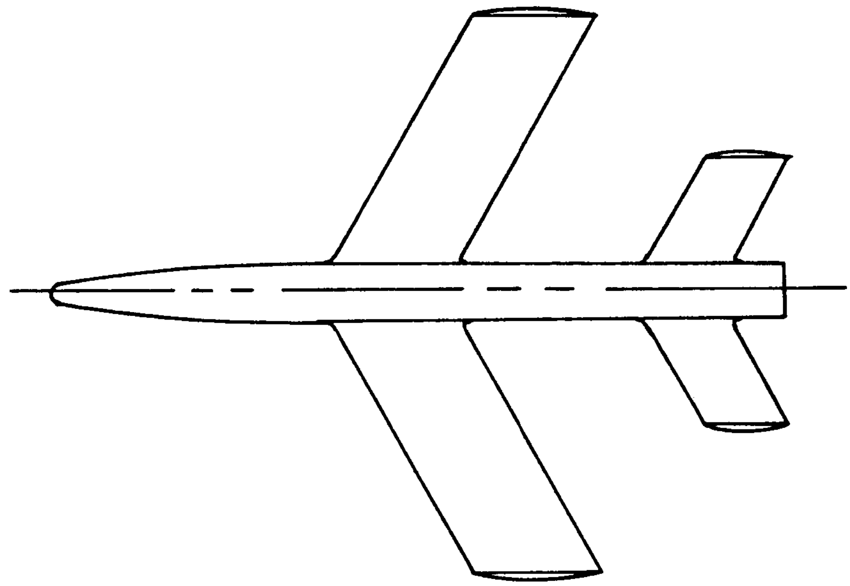

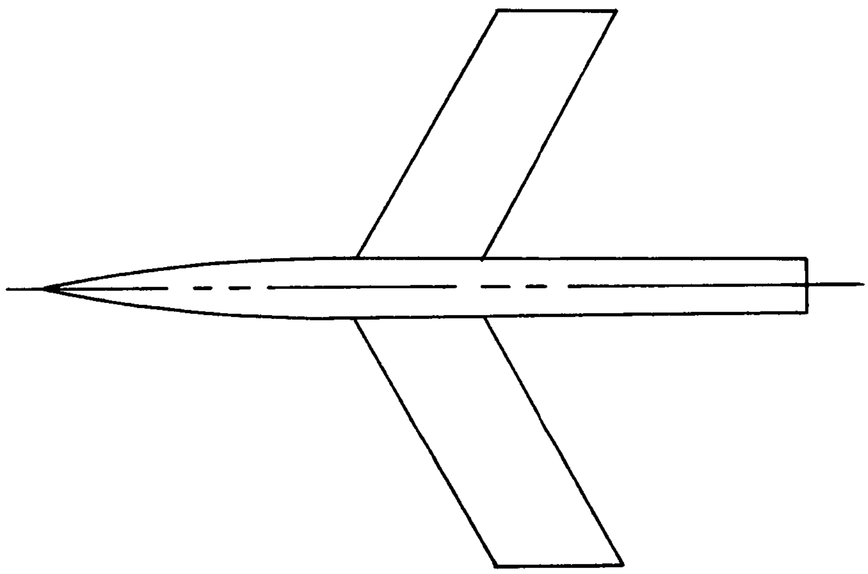

Fig. 9 Comparison of Wind Tunnel and BOPPE-Code Aircraft Geometry

required are the Mach number, Reynolds number and angle of attack. It should be noted that the Reynolds number is used to compute a boundary layer displacement thickness which is used to modify the aircraft geometry before processing. The control variables include the reference center for integrated forces and moments, number of iterations to be made on the coarse grid, and the convergence criterion, as well as output control variables.

III.3 Description of the Subsonic Wing Pressure Prediction Code (SWPP-Code)

The SWPP-Code is based on a technique detailed by A. Jagadesh Prasad (1), and represents the more specialized programs dealing with a particular class of problem. As reported by Prasad, this technique is intended to compute pressure distributions on 3-dimensional swept and tapered isolated wings of symmetrical airfoil sections at angle of attack in incompressible flow. This technique is modified for this study to include a circular fuselage of infinite length with the wing mounted along its centerline.

This technique makes use of the concept that for portions of the wing sufficiently far from the wing root or tip, a 2-dimensional solution is valid. In regions near the root or tip, the same 2-dimensional solution is used with modifications to reflect the 3-dimensional nature of the flow in these areas.

Given the symmetrical airfoil coordinates, leading edge radius, trailing edge half-angle, thickness ratio, wing planform, body radius and geometric angle of attack, this program will compute the pressure coefficients along the wing chord based on the wing span location and an estimated section lift coefficient at that span location. A detailed list of the program inputs is presented in the Appendix along with a listing of the computer program. The equations used are in closed form requiring no iteration to reach a solution. These equations and their development as presented in Reference 1, with the modifications necessary to include the cylindrical fuselage follow.

An expression for the airfoil coordinates Z/C as a function of X/C is defined such that

$$Z/C = f(X/C) = F_0 (X/C)^{1/2} + F_1 (X/C) + F_2 (X/C)^2 + F_3 (X/C)^3 + F_4 (X/C)^4 \qquad (6)$$

where F_0, F_1, F_2, F_3 and F_4 are constants determined directly from the input data based on the following five conditions.

i. $R_{LE}/C = F_0^2/2$.

ii. At the X/C corresponding to maximum airfoil thickness $Z/C = 0.5\, t/C$.

iii. At $X/C = 1.0$, Z/C must equal the trailing edge ordinate.

iv. At the X/C corresponding to maximum airfoil thickness the slope of the airfoil surface must equal zero.
$\frac{d}{d(X/C)}\left[f(X/C)\right] = 0$ at X/C giving maximum Z/C.

v. At $X/C = 1.0$ the slope of the airfoil surface must be equal to $-\tan(\theta)$ where θ is the trailing edge half angle. $\frac{d}{d(X/C)}\left[f(X/C)\right] = -\tan(\theta)$ at $X/C = 1.0$.

Having determined the values $F_0 \rightarrow F_4$, the airfoil coordinates at any position along the chord are found from equation 6. This approximate airfoil shape is then improved by using an interpolation scheme such that

$$z/c = f'(x/c) = f(x/c) + \sum_{J=1}^{H} \left[l_J(x/c) \left\{ (z/c)_J - f((x/c)_J) \right\} \right] \tag{7}$$

where H is the number of interpolation stations, input to the program

$(x/c)_J$ are interpolation stations along the chord selected from the input data by the program.

$(z/c)_J$ are airfoil coordinates from the input data corresponding to the $(x/c)_J$ values.

$l_J(x/c)$ are interpolation weighting factors determined from the x/c location and the interpolation stations $(x/c)_J$ as follows.

$$l_J(x/c) = \frac{(1-x/c)^2 \left[x/c - (x/c)_m\right]^2 \left\{ \prod_{i=1}^{J-1} \left[x/c - (x/c)_i\right] \right\} \left\{ \prod_{i=J+1}^{N} \left[x/c - (x/c)_i\right] \right\}}{(x/c)_J \left[(x/c)_J - (x/c)_m\right]^2 \left\{ \prod_{i=1}^{J-1} \left[(x/c)_J - (x/c)_i\right] \right\} \left\{ \prod_{i=J+1}^{N} \left[(x/c)_J - (x/c)_i\right] \right\}} \tag{8a}$$

for $x/c \leq (x/c)_m$.

$$l_J(x/c) = \frac{(1-x/c)^2 \left[x/c - (x/c)_m\right]^2 \left\{ \prod_{i=1}^{J-1} \left[x/c - (x/c)_i\right] \right\} \left\{ \prod_{i=J+1}^{N} \left[x/c - (x/c)_i\right] \right\}}{\left[1-(x/c)_J\right]^2 \left[(x/c)_J - (x/c)_m\right]^2 \left\{ \prod_{i=1}^{J-1} \left[(x/c)_J - (x/c)_i\right] \right\} \left\{ \prod_{i=J+1}^{N} \left[(x/c)_J - (x/c)_i\right] \right\}} \tag{8b}$$

for $x/c > (x/c)_m$.

where $(x/c)_m$ is the x/c corresponding to maximum airfoil thickness and $\prod$ indicates the product of terms. Equation 7 is used to obtain the airfoil coordinates at any position along the chord throughout the program.

Next the wing area and aspect ratio are computed directly from the input planform information. At this point it is necessary to determine the effective angle of attack at each spanwise station at which pressure coefficients are to be computed. Kuchemann (6) derived the following relation for the effective incidence at any spanwise station of a finite swept isolated wing.

$$\alpha_e = C_L \frac{\sin \pi m_o}{4\pi m \cos \phi_e} \left\{ 1 - \pi m \left(\cot \pi m - \cot \pi m_o \right) \right\} \tag{9}$$

where C_L is the estimated section lift coefficient.

$$\phi_e = \frac{\phi_{c/2}}{\left\{ 1 + \left(\frac{a_o \cos \phi_{c/2}}{\pi \cdot AR} \right)^2 \right\}^{0.25}} \tag{10}$$

$$m = 1 - \frac{1 + \lambda(Y)\, 2\, \phi_e / \pi}{2 \left\{ 1 + \left(\frac{a_o \cos \phi_e}{\pi \, AR} \right)^2 \right\}^{0.25(1 + 2\phi_e/\pi)}} \tag{11}$$

$$m_o = \tfrac{1}{2}\left(1 - \lambda(Y)\, 2\, \phi_e / \pi\right) \tag{12}$$

$$\lambda(Y) = 1.40 + 1.33Y - (0.16 + 7.3\, Y)^{0.5} \tag{13}$$

Y is the distance to the root or tip measured in terms of the local chord.

$$a_o = 2\, \pi \left(1 + 0.8\, (t/c) / \cos \phi_{c/2} \right) \tag{14}$$

$\phi_{c/2}$ is the sweep angle in radians of the 50% chord line.

This effective angle of attack α_e does not account for the presence of a fuselage. This is therefore modified by defining a new effective angle of attack α_e' .

$$\alpha_e' = \alpha_e + \Delta\alpha_{FUSE} \tag{15}$$

where $\Delta\alpha_{FUSE}$ is the increment in angle of attack due to the fuselage. To evaluate this increment $\Delta\alpha_{FUSE}$, a circular cylinder of infinite length inclined at a geometric angle of attack   is examined in Figure 10.

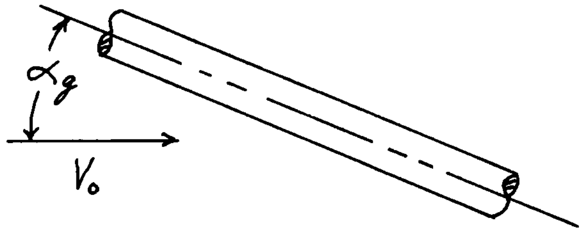

Fig. 10 Infinite Cylinder at Angle of Attack

The free stream velocity V_o is resolved into its components normal to and tangent to the fuselage centerline, as shown in Figure 11, such that the normal and tangential velocity components become

$$V_n = V_o \sin\alpha_g \tag{16}$$

$$V_p = V_o \cos\alpha_g \tag{17}$$

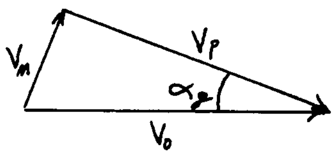

Fig. 11 Free Stream Velocity Components Relative to the Cylinder Axis

The velocity component along the cylinder axis, V_p , will be unaffected by the cylinder, but the component normal to the cylinder axis, V_n , will be influenced by the cylinder, and can be evaluated as a cylinder in cross flow. From Li and Lam (7) it can be shown that at any point (y_1, z_1) in the flowfield about a cylinder in cross flow the velocity in the z direction is

$$V_c = V_n\left(1 + \frac{R_{BODY}^2}{y^2+z^2}\left\{\frac{y^2-z^2}{y^2+z^2}\right\}\right) \tag{18}$$

as shown in Figure 12.

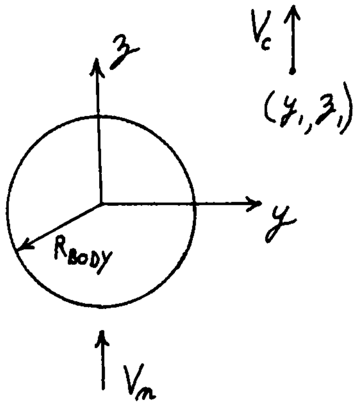

$$V_c = V_n\left(1 + \frac{R_{BODY}^2}{y_1^2+z_1^2}\left\{\frac{y_1^2-z_1^2}{y_1^2+z_1^2}\right\}\right)$$

Fig. 12 Velocity Distribution about a Cylinder in Cross Flow

In the case of a wing mounted along the centerline of the fuselage at $z=0$, the cross flow velocity at the wing plane becomes

$$V_c = V_n\left(1 + \frac{R_{BODY}^2}{y^2}\right) \tag{19}$$

where R_{BODY} and y are in any consistent set of units. Using this induced cross flow velocity V_c and the existing velocity component along the body V_p , a new angle of attack α^* is computed due to the fuselage.

$$\alpha^* = \mathrm{ArcTan}\left(\frac{V_c}{V_p}\right) = \mathrm{ArcTan}\left\{\frac{V_n(1+R_{BODY}^2/y^2)}{V_p}\right\} \tag{20}$$

$$\alpha^* = \mathrm{ArcTan}\left\{\tan\alpha_g\left(1 + \frac{R_{BODY}^2}{y^2}\right)\right\} \tag{21}$$

The increment in angle of attack at any spanwise station due to the fuselage is then the difference between α_g and α^*. Therefore

$$\Delta\alpha_{FUSE} = \alpha^{*} - \alpha_g \tag{22}$$

$$\Delta\alpha_{FUSE} = \operatorname{ArcTan}\left\{\tan\alpha_g\left(1+\frac{R^2_{BODY}}{y^2}\right)\right\} - \alpha_g \tag{23}$$

and the total effective angle of attack $\alpha_e' = \alpha_e + \Delta\alpha_{FUSE}$ becomes

$$\alpha_e' = \frac{C_L \sin\pi m_0}{4\pi m \cos\phi_e}\left\{1 - \pi m\left(\cot\pi m - \cot\pi m_0\right)\right\} + \operatorname{ArcTan}\left\{\tan\alpha_g\left(1+\frac{R^2_{BODY}}{y^2}\right)\right\} - \alpha_g \tag{24}$$

At this point expressions for the airfoil shape, wing area and aspect ratio, and the effective angle of attack at each span station of interest have been computed. Based on this the pressure coefficients are computed along the wing surface at the span stations of interest. Four equations for the pressure coefficients have been developed, with each applying to a particular region of the wing. These four regions are:

1. the portion of the wing more than one local chord length from the wing center or tip, and not at the leading edge.

2. the portion of the wing less than one local chord length from the wing center or tip, and not at the leading edge.

3. the portion of the wing more than one local chord length from the wing center or tip, and at the leading edge.

4. the portion of the wing less than one local chord length from the wing center or tip, and at the leading edge.

These four regions are shown schematically in Figure 13.

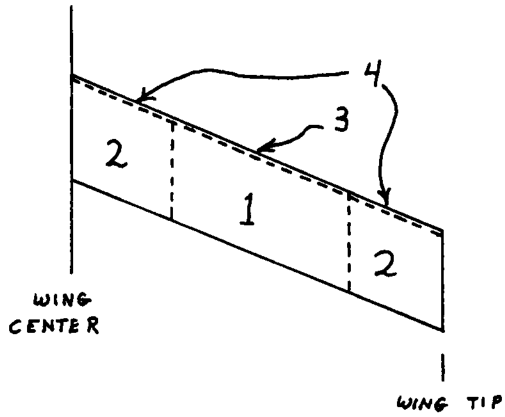

Fig. 13 Four Wing Regions used by SWPP-Code to Determine Which Equation to use to Compute C_p

For any point on the wing the equation used to compute the pressure coefficient is determined by what region the point is in. The equation used in region 1 is developed for a two dimensional airfoil at an angle of attack α_e' , in a free stream velocity V_o as shown in Figure 14.

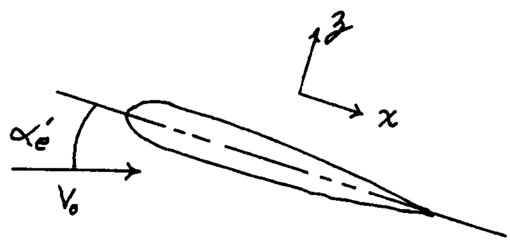

Fig. 14 Airfoil at an Effective Angle of Attack to the Flow

The velocity V_o is resolved into its components parallel to and normal to the wing chord line such that

$$V_z = V_o \sin \alpha_e' \tag{25}$$

$$V_x = V_o \cos \alpha_e' \tag{26}$$

These two flow components are then examined separately to develop a distribution of singularities which exactly cancels the stream component normal to the airfoil surface (no flow across a solid boundary).

For the flow parallel to the wing chord, at any point along the surface of the airfoil the velocity V_X is resolved into its components normal to and tangent to the surface as in Figure 15.

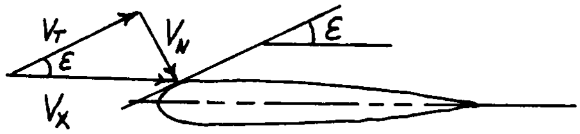

Fig. 15 Components of the Chordwise Velocity Relative to the Airfoil Surface

These components are:

$$V_N = V_X \sin \varepsilon \tag{27}$$

$$V_T = V_X \cos \varepsilon \tag{28}$$

where ε is the angle between the wing chord line and a line tangent to the surface at the point of interest. The sine and cosine of ε can be expressed in terms of the airfoil geometry as

$$\cos \varepsilon = \frac{1}{\sqrt{1+\left(\frac{dZ}{dX}\right)^2}} \tag{29}$$

$$\sin \varepsilon = \frac{dZ/dX}{\sqrt{1+\left(\frac{dZ}{dX}\right)^2}} \tag{30}$$

such that V_N and V_T become

$$V_N = \frac{V_X \frac{dZ}{dX}}{\sqrt{1+\left(\frac{dZ}{dX}\right)^2}} \tag{31}$$

$$V_T = \frac{V_X}{\sqrt{1+\left(\frac{dZ}{dX}\right)^2}} \tag{32}$$

These velocity components are then used to develop the singularity distribution needed for the solution. To do this consider the complex variable h.

$$h = X + Zi \tag{33}$$

The h-plane is transformed conformally into the $h^* = X^* + Z^* i$ plane, where the portion of the h-plane outside the contour $Z = f'(X)$ is transformed into the portion of the h^*-plane outside a slit along the X^* axis. The determination of the singularity distribution in the h-plane which produces a velocity distribution canceling the normal velocity V_N at the airfoil surface is equivalent to determining the singularity distribution in the h^*-plane which cancels the normal component V_N^* at the slit. This requires a source distribution at the slit of strength $g(X^*) = -2\,V_N^*$. This produces a tangential velocity of

$$\Delta V_T^* = \frac{1}{2\pi} \int \frac{g(X^*)}{X^* - X^{*\prime}}\, dX^{*\prime} \tag{34}$$

Using the mapping ratio dh/dh^*, the corresponding tangential velocity at the surface of the airfoil in the h-plane becomes

$$\Delta V_T(X) = \frac{V_X}{\sqrt{1-\left(\frac{dZ}{dX}\right)^2}}\, \frac{1}{\pi} \int_0^1 \frac{(X-X')/(X^*-X^{*\prime})}{dX/dX^*}\, \frac{dZ}{dX'}\, \frac{dX'}{(X-X')} \tag{35}$$

and the total velocity at the surface becomes $V(X,Z) = V_T + \Delta V_T$.

$$V(X,Z) = \frac{V_x}{\sqrt{1+\left(\frac{dZ}{dX}\right)^2}}\left[\frac{1}{\pi}\int_0^1 \frac{(X-X')/(X^*-X^{*\prime})}{dX/dX^*}\,\frac{dZ}{dX'}\,\frac{dX'}{(X-X')} + 1\right] \tag{36}$$

To find $V(X,Z)$ exactly one needs the relation between X and X^*. By requiring $[(X-X')/(X^*-X^{*\prime})]/(dX/dX^*) = 1.0$, an approximate expression for $V(X,Z)$ can be obtained which is correct to the first order of t/c. This expression for $V(X,Z)$ then becomes

$$V(X,Z) = \frac{V_x}{\sqrt{1+\left(\frac{dZ}{dX}\right)^2}}\left[1 + S_1(X)\right] \tag{37}$$

where

$$S_1(X) = \frac{1}{\pi}\int_0^1 \frac{dZ}{dX'}\,\frac{dX'}{(X-X')} \tag{38}$$

Next consider the airfoil exposed to a flow velocity normal to the chord as shown in Figure 16.

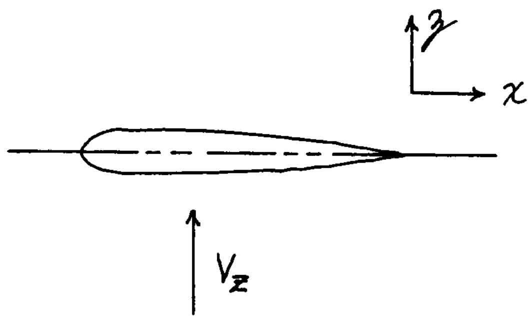

Fig. 16 Airfoil in Flow Normal to the Chord Line

For a flat plate, the velocity at the plate is given by

$$V(X,0) = \pm V_z\sqrt{\frac{1-X}{X}} \tag{39}$$

such that the velocity normal to the plate is zero and the tangential velocity is of opposite sign on the top and bottom of the plate. This can be represented by a distribution of vortices along the plate such that the strength $\gamma(X)$ is equal to the jump in tangential velocity across the plate.

$$\gamma(X) = 2 V_Z \sqrt{\frac{1-X}{X}} \tag{40}$$

For the airfoil, the vortex distribution may be taken as

$$\gamma(X) = 2 V_Z \sqrt{\frac{1-X}{X}} + \Delta\gamma(X) \tag{41}$$

where $\Delta\gamma(X)$ is due to the airfoil thickness. Keeping only the terms up to the first power of Z and satisfying the Kutta-Joukowski condition at the trailing edge, it can be shown that $\Delta\gamma(X)$ can be written as

$$\Delta\gamma(X) = \frac{2 V_Z}{\pi} \sqrt{\frac{1-X}{X}} \int_0^1 \left[\frac{dZ}{dX'} - \frac{2 Z(X')}{1-(1-2X')^2} \right] \frac{dX'}{(X-X')} \tag{42}$$

With this result, $\gamma(X)$ becomes

$$\gamma(X) = 2 V_Z \sqrt{\frac{1-X}{X}} \left[1 + S_3(X) \right] \tag{43}$$

where

$$S_3(X) = \frac{1}{\pi} \int_0^1 \left[\frac{dZ}{dX'} - \frac{2 Z(X')}{1-(1-2X')^2} \right] \frac{dX'}{(X-X')} \tag{44}$$

This distribution of singularities is along the chord line, and the total velocity on the chord line is $V(X,0) = \pm \frac{1}{2} \gamma(X)$. Hence the velocity on the airfoil surface in the uniform flow V_Z normal to its chord line is

$$V(X,Z) = \pm \frac{V_Z}{\sqrt{1+\left(\frac{dZ}{dX}\right)^2}} \sqrt{\frac{1-X}{X}} \left[1 + S_3(X) \right] \tag{45}$$

Combining this equation with the equation developed for chordwise flow, equation 37, gives the total velocity due to the flow at angle of attack α_e' .

$$V(X,Z) = \frac{V_0}{\sqrt{1+(S_2(X))^2}} \left\{ \cos\alpha_e' \left[1+S_1(X) \right] \pm \sin\alpha_e' \sqrt{\frac{1-X}{X}} \left[1+S_3(X) \right] \right\} \tag{46}$$

where

$$S_2(X) = \frac{dZ}{dX} \tag{47}$$

$$\frac{V(X,Z)}{V_0} = \frac{\cos\alpha_e' \left[1+S_1(X) \right] \pm \sin\alpha_e' \sqrt{\frac{1-X}{X}} \left[1+S_3(X) \right]}{\sqrt{1+(S_2(X))^2}} \tag{48}$$

and the plus and minus signs are used for the upper and lower surfaces respectively. Using Bernoulli's equation for incompressible flow

$$C_p = \frac{p-p_0}{\frac{1}{2}\rho V_0^2} = 1 - \left(\frac{V}{V_0} \right)^2 \tag{49}$$

Therefore

$$C_p = 1 - \frac{\left\{ \cos\alpha_e' \left[1+S_1(X) \right] \pm \sin\alpha_e' \sqrt{\frac{1-X}{X}} \left[1+S_3(X) \right] \right\}^2}{1+\left[S_2(X) \right]^2} \tag{50}$$

These results apply to an unswept airfoil, and for a swept wing this equation becomes

$$C_p = 1 - \cos^2\alpha_e' \sin^2\phi - \frac{\left\{ \cos\alpha_e' \left[\cos\phi + S_1(X) \right] \pm \sin\alpha_e' \sqrt{\frac{1-X}{X}} \left[1+\frac{S_3(X)}{\cos\phi} \right] \right\}^2}{1+\left[\frac{S_2(X)}{\cos\phi} \right]^2} \tag{51}$$

where ϕ is the local wing sweep angle. At the leading edge of the wing, region 3, this equation can be written as

$$C_p = 1 - \cos^2\alpha_e' \sin^2\phi - \left\{ \frac{\sin\alpha_e' \left[1 + S_3(x)/\cos\phi\right]}{\frac{1}{\cos\phi}\sqrt{\frac{R_{LE}}{2C}}} \right\}^2 \tag{52}$$

Equations 51 and 52 apply to points on the wing away from the wing center or tip, where the influence of the center and tip are small. Next consider the wing center line. As shown by Kuchemann (6) the wing can be replaced by a series of kinked source lines as in Figure 17.

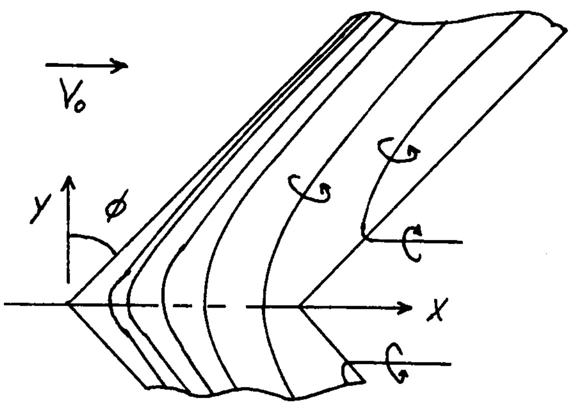

Fig. 17 Kinked Vortex Line Distribution at Wing Center Section

The velocity component V_x at the chord line is given by

$$\frac{V_x(x,0)}{V_0} = S_1(x)\cos\phi - G(\phi)\, S_2(x)\cos\phi \tag{53}$$

where

$$G(\phi) = \frac{1}{\pi} \ln\left(\frac{1+\sin\phi}{1-\sin\phi}\right) \tag{54}$$

With the spanwise component of velocity being zero due to symmetry, the velocity distribution on the surface becomes

$$\frac{V(X,Z)}{V_0} = \frac{1+\cos\phi\, S_1(X) - G(\phi)\, S_2(X)\cos\phi}{\sqrt{1+[S_2(X)]^2}} \tag{55}$$

and

$$C_p = 1 - \frac{\{1+\cos\phi\, S_1(X) - G(\phi)\, S_2(X)\cos\phi\}^2}{1+[S_2(X)]^2} \tag{56}$$

Equation 56 is modified to improve its performance near the leading edge such that

$$C_p = 1 - \frac{\left\{1+\cos\phi\, S_1(X) - G(\phi)\, S_2(X)\cos\phi\, \frac{1}{\sqrt{1+[S_2(X)]^2}}\right\}^2}{1+[S_2(X)]^2} \tag{57}$$

Next consider the velocity component normal to the chord, V_z. The vortex distribution to obtain a constant $V_z = V_0 \sin\alpha_e'$ normal to the chord is

$$\gamma(X) = 2V_0 \sin\alpha_e' \cos\phi \left(\frac{1-X}{X}\right)^{n(\phi)} \tag{58}$$

where

$$n(\phi) = \frac{1}{2}\left(1 - \phi/2\pi\right) \tag{59}$$

Accounting for wing thickness

$$\gamma(X) = 2V_0 \sin\alpha_e' \cos\phi \left(\frac{1-X}{X}\right)\left(1+S_3(X)\right) \tag{60}$$

Thus the pressure distribution due to both chordwise and normal flow becomes

$$C_p = 1 - \frac{\left\{\begin{array}{c}\cos\alpha_e'\left[1+\cos\phi\, S_1(X) - G(\phi)\cos\phi\, S_2(X)/\sqrt{1+[S_2(X)]^2}\right. \\ \pm \sin\alpha_e' \cos\phi \left(\frac{1-X}{X}\right)^{n(\phi)}\left(1+S_3(X)\right)\end{array}\right\}^2}{1+[S_2(X)]^2} \tag{61}$$

Equation 61 can be improved near the leading edge by replacing the term $\left(\frac{1-X}{X}\right)^{m(\phi)} \Big/ \sqrt{1+[S_2(X)]^2}$ by $\left(\frac{1-X}{X}\right)^{m(\phi)} \Big/ \left\{1+[S_2(X)]^2\right\}^{m(\phi)}$ such that equation 61 becomes

$$C_p = 1 - \left\{ \begin{array}{c} \left[\dfrac{1+\cos\phi\, S_1(X)}{\sqrt{1+[S_2(X)]^2}} - G(\phi)\cos\phi\, \dfrac{S_2(X)}{1+[S_2(X)]^2}\right]\cos\alpha_e' \\ \pm \sin\alpha_e' \cos\phi \left(\dfrac{1-X}{X}\right)^{m(\phi)} \dfrac{1+S_3(X)}{\left\{1+[S_2(X)]^2\right\}^{m(\phi)}} \end{array} \right\}^2 \tag{62}$$

At the wing leading edge equation 62 can be written as

$$C_p = 1 - \sin^2\alpha_e' \cos^2\phi \left\{ \frac{1+S_3(X)}{(R_{LE}/2C)^{m(\phi)}} \right\}^2 \tag{63}$$

Equations 56, 57, 62 and 63 are the equations used to compute pressure coefficients in the wing regions 1, 3, 2 and 4 respectively, shown in Figure 13, page 27. It should be noted that equation 62 and 63 were derived for the center section of the wing, and are used at the tip station as well by changing the sign of the sweep angle ϕ in the tip region.

At this point all of the equations necessary to compute the wing pressure distributions have been developed, except for expressions for the three functions $S_1(X)$, $S_2(X)$ and $S_3(X)$. These functions can be approximated at fixed points along the chord by the sum of products of the section ordinates at the points and certain coefficients determined once and for all. The pressure coefficients are subsequently evaluated at the chord positions at which these S-functions have been approximated.

Dealing with the dimensionless airfoil coordinates X/C and

Z/C , and computing the pressure coefficients at N locations along the chord, the new parameter θ_i is defined such that

$$\cos\theta_i = 2(X/C)_i - 1 \tag{64}$$

Equation 64 is then used to determine the values of X/C locations at which pressures are computed by setting

$$\theta_i = \frac{i\pi}{N} \qquad \text{for } i = 1 \text{ to } N-1 \tag{65}$$

then

$$(X/C)_i = \frac{1+\cos\theta_i}{2} \tag{66}$$

and

$$(Z/C)_i = f'[(X/C)_i] \tag{67}$$

The three S-functions are then determined by

$$S_1[(X/C)_J] = \sum_{i=1}^{N-1} \Delta_1(i,J)(Z/C)_i \tag{68}$$

$$S_2[(X/C)_J] = \sum_{i=1}^{N-1} \Delta_2(i,J)(Z/C)_i \tag{69}$$

$$S_3[(X/C)_J] = \Delta_3(N,J)\sqrt{\frac{R_{LE}}{2C}} + \sum_{i=1}^{N-1} \Delta_3(i,J)(Z/C)_i \tag{70}$$

for values of J from 1 to N-1. In addition, at the leading edge (where J = N)

$$S_1(X/C=0) = 2N\sqrt{\frac{R_{LE}}{2C}} + \sum_{i=1}^{N-1} \Delta_1(i,N)(Z/C)_i \tag{71}$$

$$S_3(X/C=0) = N\sqrt{\frac{R_{LE}}{2C}} + \sum_{i=1}^{N-1} \Delta_3(i,N)(Z/C)_i \tag{72}$$

In equations 68 to 72 the values for Δ_1 , Δ_2 and Δ_3 are determined as follows:

$$\Delta_1(i,J) = \frac{(-1)^{(i-J)}-1}{N}\,\frac{2\sin\theta_i}{(\cos\theta_i - \cos\theta_J)^2} \tag{73}$$

for $i \neq J$

$$s_1(i,J) = N/\sin\theta_i \tag{74}$$

for i = J

$$s_2(i,J) = \frac{-2(-1)^{(i-J)}\sin\theta_i}{\sin\theta_J(\cos\theta_i - \cos\theta_J)} \tag{75}$$

for i ≠ J

$$s_2(i,J) = \cot\theta_i/\sin\theta_i \tag{76}$$

for i = J

$$s_3(i,J) = s_1(i,J) + \frac{2}{N}\,\frac{1-(-1)^{(i-J)}}{\sin\theta_i(\cos\theta_i - \cos\theta_J)} \tag{77}$$

for i ≠ J

$$s_3(i,J) = s_1(i,J) \tag{78}$$

for i = J

$$s_3(N,J) = \frac{(-1)^J - 1}{N}\,\frac{1}{1+\cos\theta_J} \tag{79}$$

Equations 6 through 79 constitute a complete set of equations necessary to compute the wing pressure distributions. In the solution of a particular problem the function describing the airfoil is developed, followed by the computation of the wing area and aspect ratio. Next the S-values and then the effective angle of attack are calculated. Finally the pressure coefficients are computed and the results numerically integrated and plotted.

It should be noted that this solution is purely incompressible, and that improved results could be obtained in subsonic compressible flows by applying the Gothert compressibility factor $\beta = \sqrt{1-M^2}$. This is simply done by multiplying the aspect ratio and Z coordinates by the factor β and then computing the pressure distributions as usual. The resulting pressure coefficients are then divided by β^2 for the final results.

For this program, the differences between the wind tunnel model geometry and the geometry represented to the program are somewhat more than for the previous two programs discussed. These differences consist of no horizontal tail in the program representation, a cylindrical fuselage of infinite length, and no wing tip fairings for the program. Also, no model support system or wind tunnel walls are represented. A comparison of the wind tunnel model and the geometry used for this program are shown in Figure 18. Although these differences would appear to be substantial, with the exception of the infinite fuselage, these are the same differences that exist for the other two programs. Since none of the data examined is closer to the fuselage than 40% span, it is considered unlikely that the differences between the various computer configurations and the model geometry will affect the results.

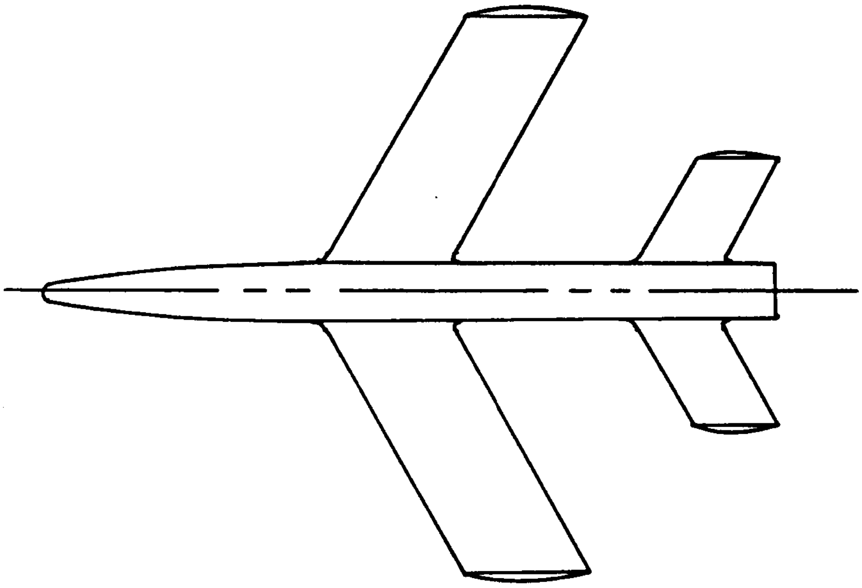

TEST GEOMETRY

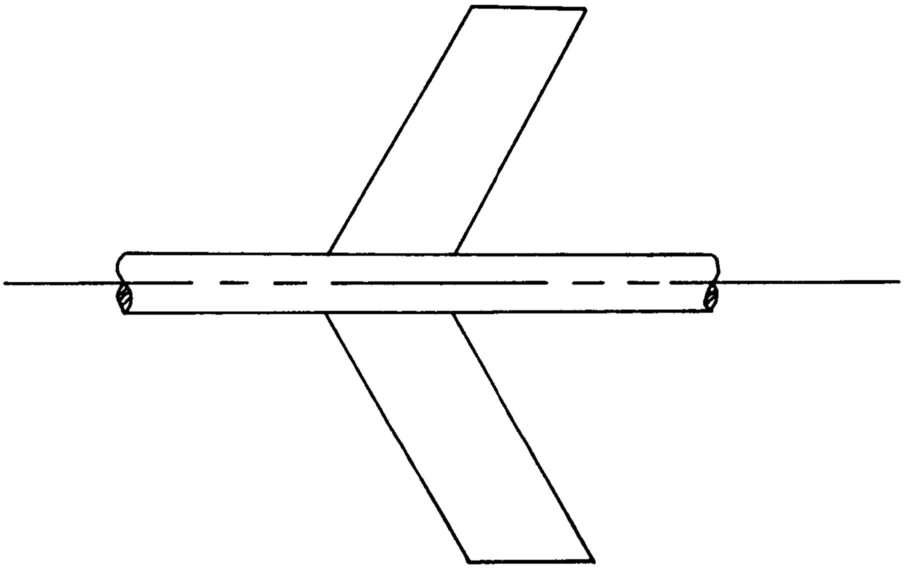

SWPP GEOMETRY

Fig. 18 Comparison of Wind Tunnel and SWPP-Code Aircraft Geometry

CHAPTER IV

RESULTS OF COMPUTER ANALYSIS

IV.1 Comparison of Computed and Experimental Results

In this section, the pressure distributions as computed by each of the computer codes are examined and evaluated in terms of their agreement or disagreement with the wind tunnel test results. Before examining these results, it is considered proper to ask whether the use of these experimental data to evaluate the performance of theoretical methods is valid. It could be argued that since none of the three programs examined a geometry that was in every way identical to the model tested, that the comparison is meaningless. Further, if the geometry were represented identically, it could still be argued that if a given program accurately solved the flow equations for a particular problem, then its results would be correct whether or not the experimental data agree. To avoid becoming involved in such a philosophical dialogue, no attempt is made to imply that the wind tunnel data is the "right answer", but merely to use this data as a yardstick for comparison of the computer results.

Presented in Figure 19 is the data obtained for 0.5 Mach number, for which the flowfield should be totally subsonic. At this Mach number it can be seen that all three programs predict pressure distributions in general agreement with the wind tunnel results. The

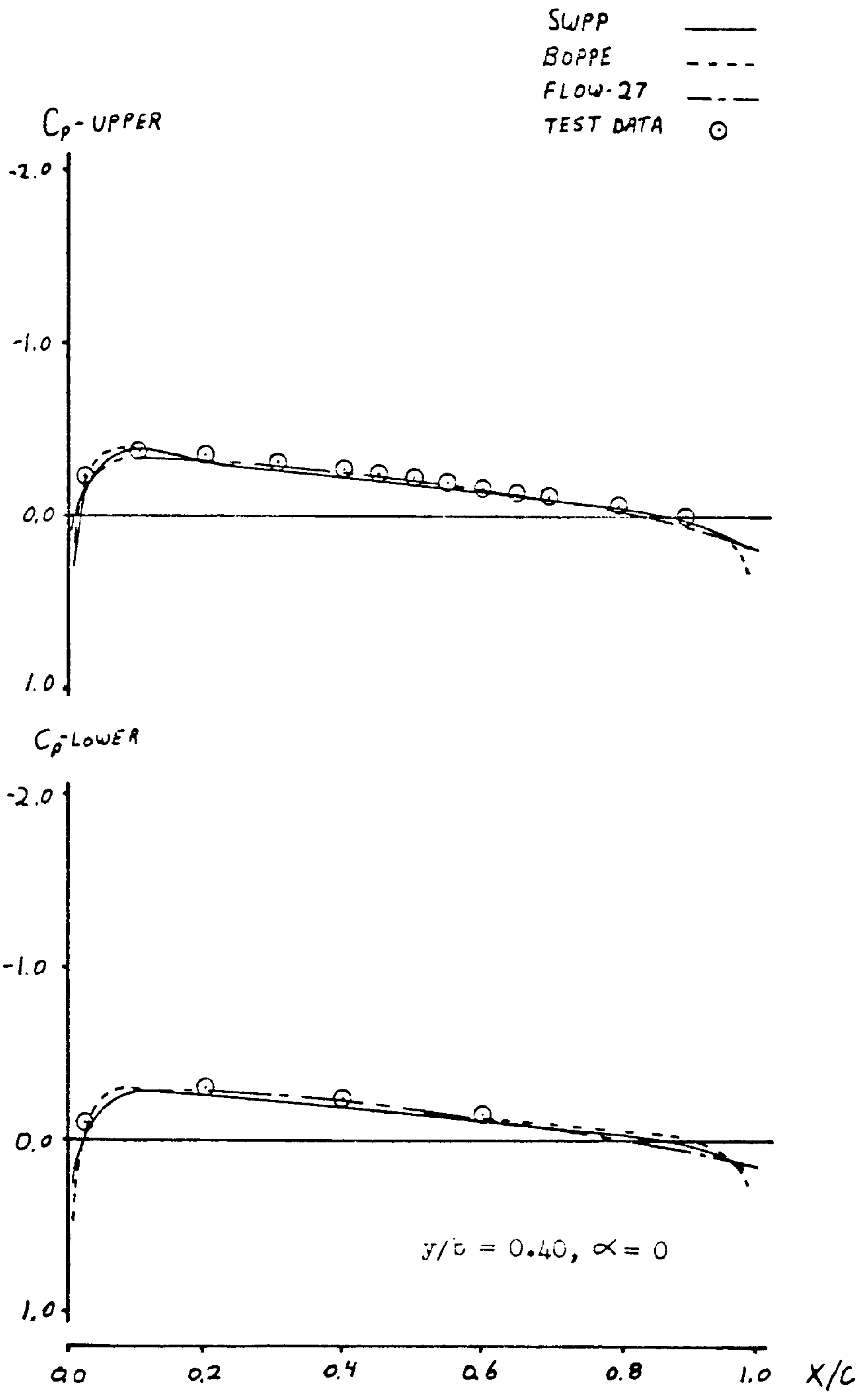

Fig. 19. Comparison of Pressure Distributions at 0.5 Mach

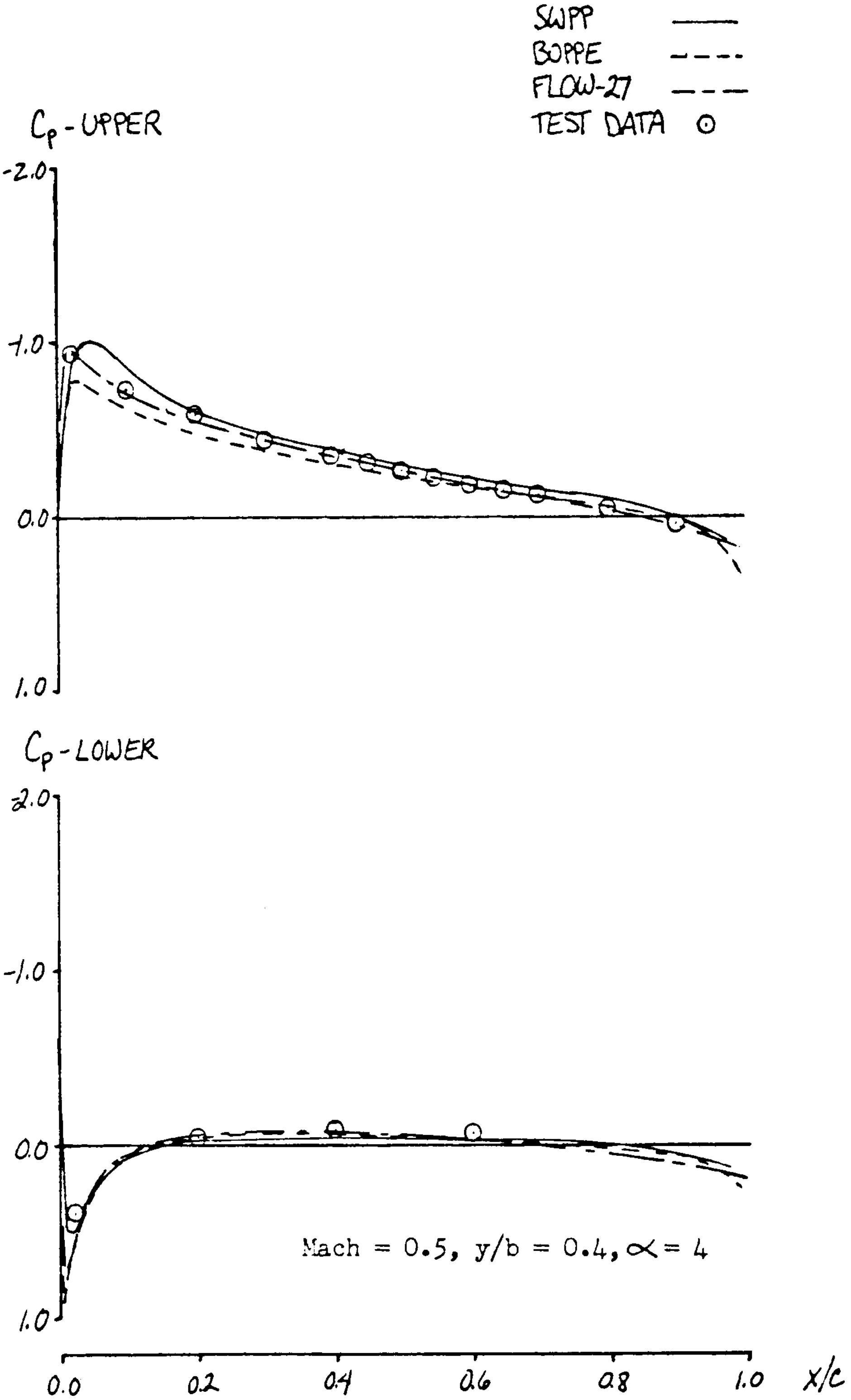

Fig. 19 (continued)

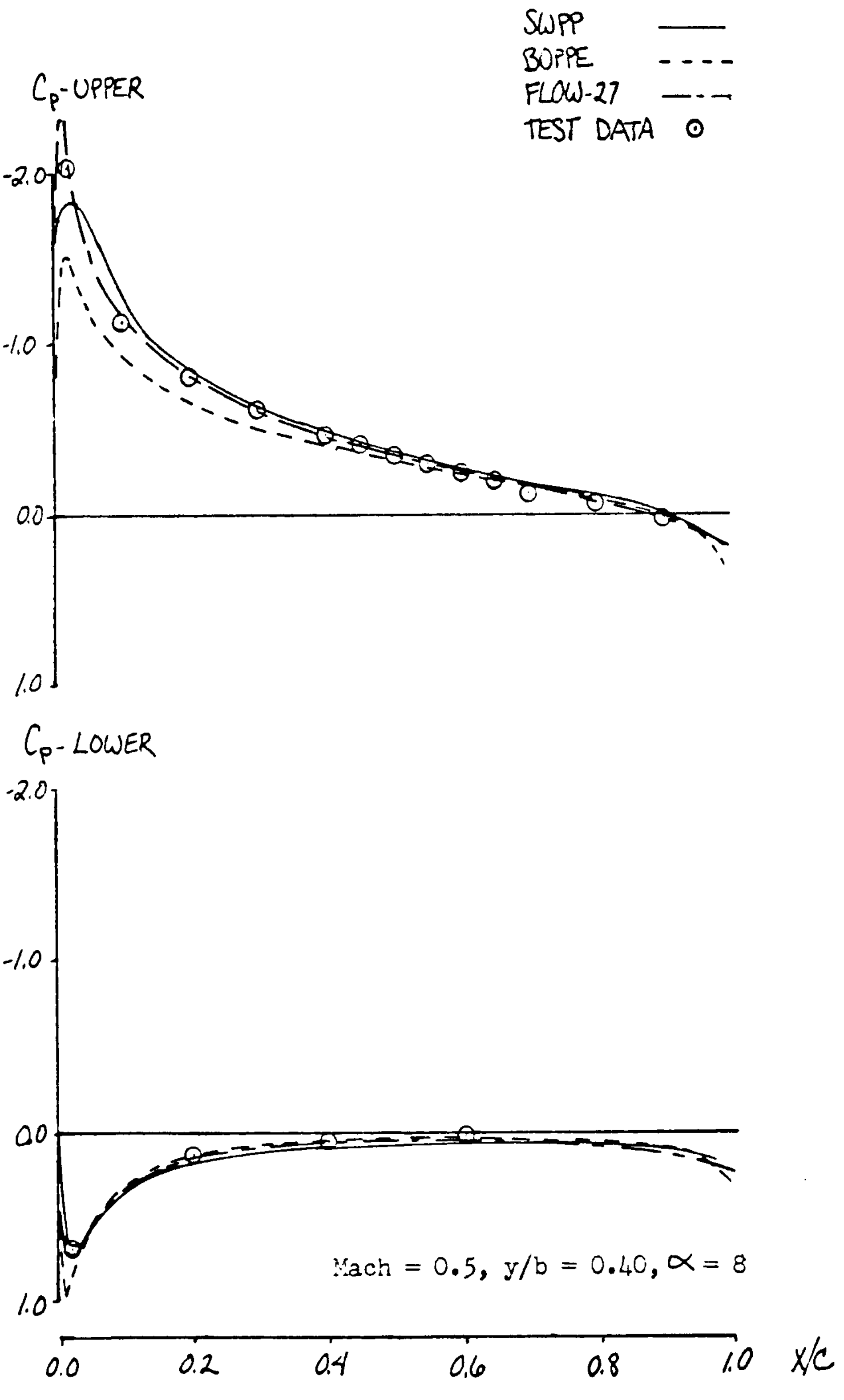

Fig. 19 (continued)

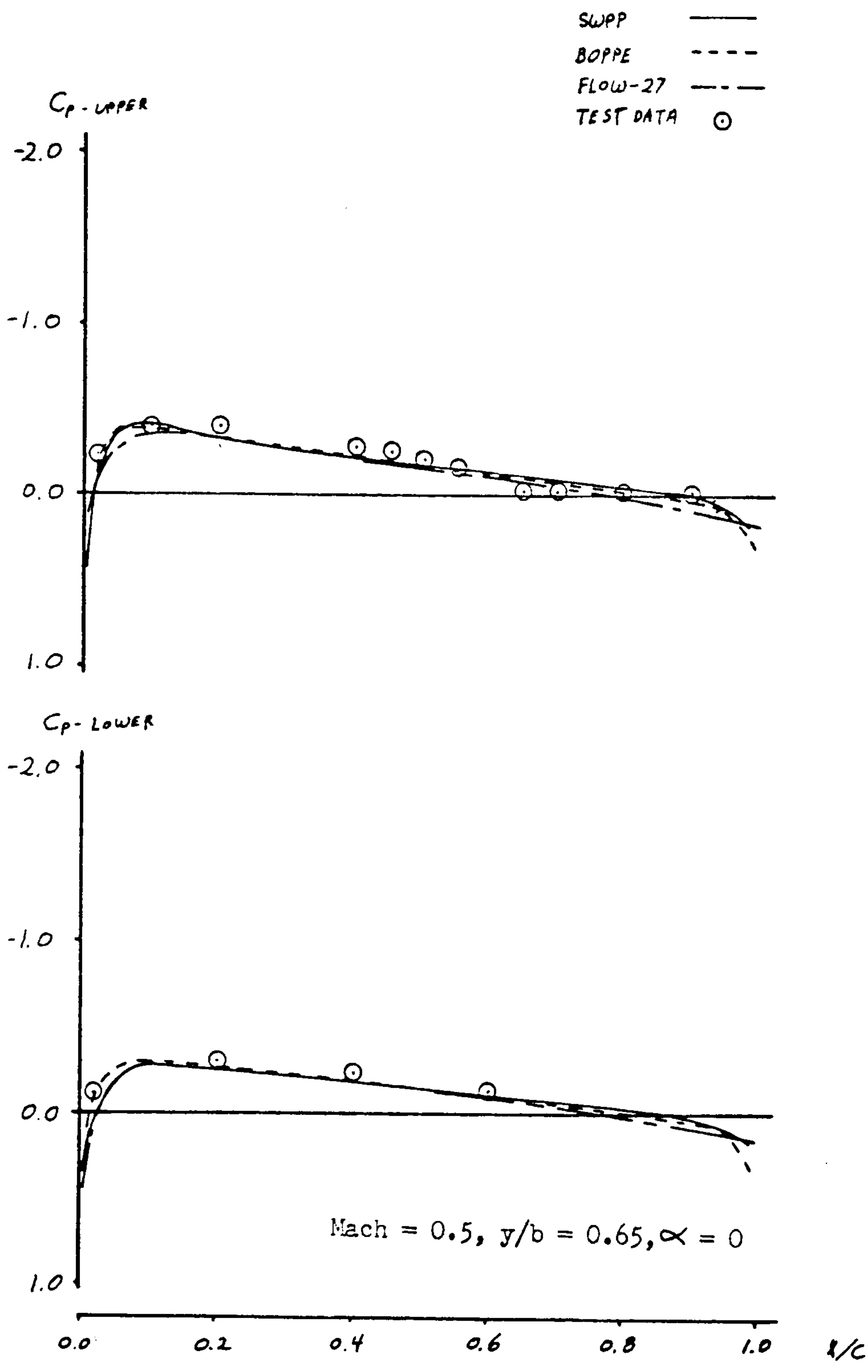

Fig. 19 (continued)

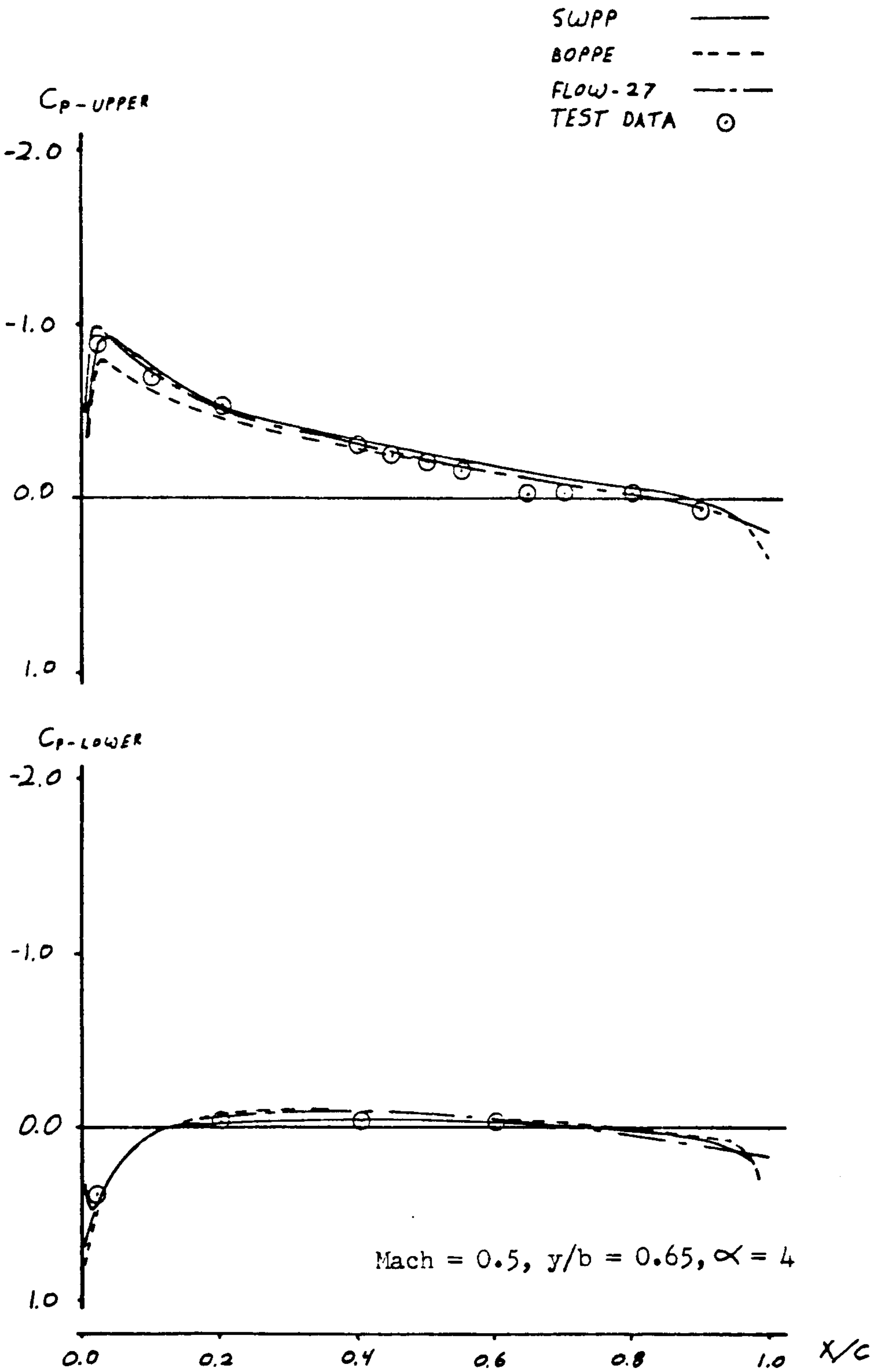

Fig. 19 (continued)

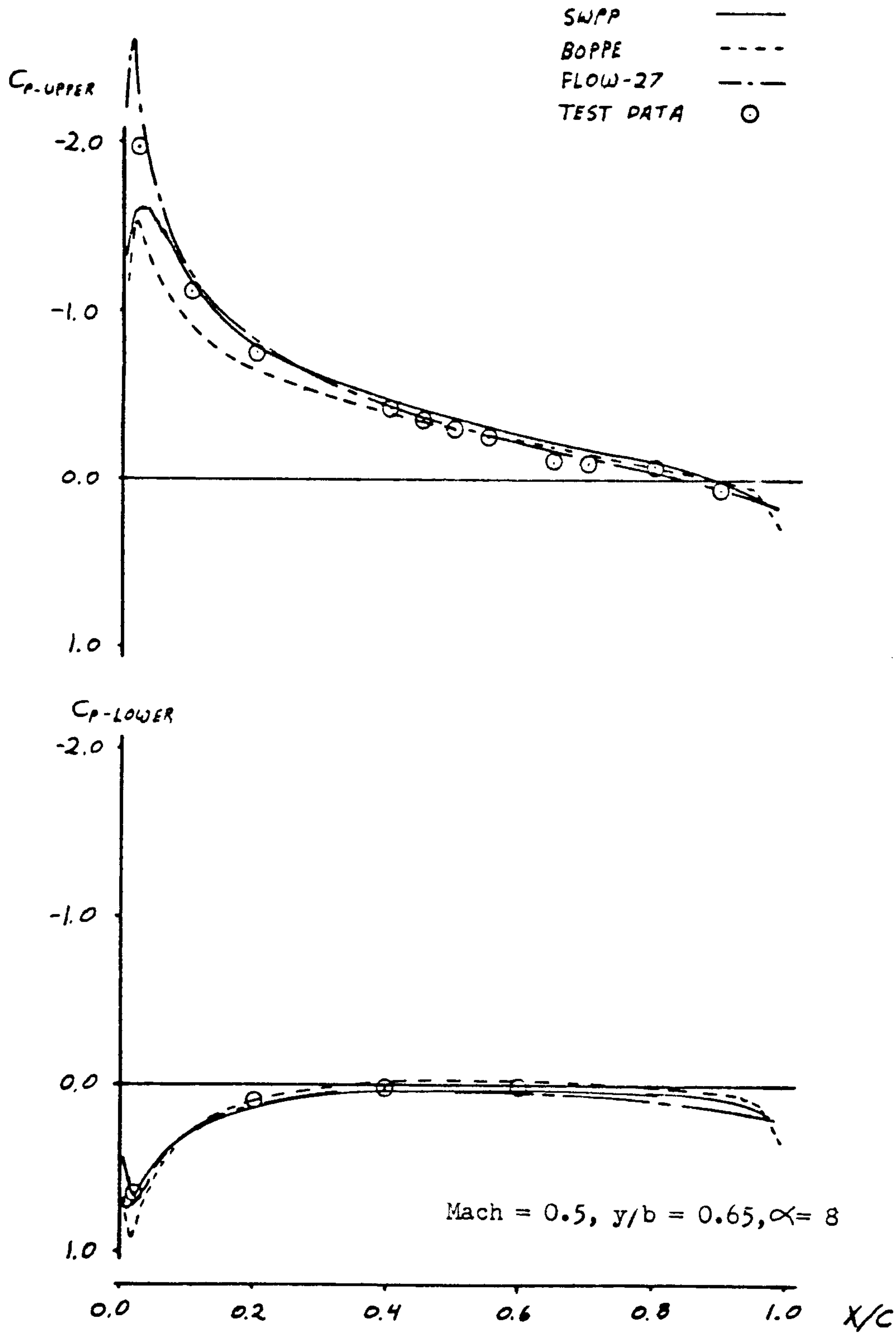

Fig. 19 (continued)

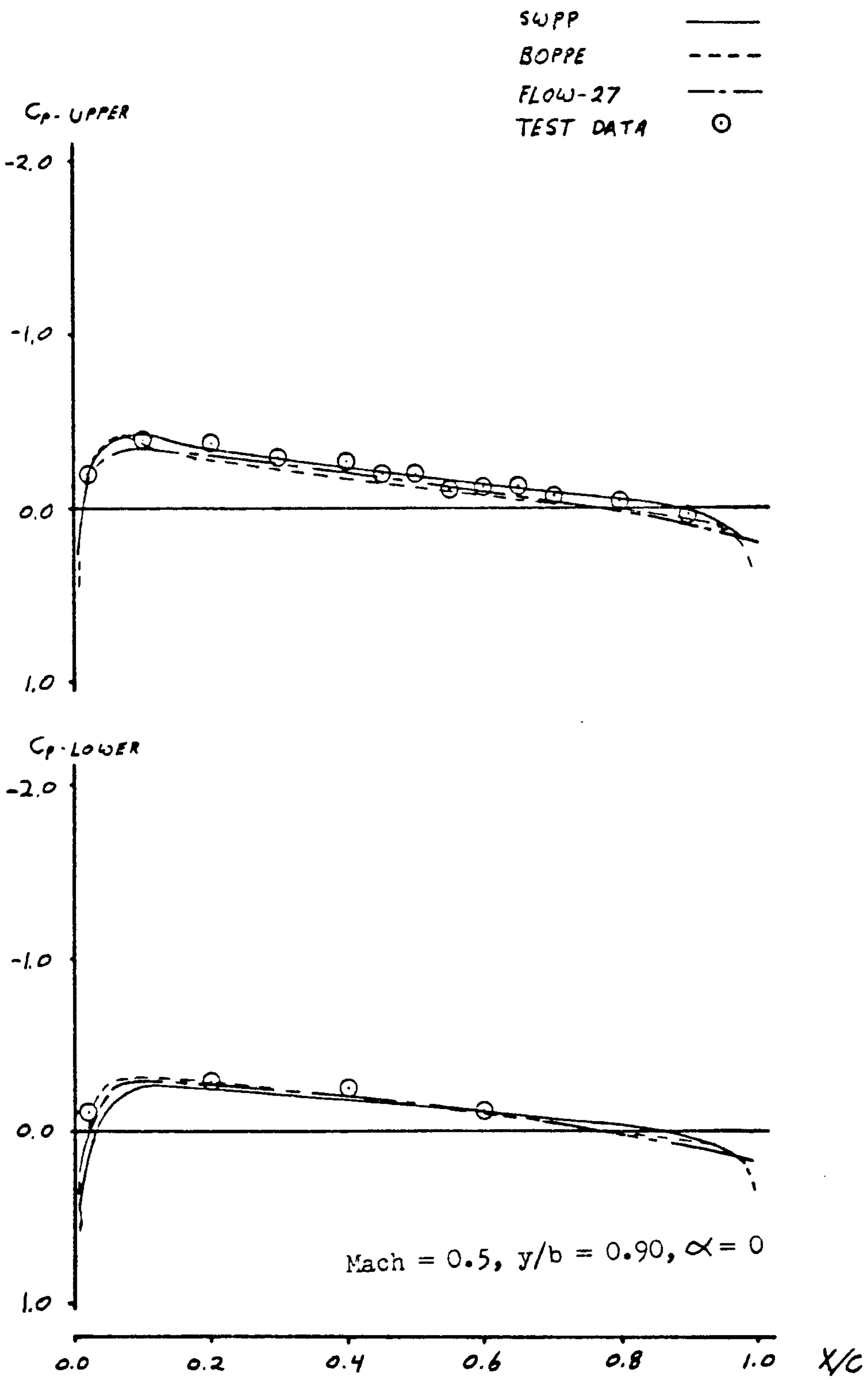

Fig. 19 (continued)

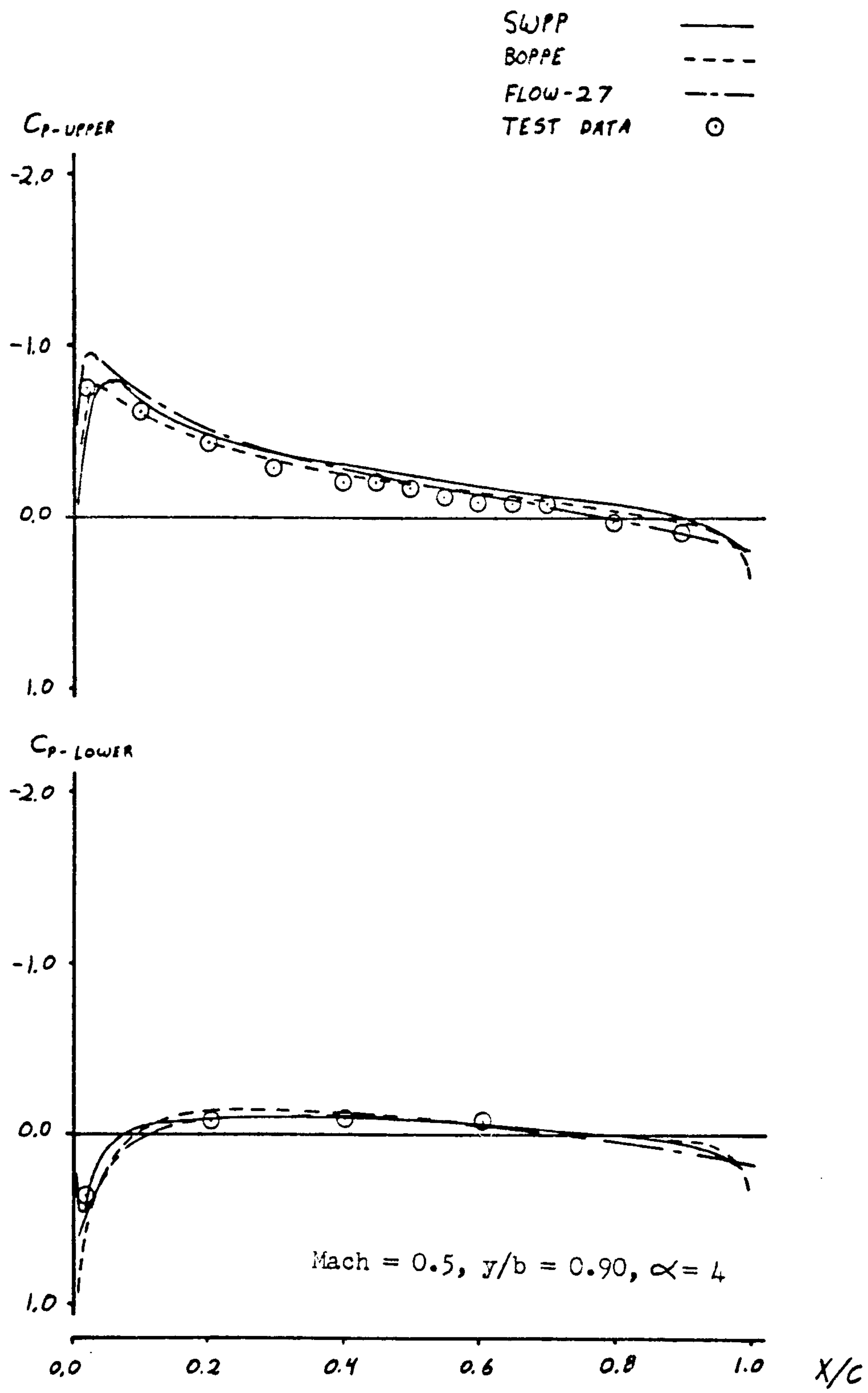

Fig. 19 (continued)

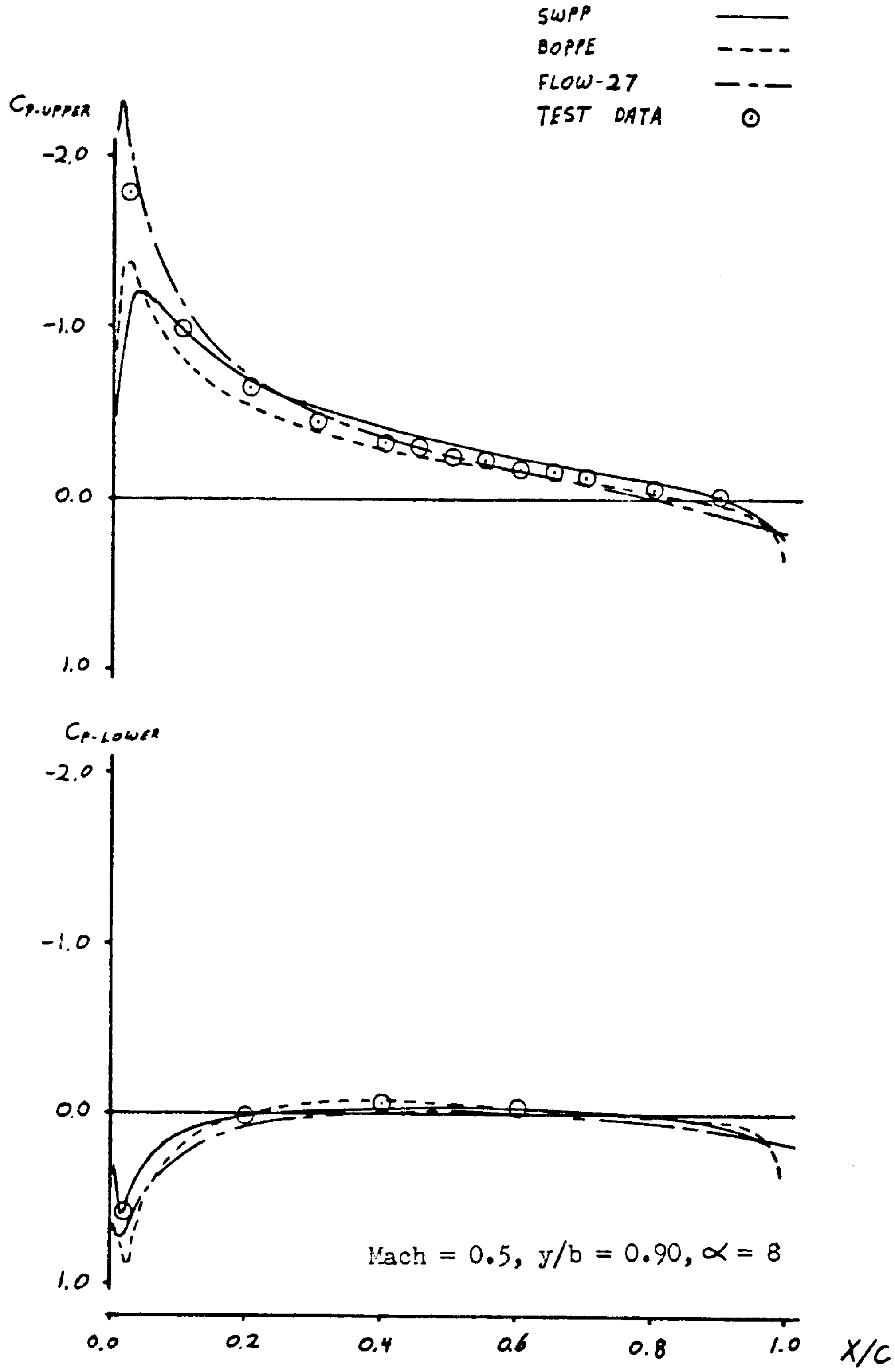

Fig. 19 (continued)

match between both the FLOW-27 and the SWPP-Code results and the test data are especially good. Although the BOPPE-Code results closely follow the data, the peak pressure predicted is somewhat smaller than the test data indicates, and remains smaller over the forward 40% of the wing section. For all spanwise locations, as the aircraft angle of attack is increased, the overall load on the wings is increased, but the agreement between the computed and measured pressure distributions is unaffected. Moving outboard along the span has little influence on the results when moving from 40 to 65% span. Moving further outboard to 90% span results in a decrease in the leading edge peak pressure and a greater variation between the three computer codes' results. This wider variation between the codes effectively brackets the experimental data, and reflects a slightly poorer performance by SWPP-Code and FLOW-27 and no change for the BOPPE-Code.

Increasing the Mach number to 0.7, the flowfield experiences the onset of transonic flow with mixed regions of subsonic and supersonic conditions. At this Mach number it is not likely that large portions of the flow are supersonic, but some localized regions of supersonic flow may occur. Shown in Figure 20 is the pressure distribution data for this Mach number. In general, the agreement with experimental data is good for all three programs at angles of attack below 8 degrees at all span stations. For these angles below 8 degrees, FLOW-27 best matches the test data, with both the SWPP-Code and BOPPE-Code predicting leading edge peak pressures below the measured values. At 8 degrees angle of attack the test data indicates the possible

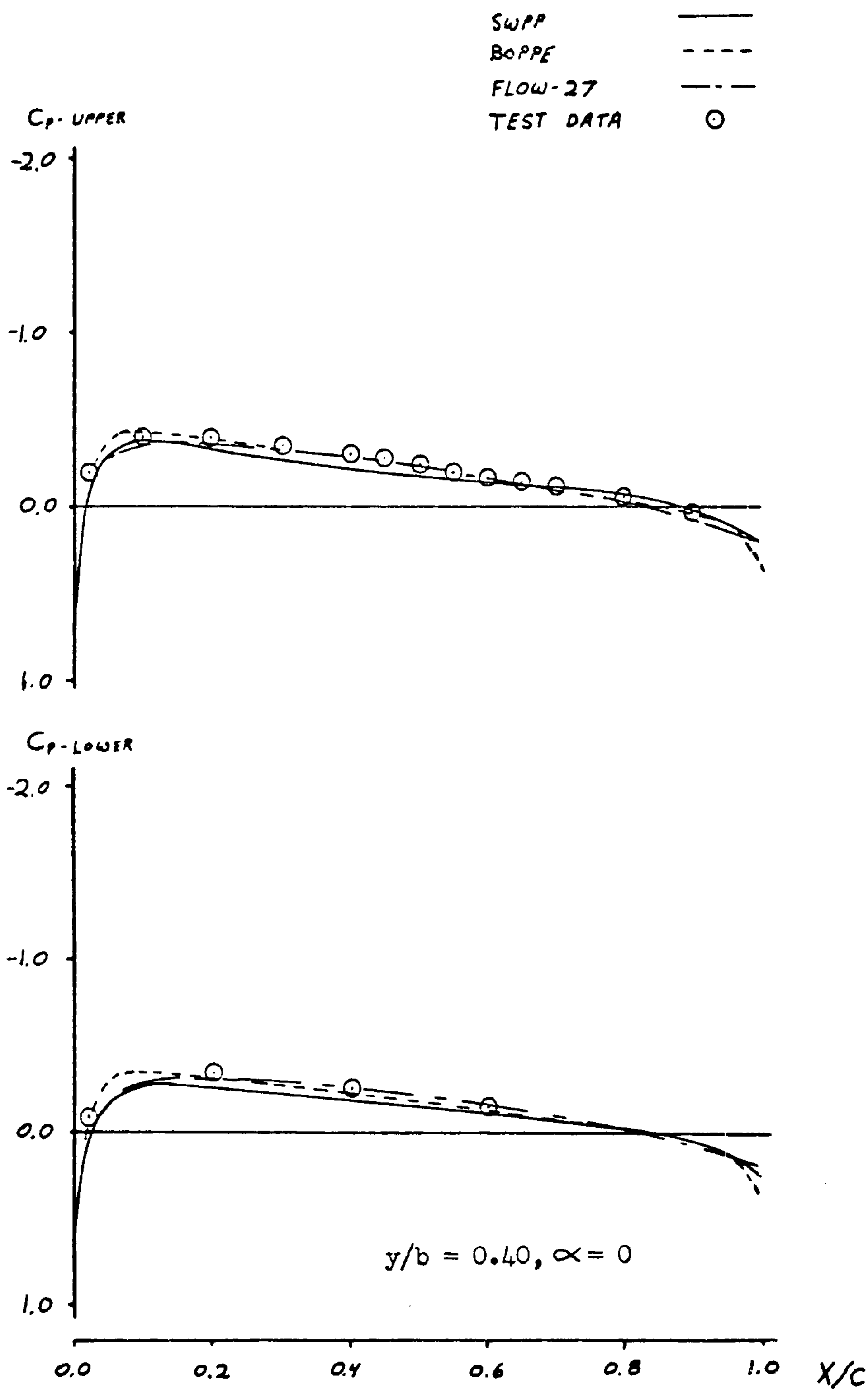

Fig. 20. Comparison of Pressure Distributions at 0.7 Mach

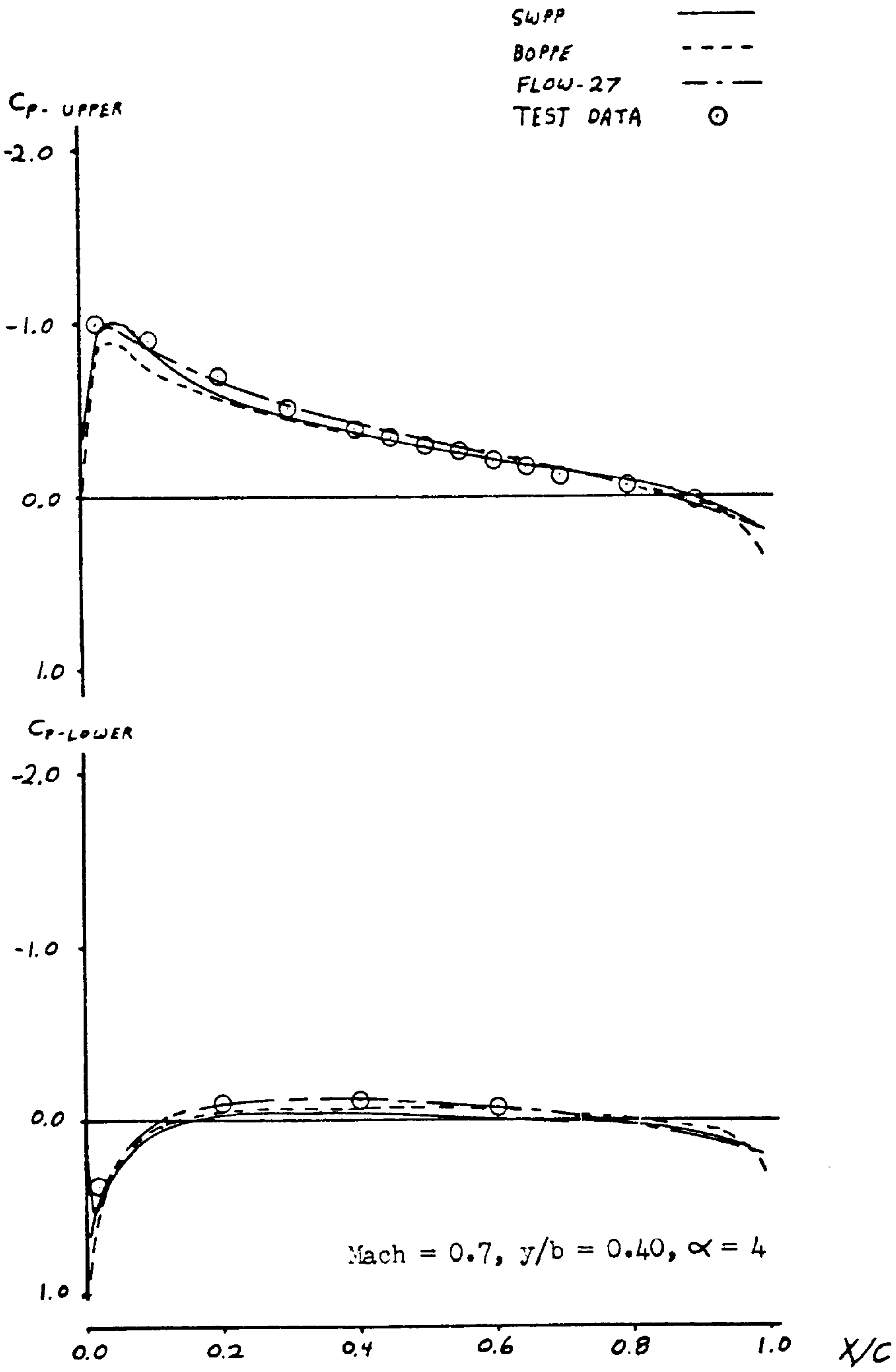

Fig. 20 (continued)

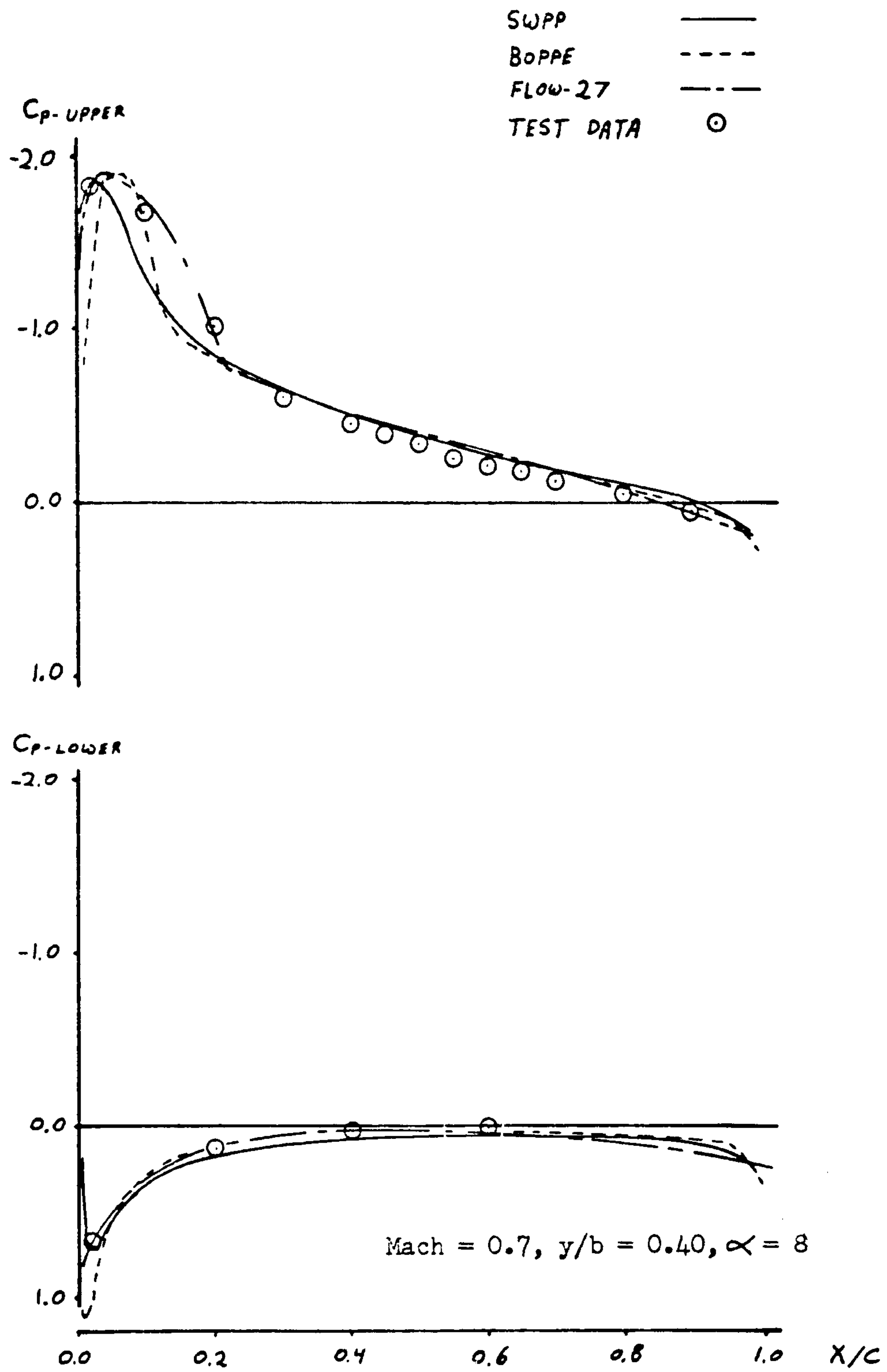

Fig. 20 (continued)

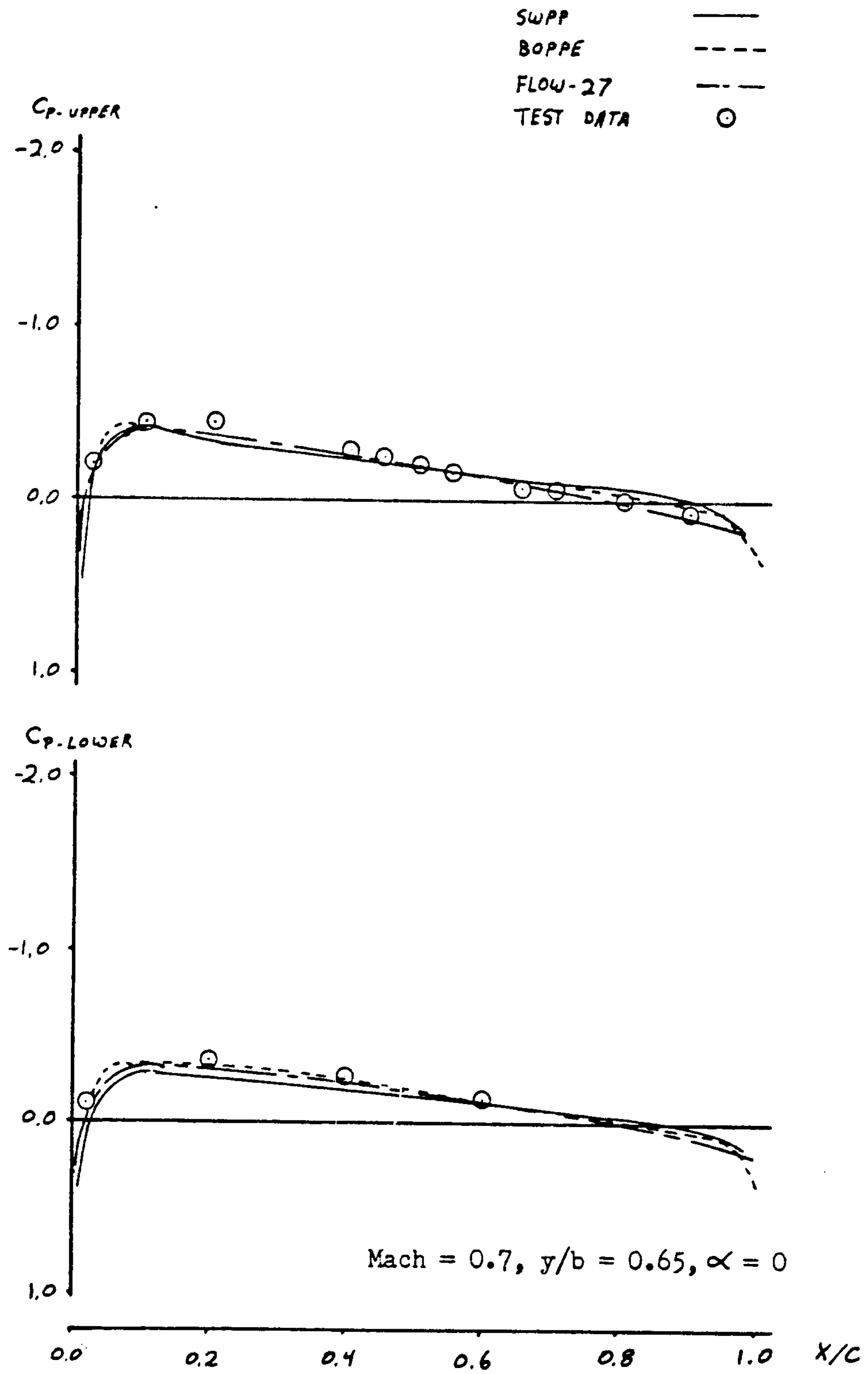

Fig. 20 (continued)

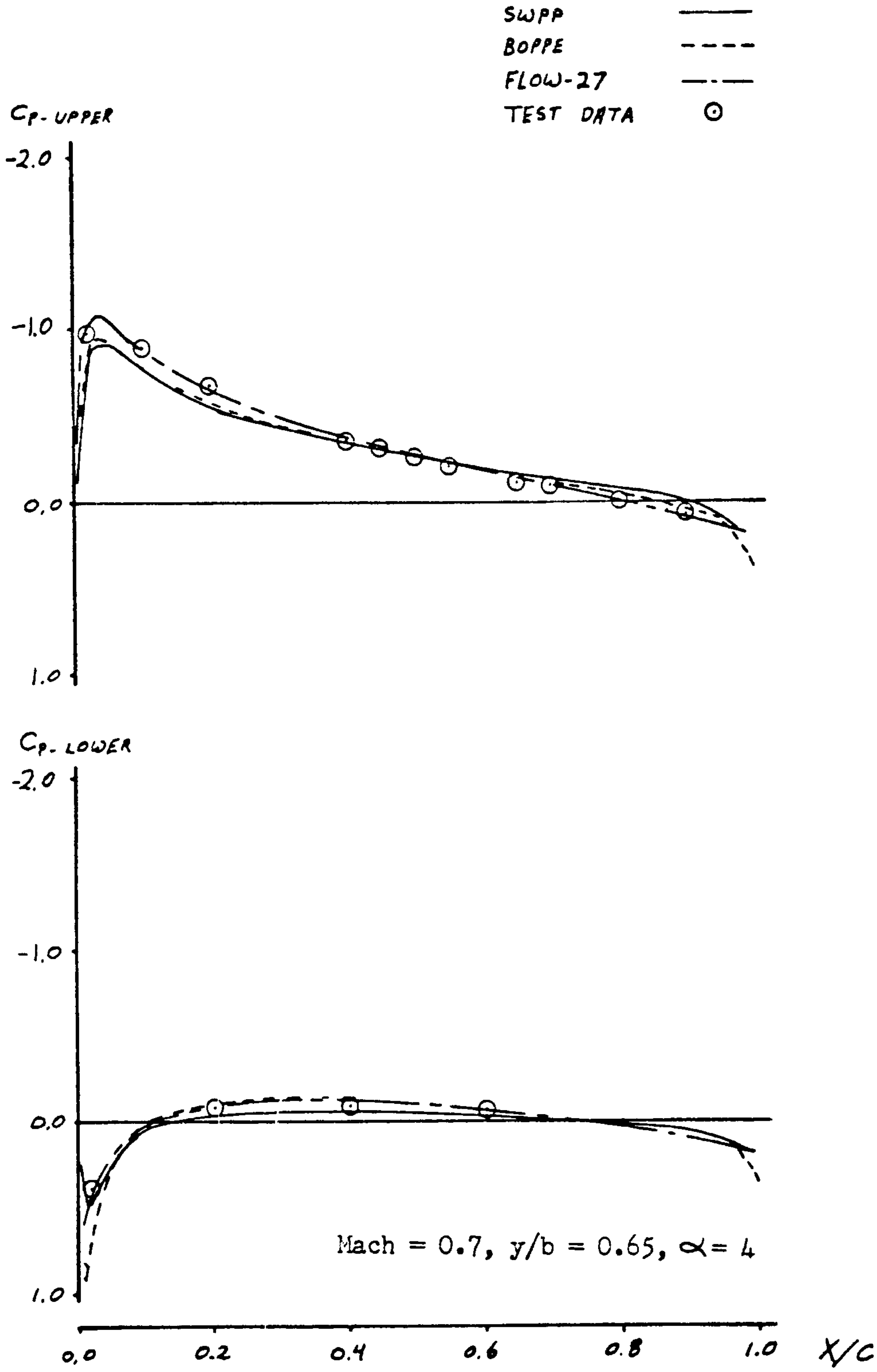

Fig. 20 (continued)

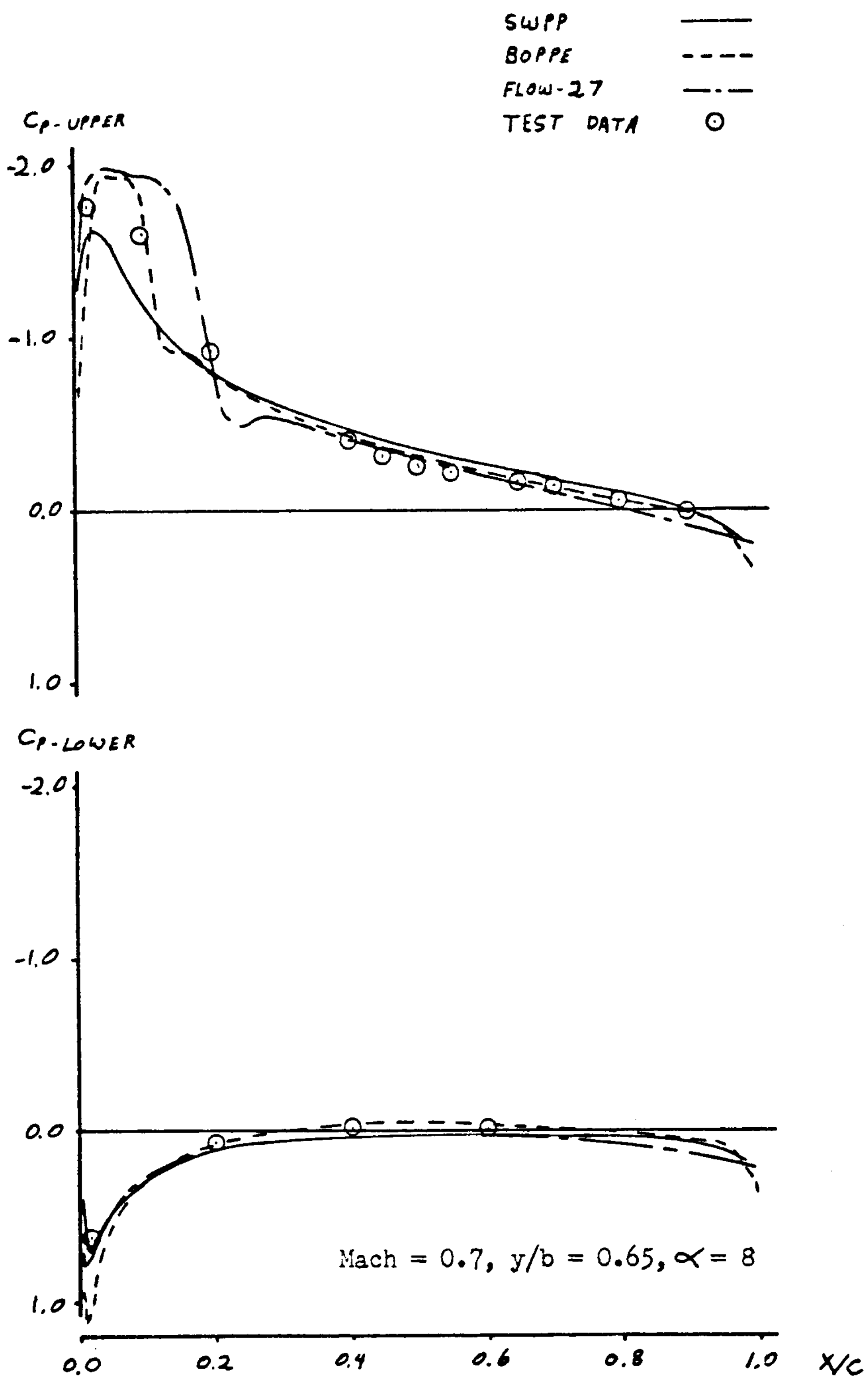

Fig. 20 (continued)

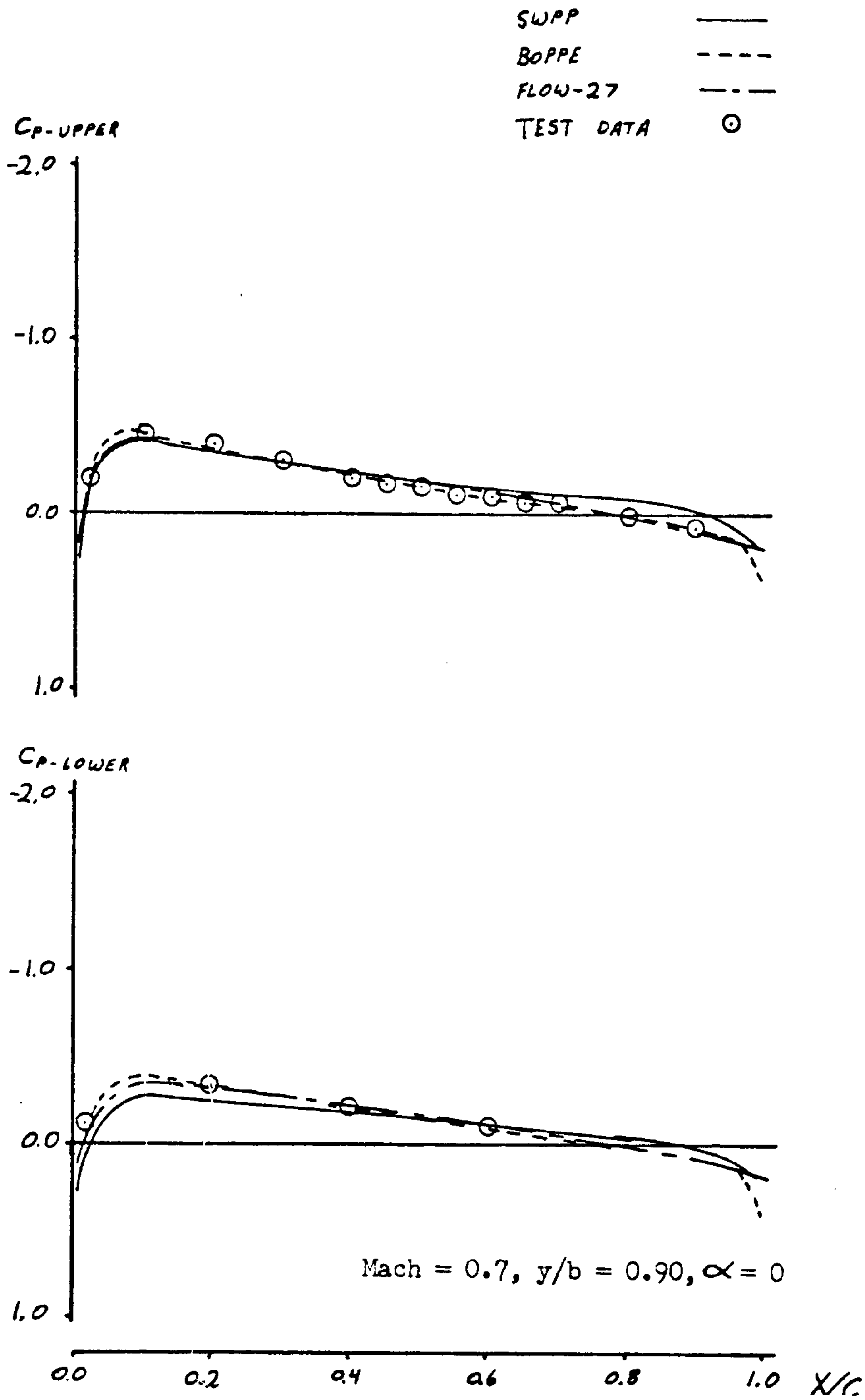

Fig. 20 (continued)

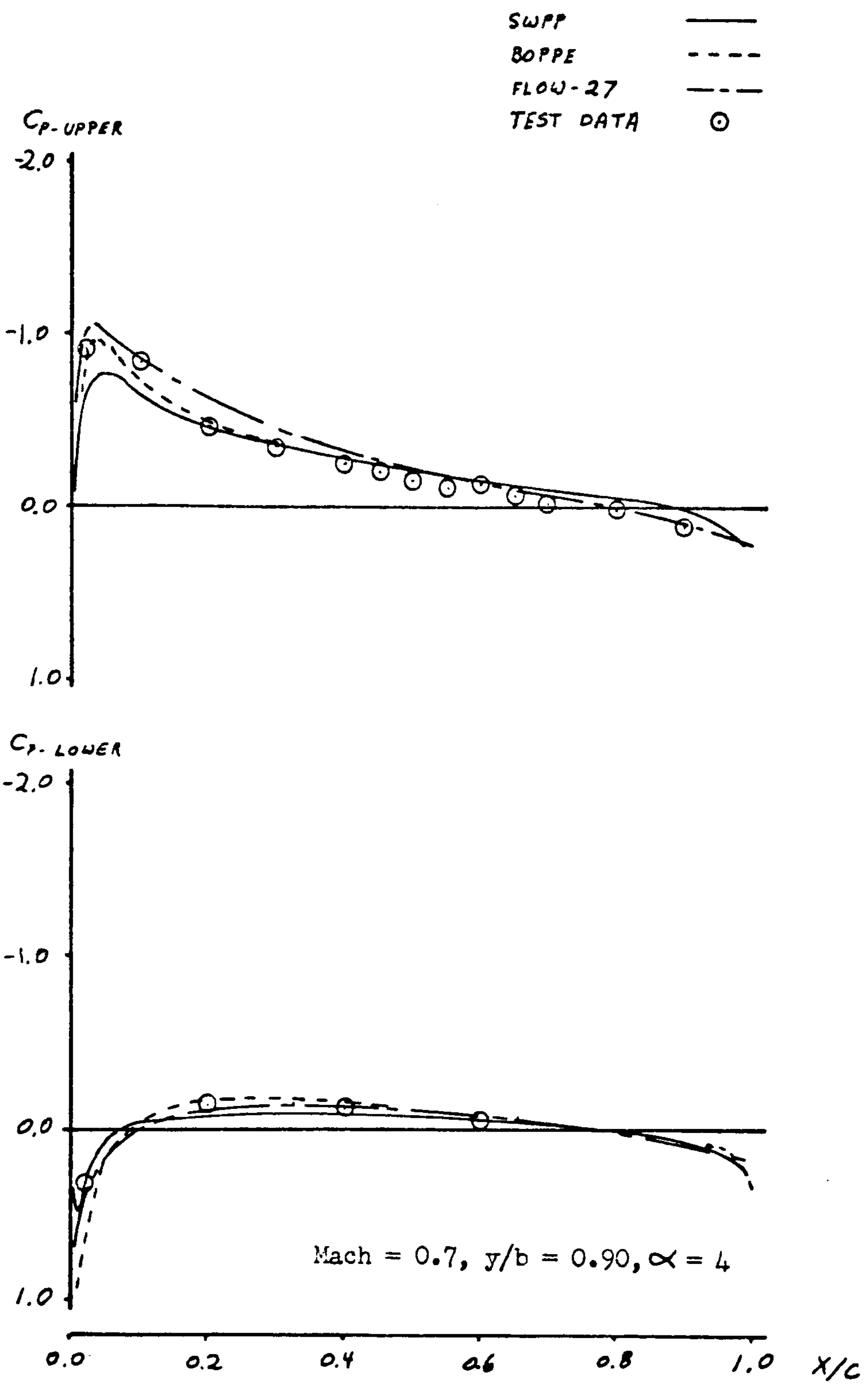

Fig. 20 (continued)

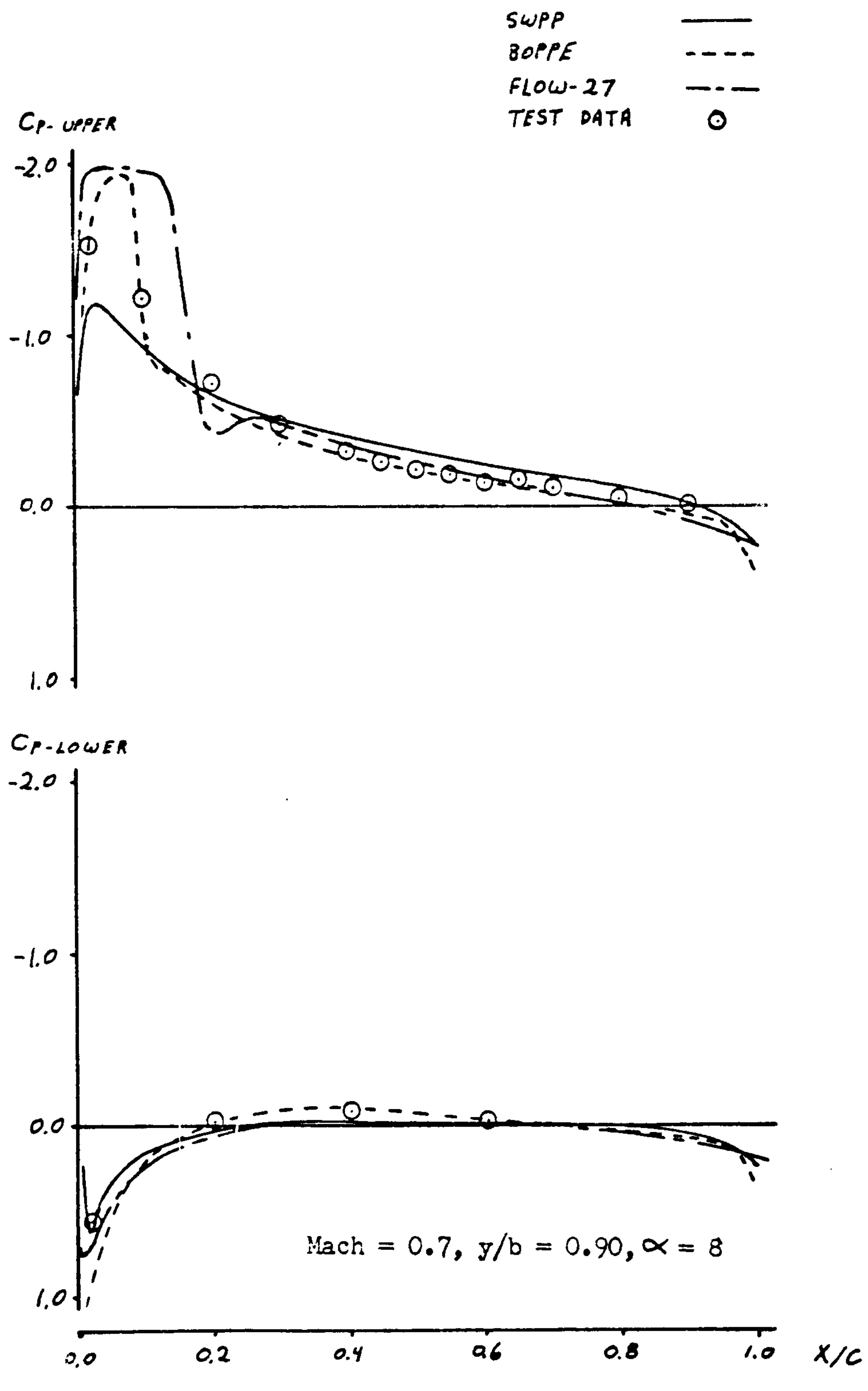

Fig. 20 (continued)

formation of a shock wave near the leading edge at all spanwise stations. Both FLOW-27 and the BOPPE-Code predict leading edge shocks at these conditions, with the BOPPE-Code results most closely matching the experimental data. A shock stronger and further aft on the wing than that observed is predicted by FLOW-27. Although the SWPP-Code predicts no shocks, its pressure distribution is seen to agree with the experimental data at 8 degrees nearly as well as the FLOW-27 results. This is coincidental in that the SWPP-Code is merely indicating the strong pressure gradient associated with subsonic flow over a wing, while FLOW-27 is predicting a shock wave which as mentioned is stronger and further aft than observed. As a result both programs differ from the experimental data, and by approximately the same amount. Moving outboard along the span at angles of attack of less than 8 degrees is seen to have little effect between 40 and 65% span. At 90% span a small reduction in the peak pressure is observed, and the BOPPE-Code better predicts this peak than it did at more inboard locations. At 8 degrees angle of attack the effect of moving along the span is seen to be somewhat different. Moving outboard is seen to move the shock slightly forward and to produce a somewhat stronger gradient across the shock. These effects of span location as described are observed in both the computed and experimental results such that the spanwise location is not observed to have a large effect on the agreement between the various results.

The final Mach number examined is 0.9. At this condition the flowfield experiences strong compressibility effects with large areas of supersonic flow, and strong shock waves. The pressure distribution data for 0.9 Mach number is presented in Figure 21. It should be noted that due to computer time limitations neither the BOPPE-Code nor FLOW-27 were able to reach a solution at 8 degrees angle of attack at this Mach number. Because of this, only 0 and 4 degree data are presented in Figure 21. At this Mach number it can be seen that the incompressible flow program, SWPP-Code, fails to predict the measured pressure distribution at any angle of attack or spanwise station. The failure of the SWPP-Code at these conditions is an expected result in that the program, which is based on incompressible assumptions, is being used to evaluate a flow in which compressibility is a primary feature. The remaining two programs, FLOW-27 and BOPPE-Code, can be seen to predict pressure distributions in general agreement with the experimental results. However, the program FLOW-27 has considerable difficulty locating the shock wave on the wing. As can be seen, at 0 degrees angle of attack FLOW-27 predicts the shock wave forward of the measured shock, while at 4 degrees the predicted shock is aft of that measured. In contrast to FLOW-27, the angle of attack is seen to have little effect on the performance of the BOPPE-Code at any span station. The BOPPE-Code is seen to consistently locate the shock wave more closely than FLOW-27. The spanwise location on the wing is seen to significantly alter the location of the shock as measured experimentally. As can be seen, the further outboard on the wing, the further forward the shock is located. This forward movement of the shock is predicted by both FLOW-27 and BOPPE-Code, but the measured movement is greater

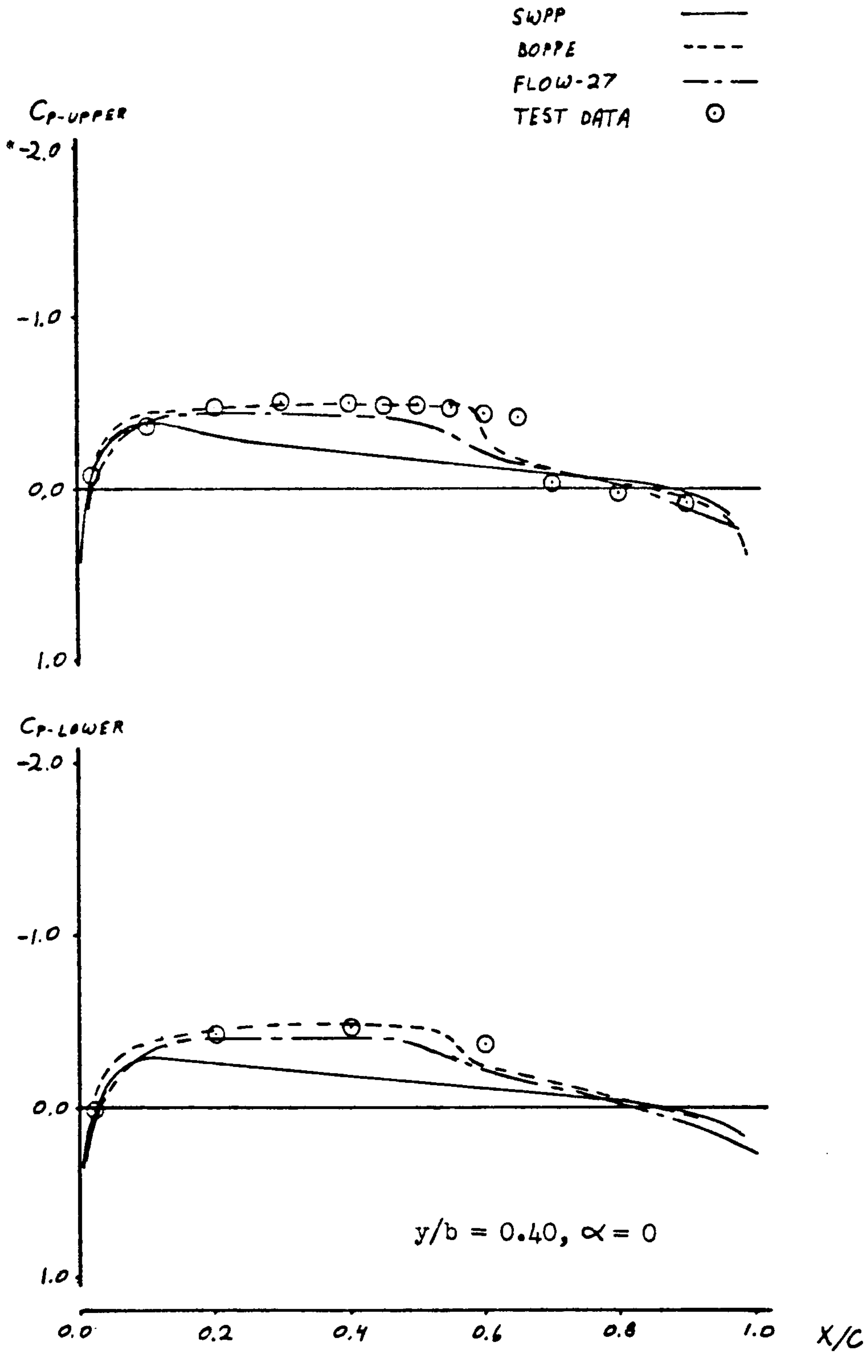

Fig. 21. Comparison of Pressure Distributions at 0.9 Mach

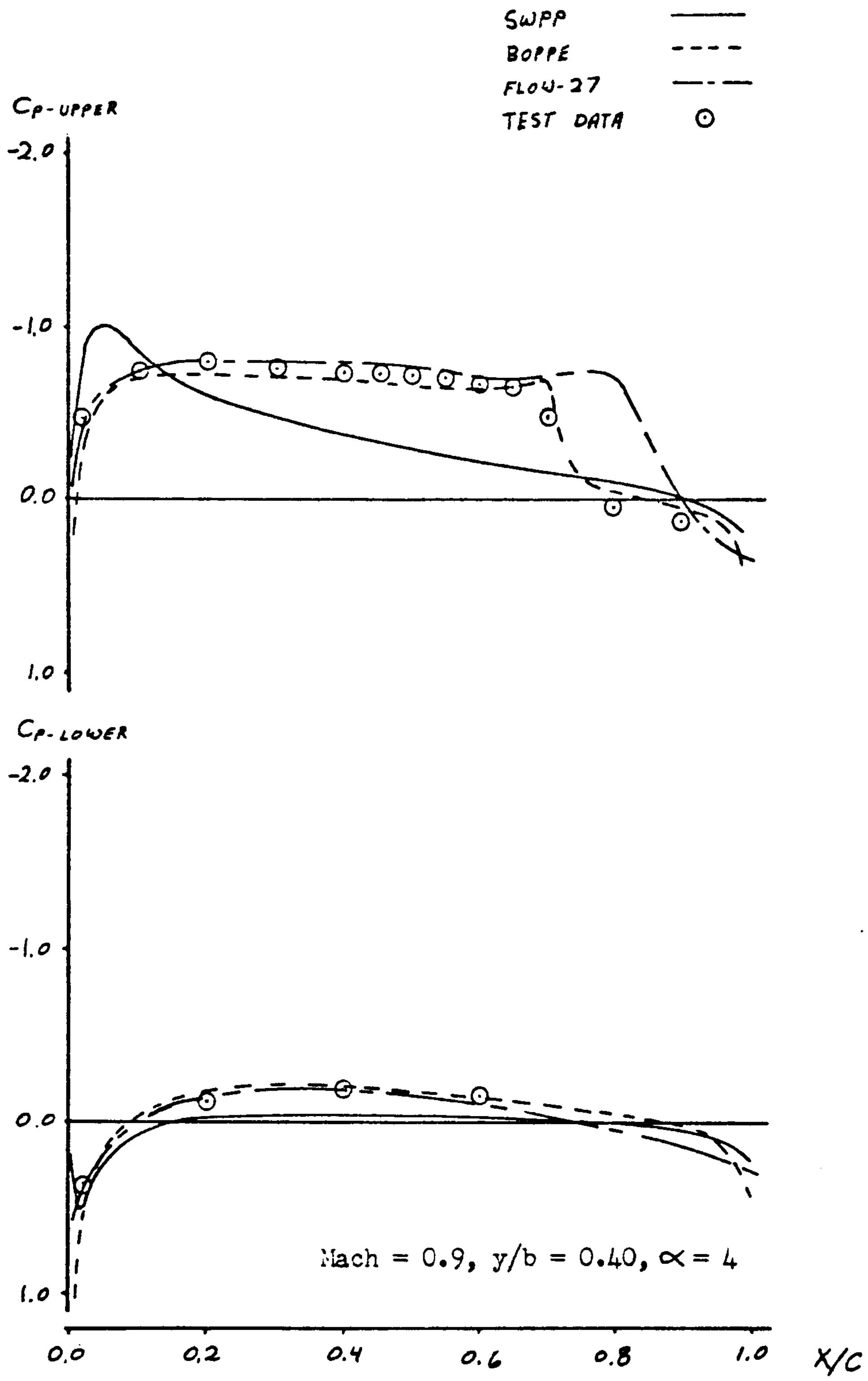

Fig. 21 (continued)

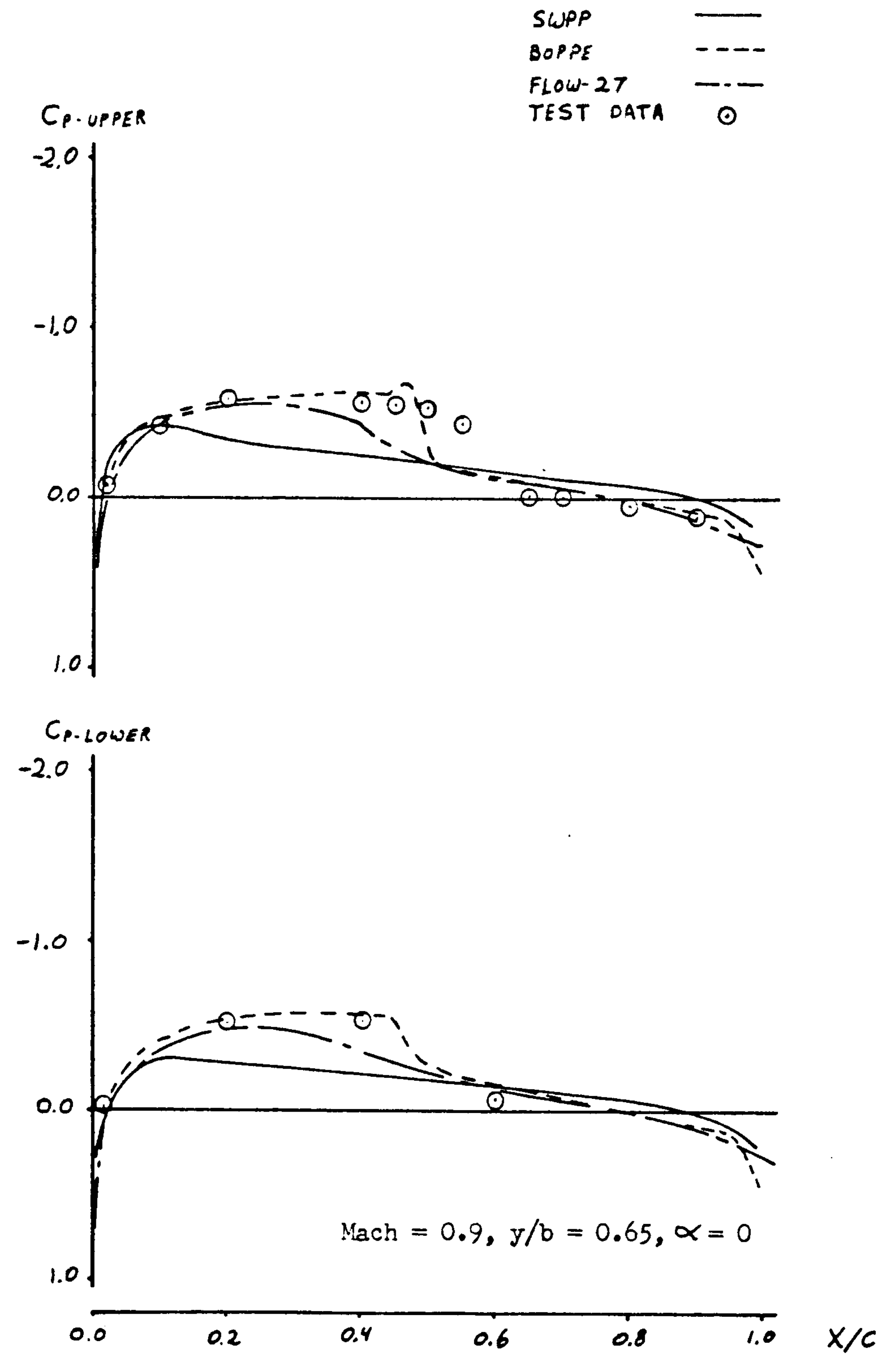

Fig. 21 (continued)

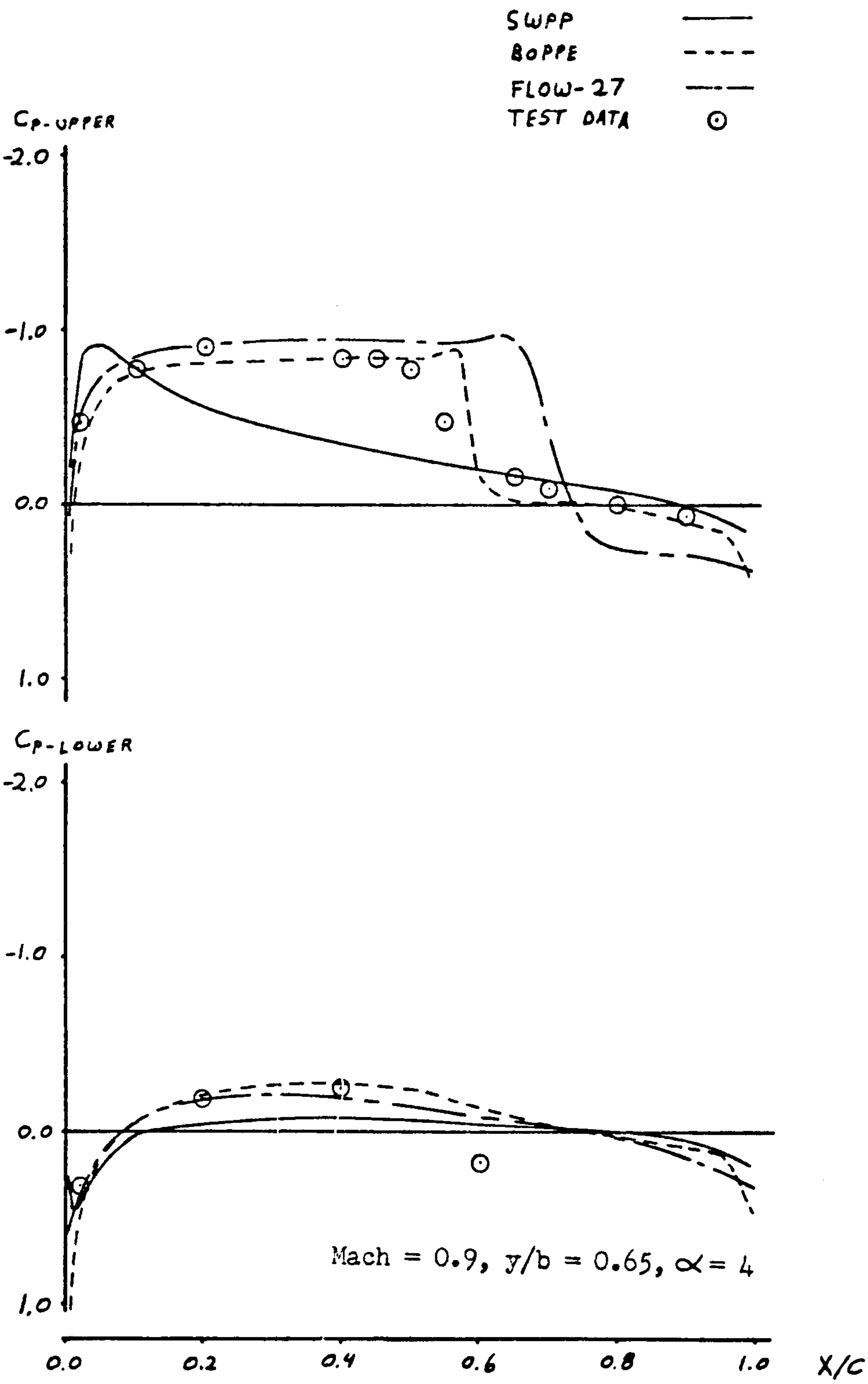

Fig. 21 (continued)

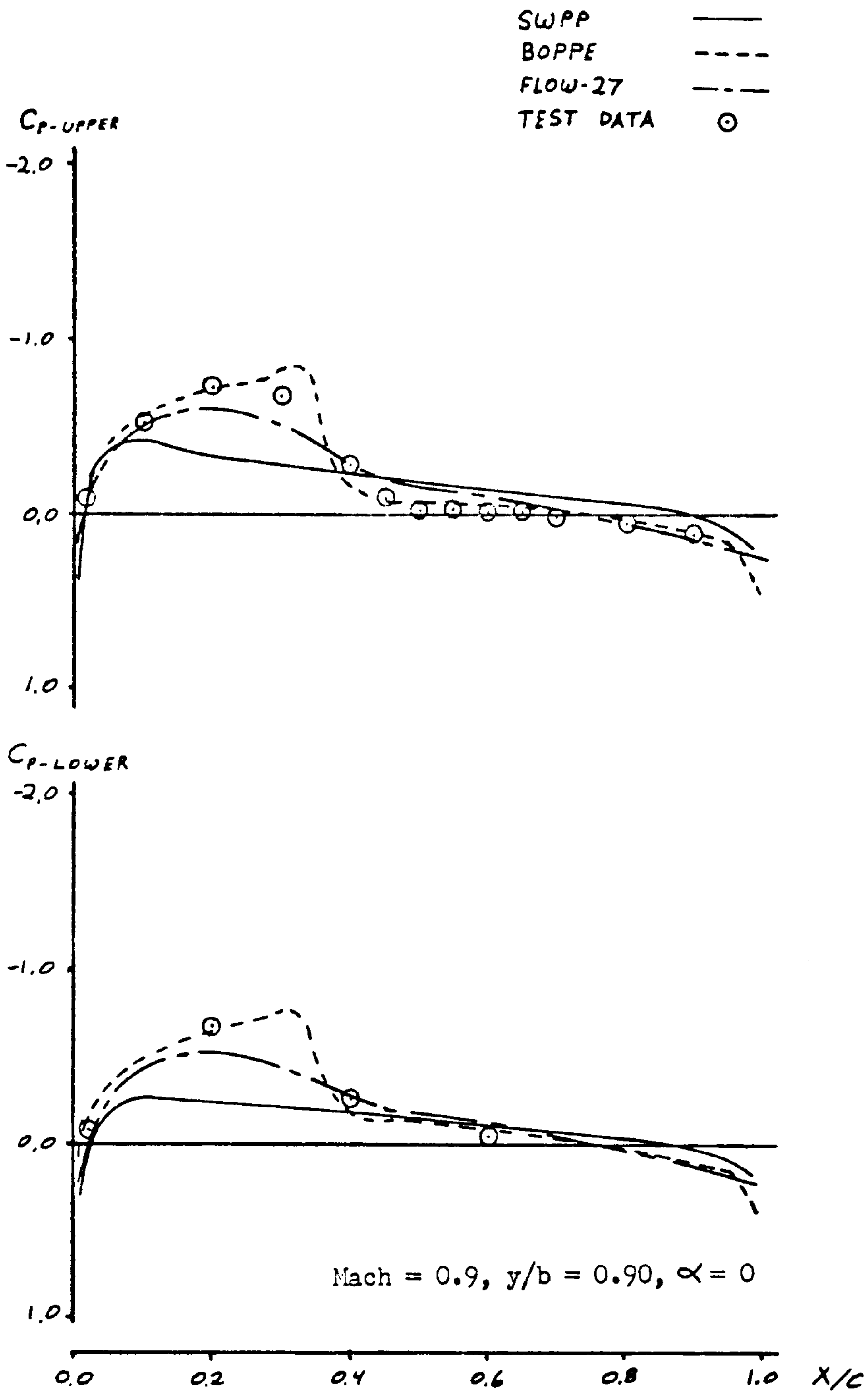

Fig. 21 (continued)

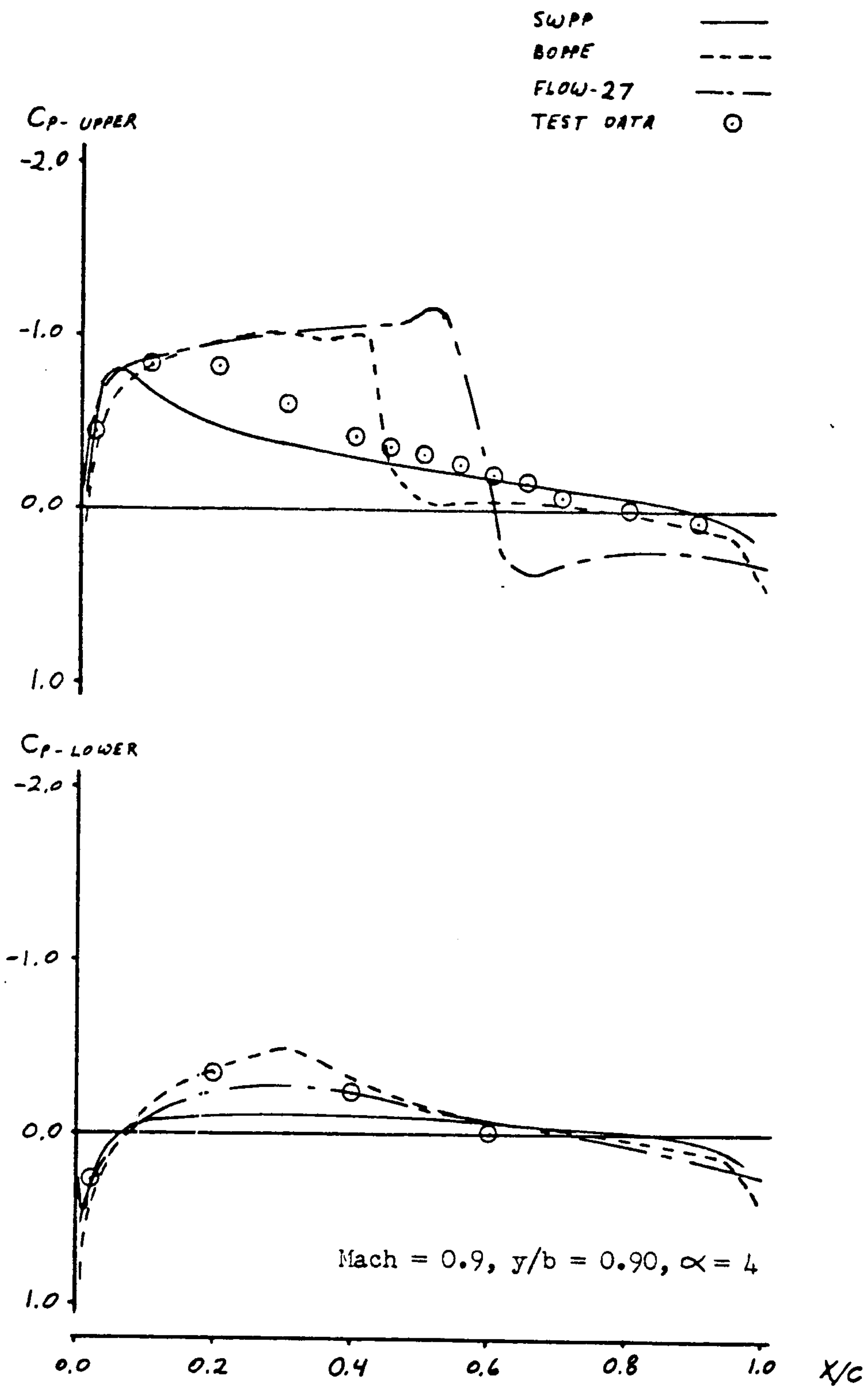

Fig. 21 (continued)

than predicted. As a result, as spanwise station is increased, the shocks predicted by both FLOW-27 and BOPPE-Code become further away from the measured shock.

In addition to these direct comparisons of pressure distributions, these pressures can be integrated to obtain section lift and pitching moment coefficients. These integrations were performed graphically and are subject to the variations introduced by such a technique. This is particularly true for the experimental data consisting of widely spaced points and having only four points along the section lower surface. With this in mind, the lift and pitching moment data are examined as data supplemental to the pressure distribution data. Presented in Figure 22 is the comparison of the section lift characteristics. Figure 22a shows the Mach 0.5 data. It can be seen that at all spanwise stations the wind tunnel data are bracketed by the computer results, showing a general agreement between all the codes. Moving outboard along the span it is seen that the variation between the codes increases, with the BOPPE-Code showing consistently the best agreement. It is notable that Mach 0.5 is the condition at which the best agreement between predicted and measured pressure distributions is seen, and that the agreement is best for FLOW-27 results. In these integrated results there is a significant difference seen between the FLOW-27 and measured results. This difference is considered to be due to the difficulty in integrating the wind tunnel data, and differences of this magnitude are likely to be seen in all integrated results presented. Figure 22b shows the

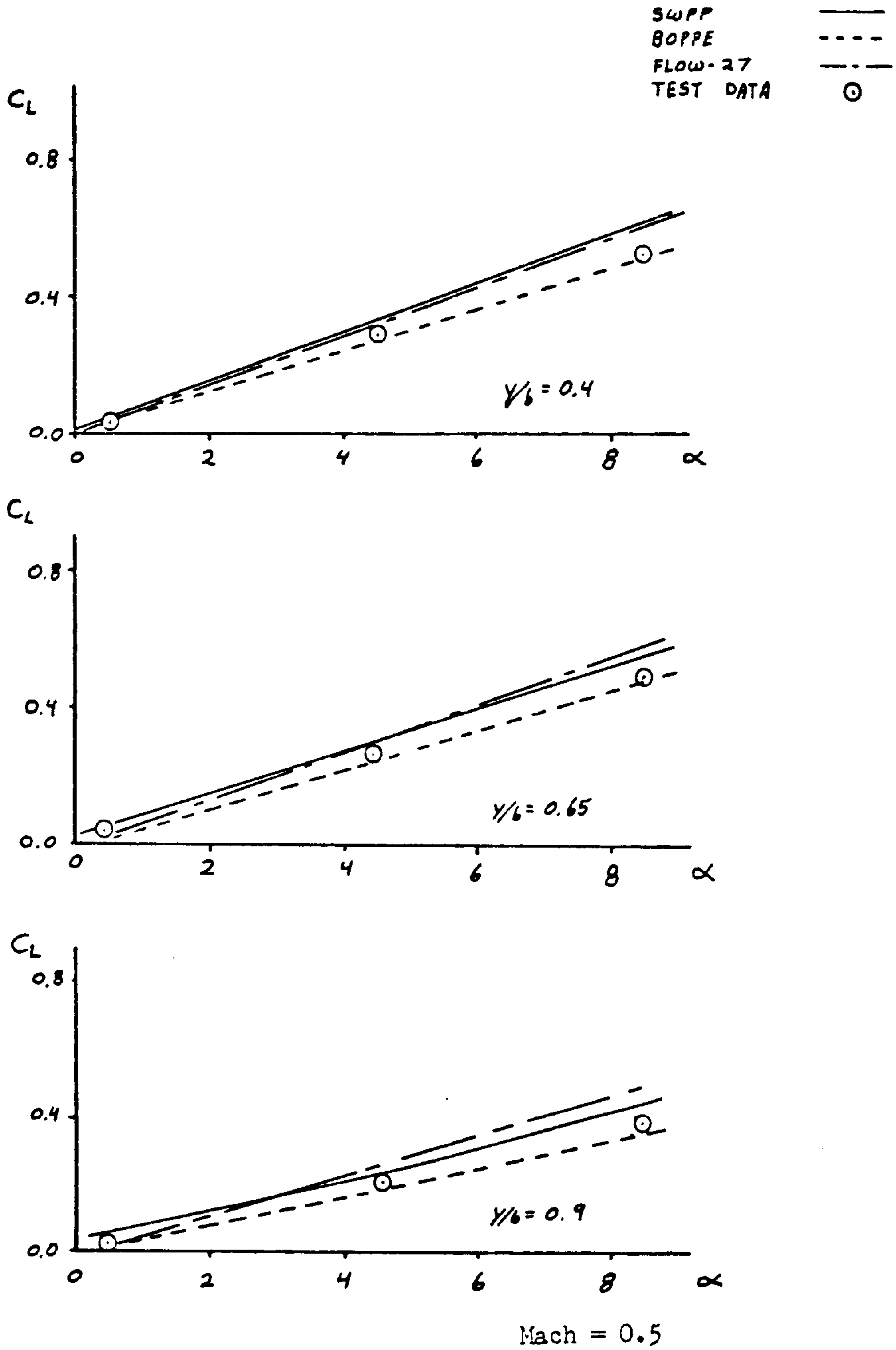

Fig. 22. Comparison of Wing Section Lift Coefficients

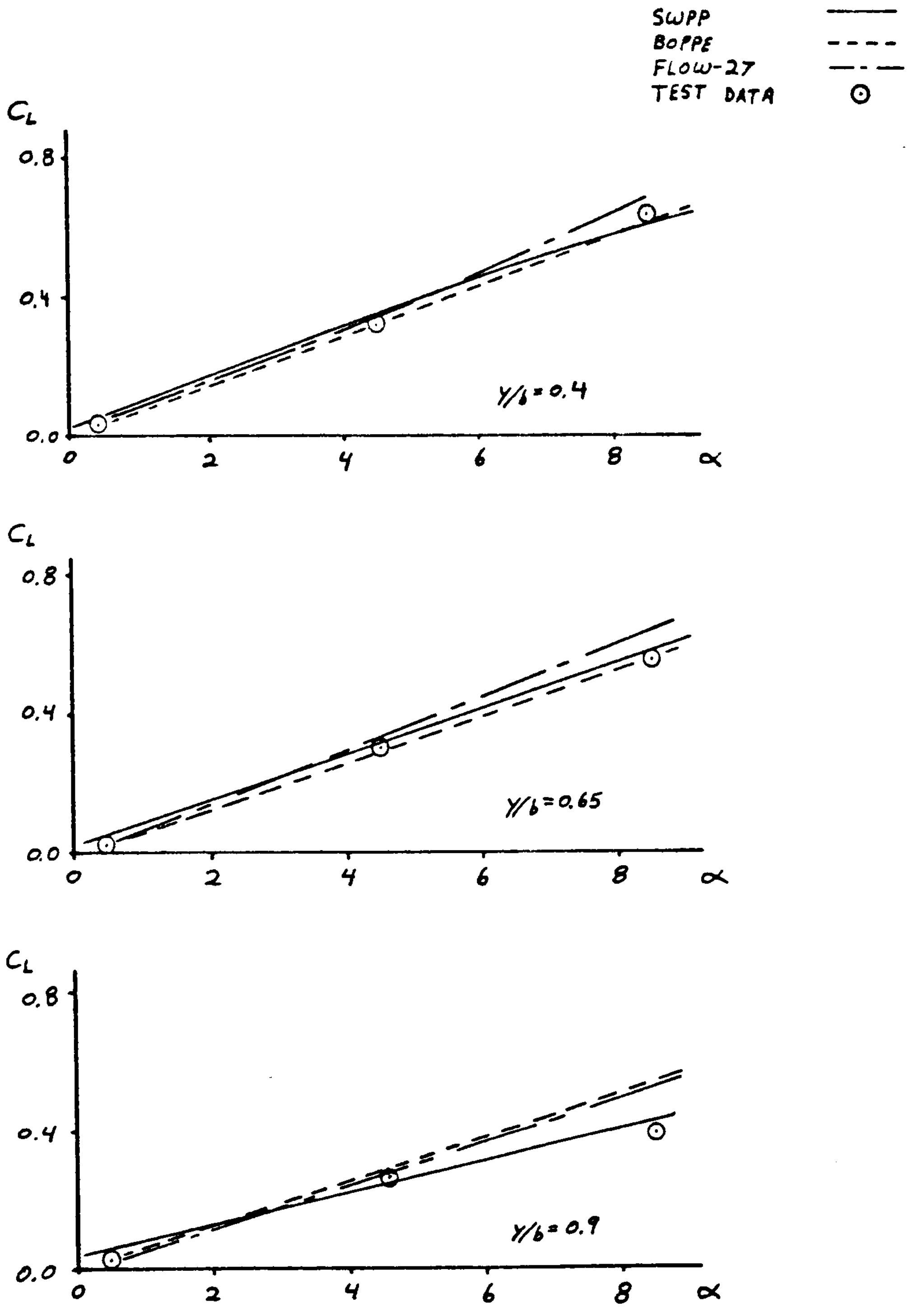

Mach = 0.7

Fig. 22 (continued)

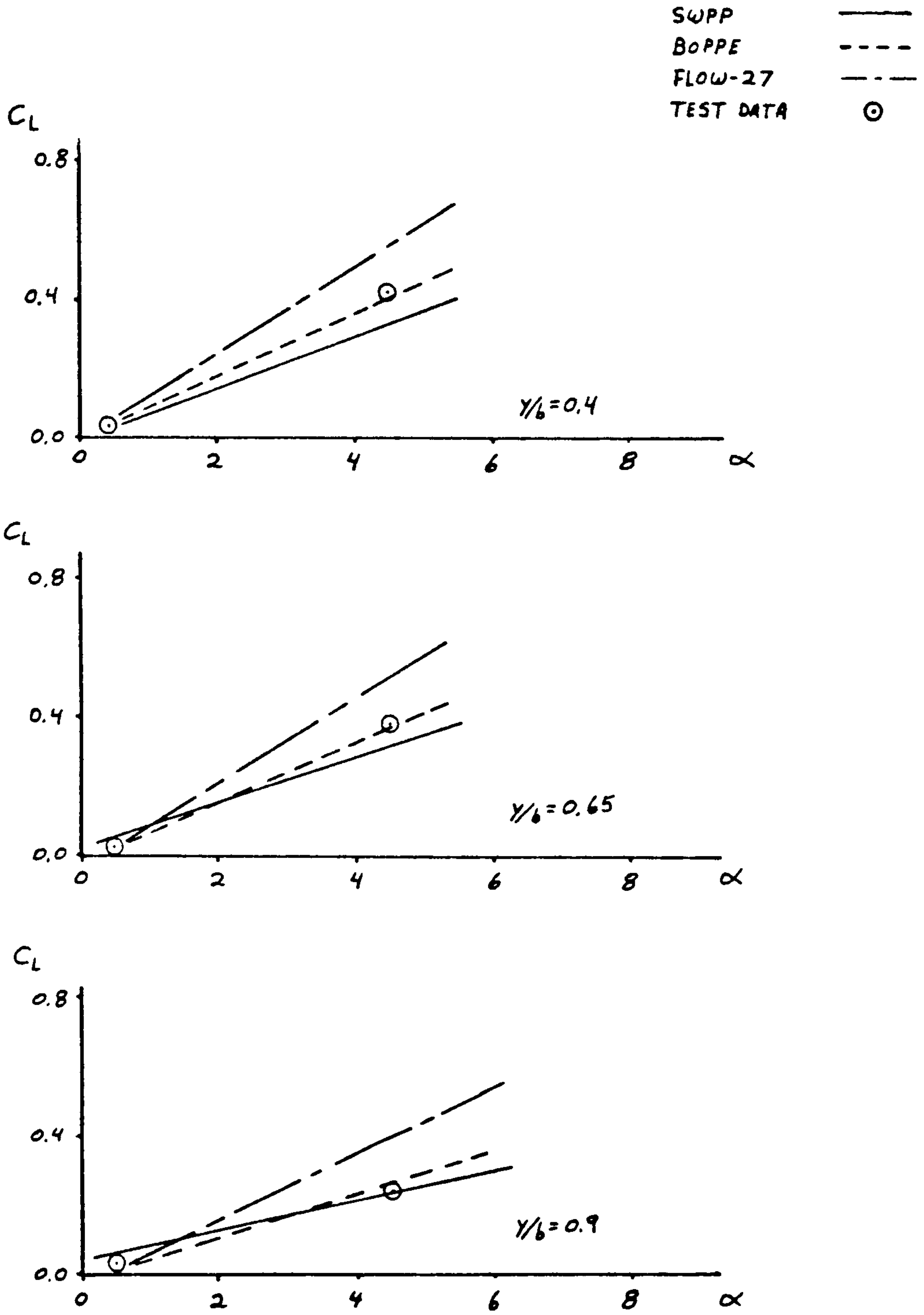

Mach = 0.9

Fig. 22 (continued)

lift data at Mach 0.7. Here again good agreement is seen for all computer codes at all span stations, with some variation seen in the SWPP-Code results at 90% span. For all techniques, a slight decrease in lift slope is seen as wing span location is increased. This loss in lift slope corresponds to the reduction in peak pressure observed in Figure 20 under similar conditions. At Mach 0.9, Figure 22c, a wide variation in lift data is seen. As noted earlier, at this Mach number the SWPP-Code results do not predict reasonable pressure distributions, such that any agreement with its lift data at this condition is only coincidental. As can be seen the BOPPE-Code closely matches the experimental results at all span stations, while the FLOW-27 results are consistently higher than the test results. This is due to the shock wave being too far aft at 4 degrees angle of attack for FLOW-27, and therefore a higher section lift coefficient is obtained. Also observed at this Mach number is the reduction in lift slope as the wing span location moves nearer the wing tip. This results from the shock wave moving forward near the tip as shown in Figure 21.

The pitching moment coefficient computed about the section leading edge is presented in Figure 23. As can be seen in Figure 23a at Mach 0.5 good agreement with the test data at all span stations is seen for FLOW-27 and the BOPPE-Code, while the SWPP-Code shows poorer agreement near the tip. At Mach 0.7, Figure 23b, the match between experimental and computed pitching moments is still good at all span stations for FLOW-27 and BOPPE-Code, while the SWPP-Code results are

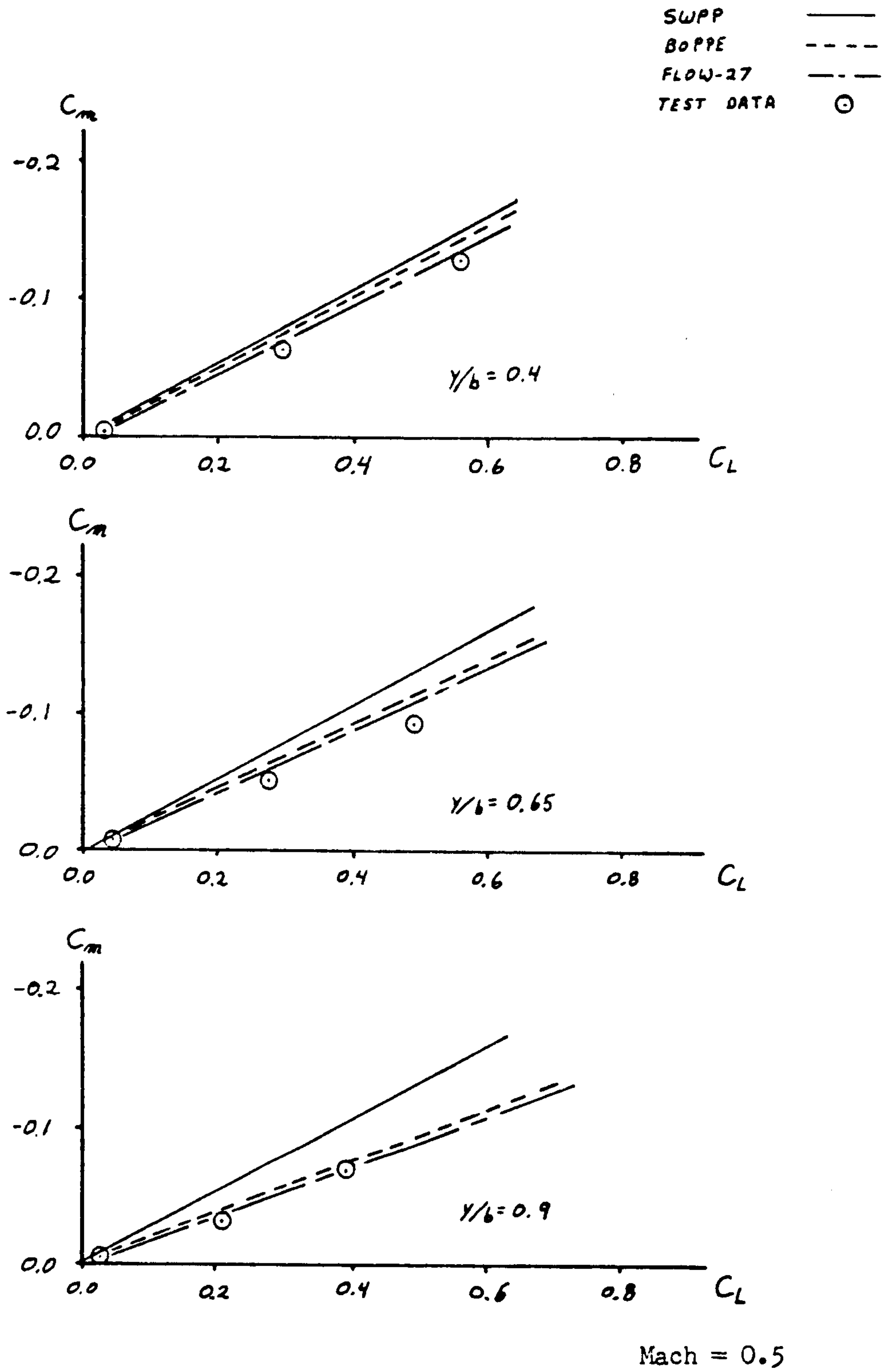

Fig. 23. Comparison of Wing Section Pitching Moment Coefficients

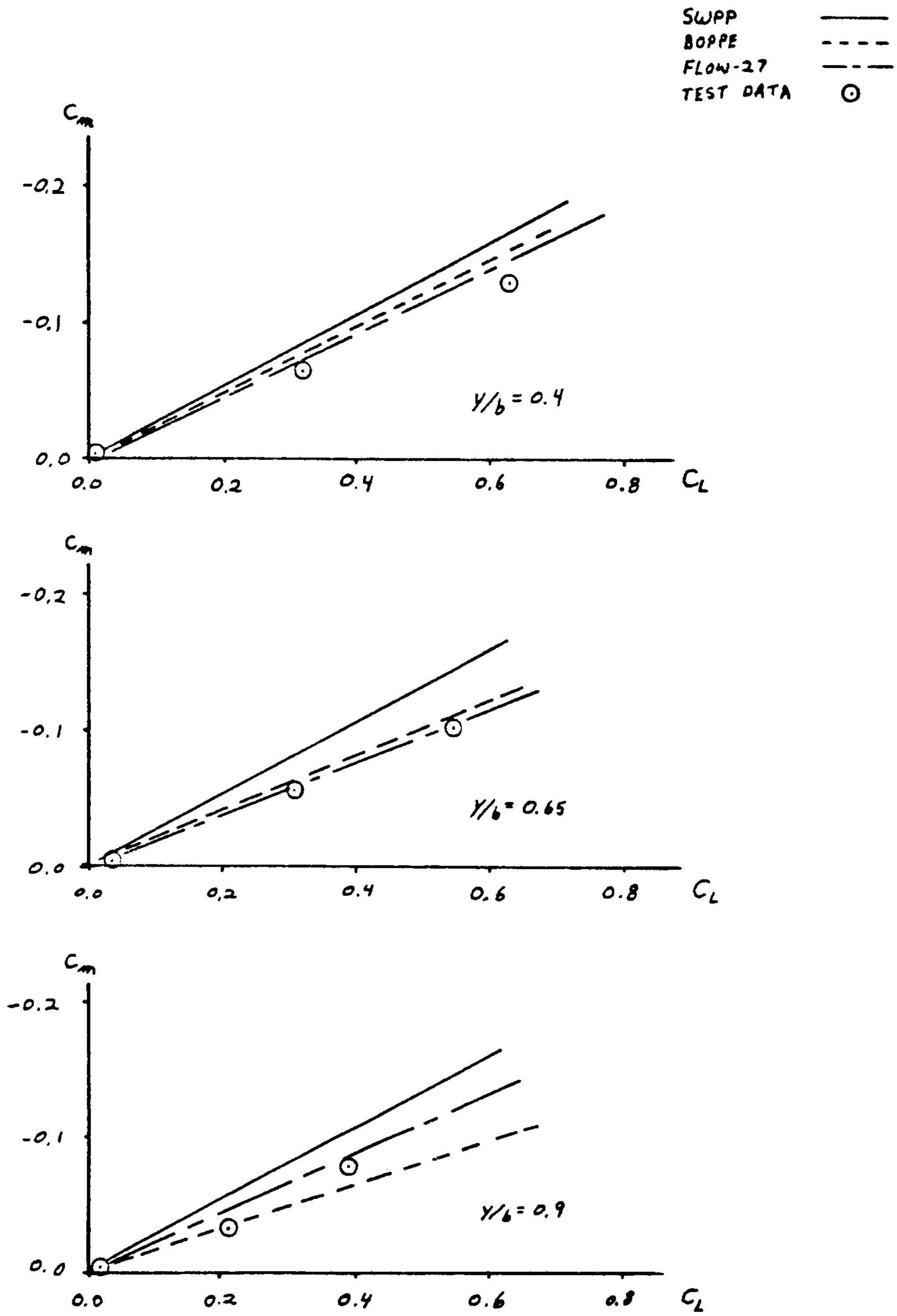

Mach = 0.7

Fig. 23 (continued)

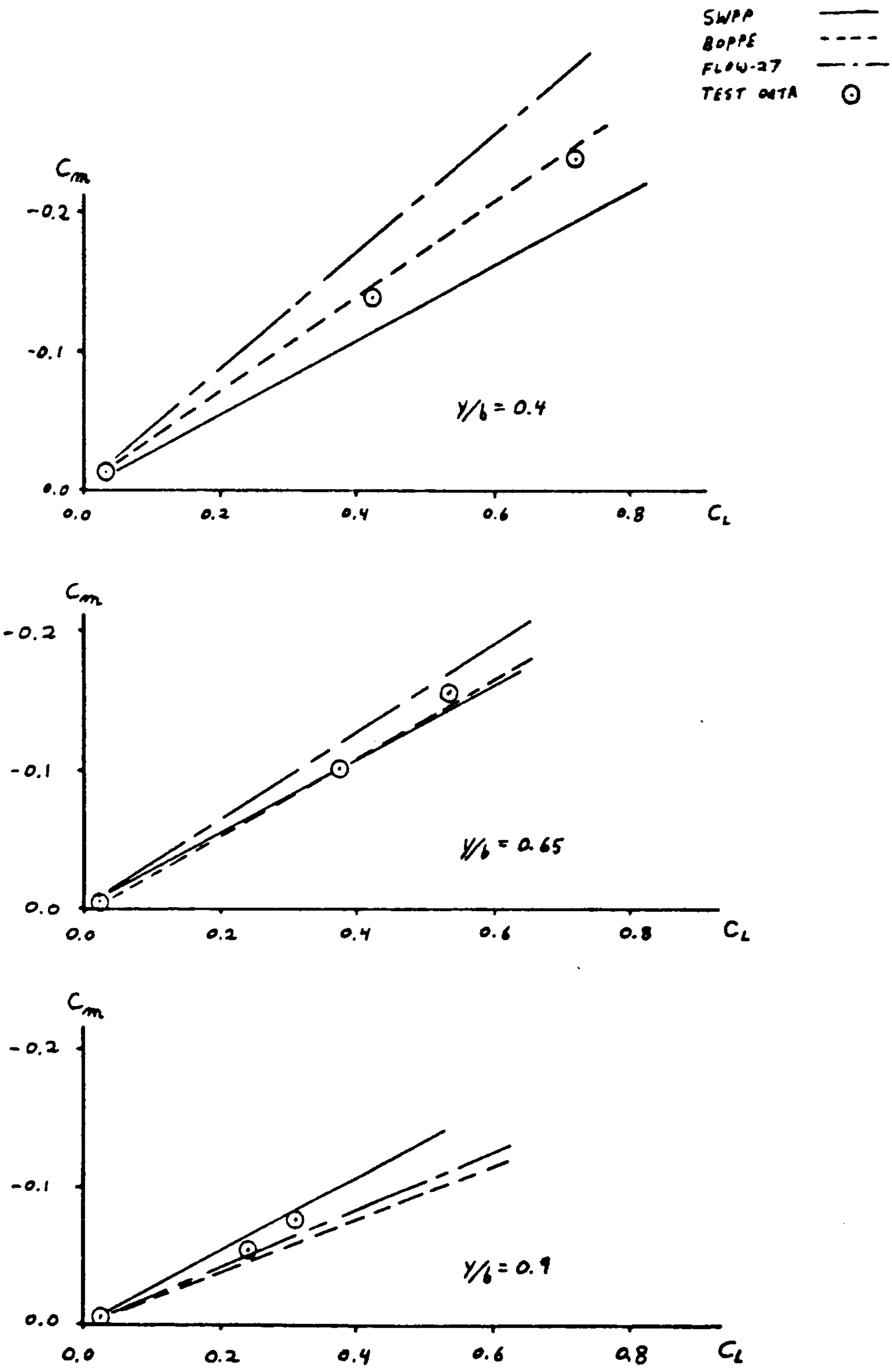

Mach = 0.9

Fig. 23 (continued)

good near mid-span but vary from the other computer codes and from test results near the tip. At this Mach number there is a greater variation in the results from all methods near the tip. In Figure 23c the Mach 0.9 pitching moments are presented. At this Mach number any agreement between the SWPP-Code and experimental pitching moments is considered coincidental due to the failure of the SWPP-Code to accurately predict the pressure distribution at this condition. As can be seen the BOPPE-Code gives good results at all spanwise stations, while the FLOW-27 results are too high on the inboard wing sections and become better near the wing tip. This is again the result of FLOW-27 predicting the shock further aft than experimentally observed.

IV.2 Comparison of Computer Resource Requirements

In discussing the computer resources used by each program, two parameters are considered of primary interest. These parameters are the amount of core memory required to execute the program, and the CPU time required to compute a single case (one angle of attack at one Mach number). The computer used for this investigation is the AEDC IBM-370, and the computer resources described are for that machine. Presented in Figure 24 is a comparison of the computer core memory required for each program. The memory required is a fixed value for each program, and not dependent on the details of the particular problem being solved. As can be seen the SWPP-Code requires less than one third the core needed by the BOPPE-Code, and only one fourth that

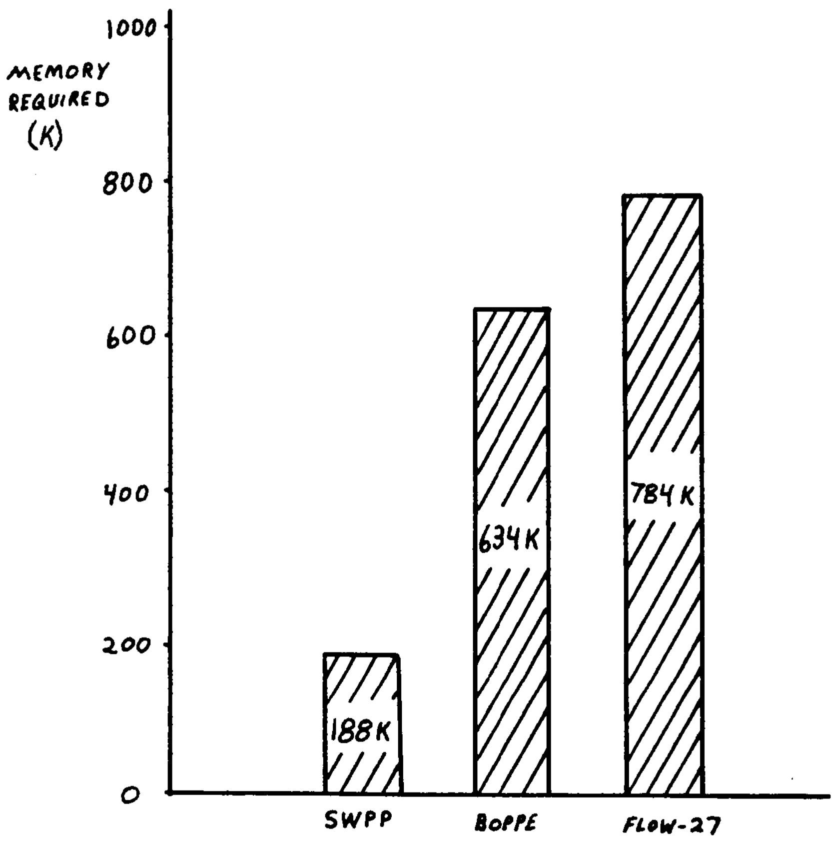

Fig. 24 Comparison of Program Memory Requirements

required by FLOW-27. Even more impressive is the CPU time requirements for these three programs presented in Figure 25. Here the details of the particular problem are a factor, the time required varying with angle of attack, Mach number and aircraft geometry. As can be seen the BOPPE-Code is relatively insensitive to angle of attack and Mach number, requiring a great deal of time for all conditions. The FLOW-27 time requirements are more moderate than the BOPPE-Code at low Mach number, but are seen to grow with both increasing angle of attack and Mach number. In contrast, the SWPP-Code is insensitive to either Mach number or angle of attack, and can require from one tenth to one hundredth of the time required for the other programs even at low Mach number. Two additional points should be made concerning the data in Figure 25. First, for a given aircraft geometry, the SWPP-Code is capable of solving more than a single case in a single computer run. By processing many cases in a single run, the time required per case can be reduced much further. If the nine Mach number, angle of attack combinations examined in this study had been computed in a single run, the CPU time per case would have been approximately one ninth that shown in Figure 25. The second point to be made is that at Mach 0.9 at 8 degrees angle of attack, both FLOW-27 and the BOPPE-Code ran out of time at one hour of CPU time without reaching a solution. The point plotted in this case was where the programs stopped.

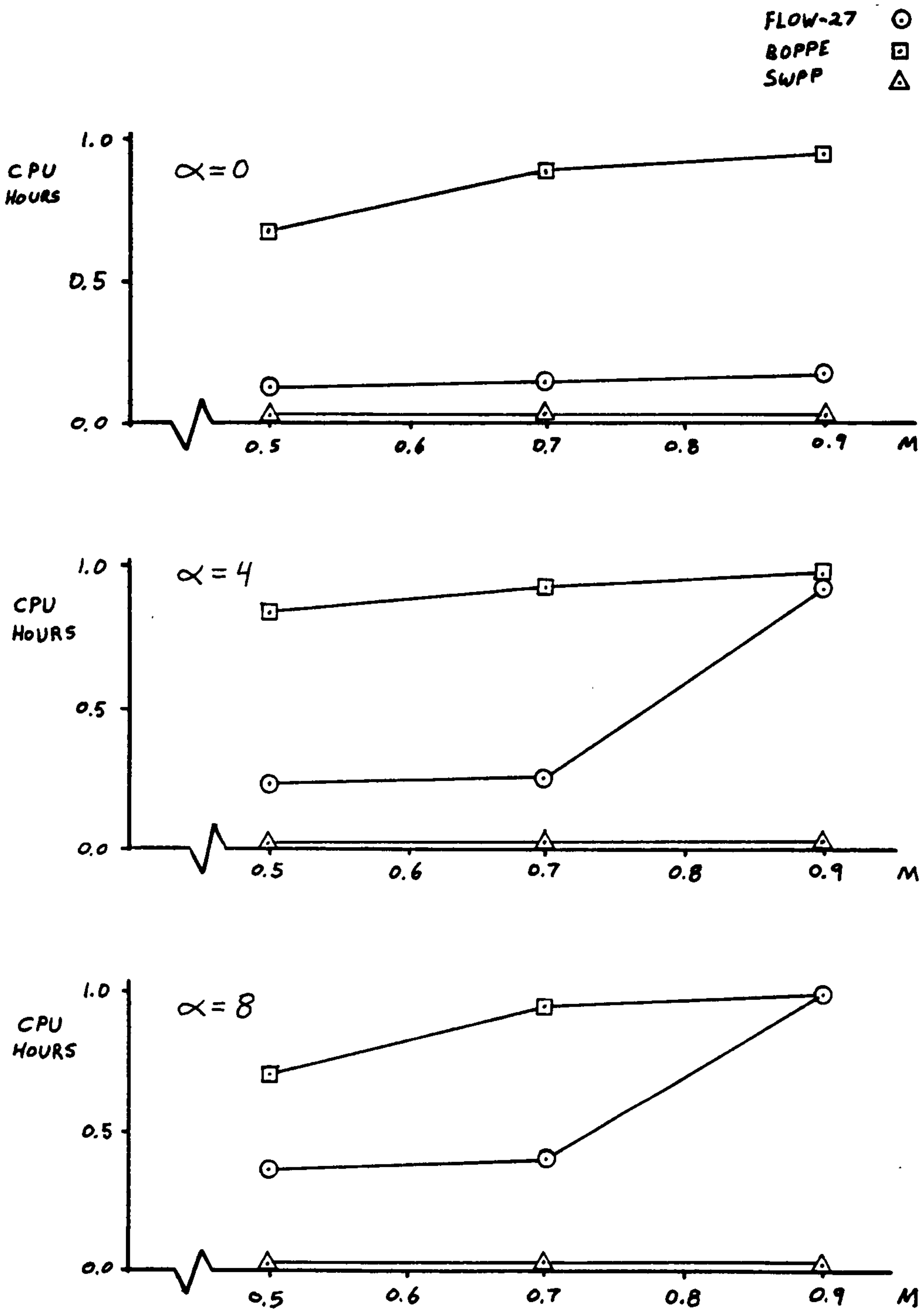

Fig. 25 Comparison of CPU Time Requirements

CHAPTER V

RESULTS AND CONCLUSIONS

A generalized transonic aircraft configuration was evaluated using three computer programs to predict the wing pressure distributions, and the results from these programs were compared with experimental results from a wind tunnel. Two of the programs were "off the shelf" numerical solutions representing the highly sophisticated programs currently available (FLOW-27 and BOPPE-Code). The third was a purely subsonic incompressible technique, the program for which was written for this investigation (SWPP-Code). Using the wind tunnel data as a basis for comparing the programs, the following observations were made.

1. At low Mach numbers all three programs predict pressure distributions in agreement with experimental results.

2. The aircraft angle of attack has little effect on the agreement between computed and measured pressures at low Mach number.

3. For conditions where no shock waves were present, the effect of spanwise location was small, affecting only the peak pressure near the wing tip, and not significantly affecting the match with experimental results.

4. At high Mach numbers the SWPP-Code fails to predict pressure distributions in agreement with test data.

5. Both FLOW-27 and BOPPE-Code predict shocks at high Mach

numbers, with the BOPPE-Code more accurately locating these shocks.

6. At high Mach number, spanwise location affected the shock location, resulting in better agreement between computed and measured values away from the wing tip.

7. The lift and pitching moments did not agree in every respect with observations made of the pressure distributions, but in general these data supported the findings based on these pressure distributions.

8. The SWPP-Code uses dramatically less computer resources than either of the other codes examined.

It can be concluded that before using any of these programs or other similar programs for a particular problem, close consideration should be given to the details of the problem. If the problem is such that the SWPP-Code or similar specialized codes can be used, large savings in computer resources can be made without compromising the results obtained. Similarly, the details of the problem may require a more general or more sophisticated program to obtain adequate results. In either event, a well thought out program selection can prevent the use of a program that is either too simplistic or too sophisticated for the problem at hand, and result in savings of both computer resources and the time of the investigator.

LIST OF REFERENCES

LIST OF REFERENCES

1. A. Jagadesh Prasad, The Calculation of the Pressure Distribution Over the Surface of a Double Delta Wing with Symmetrical Airfoil Sections. Master's Thesis, India Institute of Science, 1961

2. Charles W. Boppe, Transonic Flow Field Analysis for Wing-Fuselage Configurations. Grumman Aerospace Corporation, 1978

3. Antony Jameson and D. A. Caughey, Numerical Calculation of Transonic Potential Flow About Wing-Fuselage Combinations. AIAA 10th Fluid and Plasmadynamics Conference, June, 1977

4. Antony Jameson and D. A. Caughey, A Finite Volume Method for Transonic Potential Flow Calculations. AIAA 3rd Computational Fluid Dynamics Conference, June, 1977

5. Joe F. Herman and Robert A. Paulk, Documentation of the AEDC Adaptive and Transonic Wall Study Tests in Tunnel 4T. AEDC-TSR-78-P25, August, 1978

6. D. Kuchemann, Royal Aircraft Establishment, The Distribution of Lift Over the Surface of Swept Wings. The Aeronautical Quarterly, Volume IV, August, 1953

7. Wen-Shiung Li and San-Hai Lam, Priciples of Fluid Mechanics. Addison Wesley Publishing Co., 8th printing, August, 1976

8. R. L. Parker Jr. and W. L. Sickles, Application of Adaptive Wall Techniques in a Three-Dimensional Wind Tunnel with Variable Wall Porosity. AIAA 18th Aerospace Sciences Meeting, January, 1980

APPENDIX

PROGRAM INPUTS REQUIRED FOR SWPP-CODE

NAME	FORMAT	DESCRIPTION
NXY	I10	Number of (X,Y) points defining airfoil section.
X/C	8F10.0	NXY-points along chord, X/C.
Z/C	8F10.0	NXY-points along chord, Z/C.
RLE	F10.0	Leading edge radius/C.
THETA	F10.0	Trailing edge half angle, deg.
H	I10	Number of interpolation stations to use to improve airfoil fit (usually three).
N	I10	Number of points along chord to calculate C_ps.
SP	F10.0	Wing semi-span, consistent units.
T/C	F10.0	Airfoil thickness ratio, t/C.
NBRK	F10.0	Number of stations along span at which wing sweep changes including center and tip.
ALE TE YBREAK	3F10.0	X-coordinate of wing leading edge and trailing edge in consistent units and fraction span at stations where wing sweep changes. NBRK cards.
RBODY	F10.0	Body radius, in consistent units.
ALGEO	F10.0	Geometric angle of attack, deg.
NSP	I10	Number of span stations for C_p calculations.
ETA	8F10.0	Span stations for C_p calculations, fraction of span.
CL	8F10.0	Estimated section lift coefficients, NSP values.

```
C
C
C      THIS PROGRAM ENTITLED THE SUBSONIC WING PRESSURE
C      PREDICTION CODE (SWPP-CODE), COMPUTES THE PRESSURE
C      DISTRIBUTIONS ON ISOLATED WING AND WING BODY
C      COMBINATIONS.  THE PROGRAM CONSISTS OF A MAIN
C      PROGRAM AND A SERIES OF SUBROUTINES.  ALL
C      INPUT AND OUTPUT AS WELL AS SOME LIMITED
C      COMPUTING IS DONE IN THE MAIN PROGRAM, WHILE
C      MOST OF THE COMPUTING AND SPECIAL OPERATIONS ARE
C      PERFORMED IN THE SUBROUTINES.
C
       DIMENSION X(50),Y(50),F(5),T1(10),T2(10)
       DIMENSION SS1(50,50),SS2(50,50),SS3(50,50),S1(50)
      * ,S2(50),S3(50)
       DIMENSION ALE(6),TE(6),ETA(10),CL(10),YBREAK(6)
       DIMENSION ALPHE(10),PHIE(10),CPU(50),CPL(50)
       DIMENSION XARY(50,2),YARY(50,2)
       DATA SS1,SS2,SS3,S1,S2,S3/7650*0.0/
       IFLAG=0
C
C      INPUT AIRFOIL GEOMETRY.
C
       READ(5,1) NXY
1      FORMAT(8I10)
       READ(5,2) (X(I),I=1,NXY)
       READ(5,2) (Y(I),I=1,NXY)
2      FORMAT(8F10.0)
       WRITE(6,30) (X(I),Y(I),I=1,NXY)
30     FORMAT(1H1,10X,'AIRFOIL COORDINATES',//,5X,'X/C',
      * 10X,'Z/C',/,
      * 50(3X,2F10.5,/))
       READ(5,2) RLE,THETA
       WRITE(6,32) RLE,THETA
32     FORMAT(///,5X,'LEADING EDGE RADIUS/C = ',F10.5,//
      * ,5X,
      * 'TRAILING EDGE ANGLE = ',F10.5,' DEG.',//)
C
C      COMPUTE THE COEFFICIENTS DEFINING THE AIRFOIL.
C
       CALL COEF(NXY,X,Y,RLE,THETA,F)
       WRITE(6,3) F
3      FORMAT(1H1,5X,'F0 TO F4 =',5F13.5,/)
C
C      INPUT THE NUMBER OF INTERPOLATION STATIONS, AND
C      SELECT THE SPECIFIC STATIONS.
C
       READ(5,1) NP
       CALL STATIO (NP,T1,T2,NXY,X,Y)
       WRITE(6,7)
```

```
7     FORMAT(//,12X,'X/C',10X,'Z/C',11X,'ZA',11X,'Z1',
     * 7X,'Z/C-ZA',
     * 7X,'Z/C-Z1',/)
C
C     A COMPARISON BETWEEN INTERPOLATED AND NON-
C     INTERPOLATED AIRFOIL COORDINATES IS MADE AND THE
C     RESULTS PRINTED.
C
      DO 4 I=1,NXY
      Z=ZA(F,X(I))
      CALL INTERP(NXY,X,Y,T1,T2,NP,F,X(I),ZP)
      DEL1=Y(I)-Z
      DEL2=Y(I)-ZP
4     WRITE(6,5) X(I),Y(I),Z,ZP,DEL1,DEL2
5     FORMAT(5X,6F13.5)
C
C     ALL REMAINING VARIABLES ARE INPUT.  THESE INCLUDE
C     WING SPAN AND THICKNESS RATIO, PLANFORM,BODY
C     RADIUS AND GEOMETRIC ANGLE OF ATTACK, AS WELL AS
C     THE SPAN STATIONS OF INTEREST, ESTIMATED LIFT
C     COEFFICIENTS AND THE NUMBER OF POINTS ALONG
C     THE CHORD AT WHICH TO COMPUTE PRESSURE COEFFICIENTS.
C
      READ(5,1) NPT
      READ(5,2) SP,TC
      READ(5,1) NBRK
      DO 13 I=1,NBRK
13    READ(5,2) ALE(I),TE(I),YBREAK(I)
      READ(5,2) RBOD
      READ(5,2) ALGEO
      READ(5,1) NSP
      READ(5,2) (ETA(I),I=1,NSP)
      READ(5,2) (CL(I),I=1,NSP)
C
C     WING AREA AND ASPECT RATIO ARE COMPUTED AND PRINTED.
C
      AREA=0.0
      L=NBRK-1
      DO 14 I=1,L
      J=I+1
14    AREA=AREA+0.5*(TE(I)-ALE(I)+TE(J)-ALE(J))*
     * (YBREAK(J)-YBREAK(I))*SP
      AR=2.0*SP*SP/AREA
      WRITE(6,31)
31    FORMAT(1H1,15X,'WING PLANFORM',//)
      WRITE(6,33) SP,TC
33    FORMAT(/,5X,'WING SEMI-SPAN = ',6X,F10.4,//,5X,
     * 'WING THICKNESS RATIO = ',F10.4,/)
      WRITE(6,34) AREA,AR
34    FORMAT(/,5X,'WING AREA = ',11X,F10.4,//,5X,
```

```
     * 'ASPECT RATIO = ',8X,F10.4,/)
      WRITE(6,35) (ALE(I),TE(I),YBREAK(I),I=1,NBRK)
35    FORMAT(//,5X,'X-LEADING EDGE      X-TRAILING EDGE'
     * '       ETA-BREAK',
     * //,50(9X,F10.4,10X,F10.4,5X,F10.4,/),/)
      WRITE(6,36) RBOD
36    FORMAT(//,5X,'BODY RADIUS =',F10.4)
      K=NPT-1
C
C     THE S PARAMETERS ARE COMPUTED AND PRINTED AS AN
C     INTERMEDIATE STEP.
C
      CALL SCAL(NPT,SS1,SS2,SS3)
      CALL OUTT(NPT,NPT,SS1,40H SS1
     * K,NPT)
      CALL OUTT(NPT,NPT,SS2,40H SS2
     * K,K)
      CALL OUTT(NPT,NPT,SS3,40H SS3
     * NPT,NPT)
      CALL CAPS(NPT,SS1,SS2,SS3,S1,S2,S3,NXY,X,Y,NP,T1,
     * T2,F,RLE,1.0)
      CALL OUTT(NPT,1,S1,40H  S1
     * NPT,1)
      CALL OUTT(NPT,1,S2,40H  S2
     * K,1)
      CALL OUTT(NPT,1,S3,40H  S3
     * NPT,1)
24    IF(IFLAG.EQ.0) GO TO 25
C
C     FOR ADDITIONAL CASES INVOLVING THE SAME AIRCRAFT,
C     NEW INPUTS ARE MADE.
C
      READ(5,2,END=999) ALGEO
      READ(5,1) NSP
      READ(5,2) (ETA(I),I=1,NSP)
      READ(5,2) (CL(I),I=1,NSP)
25    DO 9 I=1,NSP
      ETB=ETA(I)
      CN=CL(I)
      CO=CLOC(ALE,TE,YBREAK,ETB)
      M=NPT/2
      PHC=PHC2(ALE,TE,YBREAK,ETB,SP,M,NPT)
C
C     AT EACH SPANWISE STATION THE EFFECTIVE ANGLE OF
C     ATTACK AND LOCAL WING SWEEP ANGLES ARE COMPUTED.
C
      CALL INCID(PHC,SP,ETB,CN,TC,AE,PHI,AR,CO)
      ALPHE(I)=AE
      A=ATAN((1.+(RBOD*RBOD)/(SP*SP*ETA(I)*ETA(I)))*
     * TAN(ALGEO*
```

```
     * 3.1415926/180.0))
      DA=A-ALGEO*3.1415926/180.0
      ALPHE(I)=ALPHE(I)+DA
9     PHIE(I)=PHI
      DO 11 I=1,NSP
      AE=ALPHE(I)
      PHI=PHIE(I)
      ETB=ETA(I)
C
C     PRESSURE DISTRIBUTIONS ARE COMPUTED AT EACH
C     SPANWISE STATION.
C
      CALL PRESS(AE,PHI,NPT,S1,S2,S3,RLE,CO,SP,ETB,CPU,
     * CPL,
     * ALE,TE,YBREAK)
      AE=AE*180.0/3.1415926
      WRITE(6,16) AE,ETB
16    FORMAT(1H1,10X,'EFFECTIVE ANGLE OF ATTACK = ',
     *F10.4,//,11X,
     * 'SPANWISE STATION = ',F10.4,///,8X,'STATION'8X,
     * 'X/C',5X,'CP-UPPER'
     * ,5X,'CP-LOWER',5X,'DELTA-CP',/)
C
C     PRESSURE DISTRIBUTIONS ARE NUMERICALLY
C     INTEGRATED TO GIVE LIFT AND PITCHING MOMENT.
C
      CN=CL(I)
      SUM=0.0
      SUM2=0.0
      SUM3=0.0
      XL=0.0
      DO 17 J=1,NPT
      H=XL
      L=NPT-J+1
      XL=(COS(FLOAT(L)*3.1415926/FLOAT(NPT))+1.0)/2.0
      XARY(L,1)=XL
      XARY(L,2)=XL
      YARY(L,1)=CPU(L)
      YARY(L,2)=CPL(L)
      XLA=(H+XL)/2.0
      K=L-1
      XLB=(COS(FLOAT(K)*3.1415926/FLOAT(NPT))+1.0)/2.0
      XLB=(XLB+XL)/2.0
      DCP=CPL(L)-CPU(L)
      DX=XLB-XLA
      SUM=SUM+DCP*DX
      SUM2=SUM2-DCP*(XL-0.25)*DX
      IF(L.EQ.NPT) GO TO 17
      SUM3=SUM3+CPU(L)*DZ(F,XL)*DX-CPL(L)*DZ(F,XL)*DX
C
```

```
C     PRESSURE DISTRIBUTIONS AND INTEGRATED
C     COEFFICIENTS ARE PRINTED.
C
17    WRITE(6,12) J,XL,CPU(L),CPL(L),DCP
12    FORMAT(5X,I10,1X,4F12.5)
      WRITE(6,6) ALGEO,SUM
6     FORMAT(//,10X,'FOR A GEOMETRIC ANGLE OF ATTACK OF'
     * ,F8.3,'  THE IN
     *TEGRATED NORMAL FORCE COEFFICIENT IS ',F8.5,/)
      IF(ETB.NE.0.0) GO TO 20
      ALIFT=SUM*COS(ALGEO*3.1415926/180.)-SUM3*
     * SIN(ALGEO*3.1415926/180.)
      DRAG= SUM*SIN(ALGEO*3.1415926/180.)+SUM3*
     * COS(ALGEO*3.1415926/180.)
      GO TO 21
20    ALIFT=SUM/COS(ALGEO*3.1415926/180.0)
      DRAG=0.0
      SUM3=0.0
21    XCP=0.25-SUM2/SUM
      WRITE(6,22) ALIFT,DRAG,SUM2,XCP,SUM3
22    FORMAT(/,5X,'LIFT =',F7.4,5X,'DRAG =',F7.4,5X,
     * 'CM =',F7.4,5X,
     * 'X-CP =',F7.4,5X,'CT =',F7.4)
C
C     PRESSURE DISTRIBUTIONS ARE THEN PLOTTED ON THE
C     LINE-PRINTER.
C
      CALL PLOT(XARY,YARY,0.0,1.0,1.0,-3.0,NPT,2)
11    CONTINUE
      IFLAG=1
C
C     THE PROGRAM THEN RETURNS TO THE INPUT SECTION
C     FOR ADDITIONAL CASES USING THE SAME AIRCRAFT
C     GEOMETRY.
C
      GO TO 24
999   CONTINUE
      STOP
      END
      SUBROUTINE COEF(NXY,X,Y,RLE,THETA,F)
C
C     THIS ROUTINE COMPUTES THE 5 COEFFICIENTS
C     DESCRIBING THE AIRFOIL.
C
      DIMENSION A(5,5),X(NXY),Y(NXY),F(5),S(5)
      PI=3.1415926
      L=IMAX(Y,NXY)
      S(1)=(2.0*RLE)**0.5
      S(2)= Y(NXY)
      S(3)=0.0
```

```
      S(4)=Y(L)
      S(5)=-TAN(THETA*PI/360.0)
      CALL SETUP(A,X,L,NXY)
C
C     SUBROUTINE VERT IS THE ONLY ROUTINE USED FROM
C     A SYSTEM LIBRARY, AND IS USED TO INVERT THE
C     MATRIX A.
C
      CALL VERT(5,5,A,NFLAG)
      CALL MULT(A,S,F)
      RETURN
      END
      SUBROUTINE INTERP(NXY,X,Y,T1,T2,NPTS,F,X1,ZP)
C
C     THIS ROUTINE COMPUTES THE INTERPOLATED AIRFOIL
C     COORDINATES.
C
      DIMENSION X(NXY),Y(NXY),T1(NPTS),T2(NPTS),F(5),
     * AL(10)
      L=IMAX(Y,NXY)
      XM=X(L)
      Z1=ZA(F,X1)
      IF(X1.GT.XM) GO TO 11
      CALL COREC(T1,AL,NPTS,X1,XM)
      J=1
      K=IMAX(Y,NXY)
      SUM=0.0
      DO 13 I=1,NPTS
      DO 14 JJ=J,K
      IF(X(JJ).NE.T1(I)) GO TO 14
      SUM=SUM+AL(I)*(Y(JJ)-ZA(F,X(JJ)))
14    CONTINUE
13    CONTINUE
      GO TO 12
11    CALL COREC(T2,AL,NPTS,X1,XM)
      J=IMAX(Y,NXY)+1
      K=NXY
      SUM=0.0
      DO 15 I=1,NPTS
      DO 16 JJ=J,K
      IF(X(JJ).NE.T2(I)) GO TO 16
      SUM=SUM+AL(I)*(Y(JJ)-ZA(F,X(JJ)))
16    CONTINUE
15    CONTINUE
12    ZP=Z1+SUM
      RETURN
      END
      SUBROUTINE MULT(A,S,F)
C
C     THIS ROUTINE MULTIPLIES A 5 BY 5 MATRIX BY A
```

```
C     5 BY 1 MATRIX AND RETURNS THE RESULTING PRODUCT
C     MATRIX.
C
      DIMENSION A(5,5),S(5),F(5)
      DO 1 I=1,5
      SUM=0.0
      DO 2 J=1,5
2     SUM=SUM+A(I,J)*S(J)
1     F(I)=SUM
      RETURN
      END
      FUNCTION DZ(F,X)
C
C     THIS ROUTINE EVALUATES THE AIRFOIL SLOPE AT ANY
C     POINT BASED ON THE NON-INTERPOLATED AIRFOIL
C     SHAPE FUNCTION.
C
      DIMENSION F(5)
      DZ=0.5*F(1)/(X**0.5)+F(2)+2.0*F(3)*X+3.0*F(4)*X*X
     * +4.0*F(5)*X*X*X
      RETURN
      END
      FUNCTION IMAX(Z,N)
C
C     THIS ROUTINE DETERMINES THE POINT OF MAXIMUM
C     THICKNESS ON THE AIRFOIL.
C
      DIMENSION Z(N)
      IMAX=1
      A=Z(1)
      DO 1 I=2,N
      IF(Z(I).LE.A) GO TO 1
      A=Z(I)
      IMAX=I
1     CONTINUE
      RETURN
      END
      SUBROUTINE SETUP(A,X,L,N)
C
C     THIS ROUTINE SETS UP THE COEFFICIENT MATRIX USED
C     IN SOLVING FOR THE CONSTANTS DEFINING THE
C     AIRFOIL SHAPE.
C
      DIMENSION A(5,5),X(N)
      A(1,1)=1.0
      A(1,2)=0.0
      A(1,3)=0.0
      A(1,4)=0.0
      A(1,5)=0.0
      A(2,1)=1.0
```

```
      A(2,2)=1.0
      A(2,3)=1.0
      A(2,4)=1.0
      A(2,5)=1.0
      A(3,1)=0.5/(X(L)**0.5)
      A(3,2)=1.0
      A(3,3)=X(L)*2.0
      A(3,4)=3.0*X(L)**2.0
      A(3,5)=4.0*X(L)**3.0
      A(4,1)=X(L)**0.5
      A(4,2)=X(L)
      A(4,3)=X(L)**2.0
      A(4,4)=X(L)**3.0
      A(4,5)=X(L)**4.0
      A(5,1)=0.5
      A(5,2)=1.0
      A(5,3)=2.0
      A(5,4)=3.0
      A(5,5)=4.0
      RETURN
      END
      SUBROUTINE COREC(A,C,N,X,XM)
C
C     THIS ROUTINE COMPUTES THE L-VALUES USED TO
C     INTERPOLATE THE AIRFOIL COORDINATES.
C
      DIMENSION A(N),C(N)
      DO 1 J=1,N
      PROD=1.0
      DIM=1.0
      DO 2 I=1,N
      IF(I.EQ.J) GO TO 2
      PROD=PROD*(X-A(I))
      DIM=DIM*(A(J)-A(I))
2     CONTINUE
      IF(X.GT.XM) GO TO 3
      C(J)=X*PROD/(DIM*A(J))
      GO TO 4
3     C(J)=((1.0-X)/(1.0-A(J)))**2.0*PROD/DIM
4     C(J)=C(J)*(ABS(X-XM))**2.0/(ABS(A(J)-XM)**2.0)
1     CONTINUE
      RETURN
      END
      FUNCTION ZA(F,X)
C
C     THIS ROUTINE COMPUTES THE AIRFOIL COORDINATES
C     PRIOR TO INTERPOLATION.
C
      DIMENSION F(5)
      ZA=F(1)*X**0.5
```

```
      DO 1 J=2,5
1     ZA=ZA+F(J)*X**(FLOAT(J-1))
      RETURN
      END
      SUBROUTINE SCAL(NPT,S1,S2,S3)
C
C     THIS ROUTINE COMPUTES THE SMALL S PARAMETERS.
C
      DIMENSION S1(NPT,NPT),S2(NPT,NPT),S3(NPT,NPT)
      DO 1 I=1,NPT
      THI=FLOAT(I)*3.1415926/ FLOAT(NPT)
      DO 2 J=1,NPT
      THJ=FLOAT(J)*3.1415926/FLOAT(NPT)
      A=1.0
      B=1.0
      IF(((I-J)/2)*2.NE.(I-J)) A=-1.0
      IF((J/2)*2.NE.J) B=-1.0
      IF(I.EQ.J) GO TO 3
      IF(I.EQ.NPT) GO TO 5
      S1(I,J)=(A-1.0)*2.0*SIN(THI)/(FLOAT(NPT)*ABS
     * (COS(THI)-COS(THJ))
     X **2.0)
5     IF((I.EQ.NPT).OR.(J.EQ.NPT)) GO TO 6
      S2(I,J)=-2.0*A*SIN(THI)/(SIN(THJ)*(COS(THI)-
     * COS(THJ)))
6     IF(I.EQ.NPT) GO TO 4
      S3(I,J)=S1(I,J)+(2.0-2.0*A)/(FLOAT(NPT)*SIN(THI)*
     * (COS(THI)-
     X COS(THJ)))
      GO TO 4
3     IF(I.EQ.NPT) GO TO 7
      S1(I,J)=FLOAT(NPT)/SIN(THJ)
      S2(I,J)=COS(THJ)/(SIN(THJ)**2.0)
7     S3(I,J)=S1(I,J)
4     IF((J.EQ.NPT).AND.(I.EQ.NPT)) GO TO 2
      IF(I.EQ.NPT) S3(I,J)=(B-1.0)/(FLOAT(NPT)*(1.0+
     * COS(THJ)))
2     CONTINUE
1     CONTINUE
      RETURN
      END
      SUBROUTINE CAPS(NPT,SS1,SS2,SS3,S1,S2,S3,NXY,X,Y,
     * NP,T1,T2,F,RLE,C)
C
C     THIS ROUTINE COMPUTES THE CAPITAL S PARAMETERS.
C
      DIMENSION SS1(NPT,NPT),SS2(NPT,NPT),SS3(NPT,NPT),
     * S1(NPT),S2(NPT),
     * S3(NPT),X(NXY),Y(NXY),T1(NP),T2(NP),F(5)
      DO 6 I=1,NPT
```

```
      AX=0.5*(COS(FLOAT(I)*3.1415926/FLOAT(NPT))+1.0)
      NM1=NPT-1
      SUM1=0.0
      SUM2=0.0
      SUM3=0.0
      DO 7 J=1,NM1
      BX=0.5*(COS(FLOAT(J)*3.1415926/FLOAT(NPT))+1.0)
      CALL INTERP(NXY,X,Y,T1,T2,NP,F,BX,ZM)
      SUM1=SUM1+SS1(J,I)*ZM
      SUM2=SUM2+SS2(J,I)*ZM
7     SUM3=SUM3+SS3(J,I)*ZM
      S1(I)=SUM1
      S2(I)=SUM2
      S3(I)=SUM3+SS3(NPT,I)*(RLE*0.5   )**0.5
      IF(I.NE.NPT) GO TO 6
      S1(I)=SUM1+2.0*FLOAT(NPT)*(RLE*0.5   )**0.5
      S3(I)=SUM3+FLOAT(NPT)*(RLE*0.5/C)**0.5
6     CONTINUE
      RETURN
      END
      SUBROUTINE OUTT(N,M,A,L,K1,K2)
C
C     THIS ROUTINE OUTPUTS THE COMPUTED S VALUES.
C
      DIMENSION A(N,M),L(10)
      KA=1
8     KB=KA+24
      IF(KB.GT.K1) KB=K1
      KC=1
5     KD=KC+9
      IF(KD.GT.K2) KD=K2
      WRITE(6,4) L
      WRITE(6,9) (I,I=KC,KD)
      DO 1 II=KA,KB
      WRITE(6,2) II,(A(II,J),J=KC,KD)
1     WRITE(6,3)
      IF(KD.EQ.K2) GO TO 6
      KC=KD+1
      GO TO 5
6     IF(KB.EQ.K1) GO TO 7
      KA=KB+1
      GO TO 8
7     RETURN
4     FORMAT(1H1,5X,10A4,/)
9     FORMAT(5X,10(I8,4X),/)
2     FORMAT(1X,I4,1X,10F12.6)
3     FORMAT(1H )
      END
      FUNCTION ALAM(YC,YT)
C
```

```
C      THIS FUNCTION COMPUTES THE PARAMETER LAMDA.
C
       ALAM=1.4+1.33*YC-(0.16+7.3*YC)**0.5
       RETURN
       END
       SUBROUTINE INCID(PHC,SP,ETA,CL,TC,AE,PHI,AR,CLOCAL)
C
C      THIS ROUTINE COMPUTES THE EFFECTIVE ANGLE OF ATTACK.
C
       YO=ETA*SP/CLOCAL
       YT=(1.0-ETA)*SP/CLOCAL
       AO=2.0*3.1415926*(1.0+0.8*TC/COS(PHC))
       B=AO*COS(PHC)/(3.1415926*AR)
       PHI=PHC/(1.0+B*B)**0.25
       ANO=0.5*(1.0-2.0*PHI*ALAM(YO,YT)/3.1415926)
       D=4.0*(1.0+2.0*ABS(PHI)/3.1415926)
       D=1.0/D
       B=AO*COS(PHI)/(3.1415926*AR)
       DE=2.0*(1.0+B*B)**D
       AN=1.0-(1.0+2.0*PHI*ALAM(YO,YT)/3.1415926)/DE
       A=1.0-3.1415926*AN*(COTAN(3.1415926*AN)-
      * COTAN(3.1415926*ANO))
       AE=A*CL*SIN(3.1415926*ANO)/(4.0*3.1415926*AN*
      * COS(PHI))
       RETURN
       END
       SUBROUTINE STATIO (N,T1,T2,M,X,Y)
C
C      THIS ROUTINE SELECTS WHICH STATIONS WILL BE USED
C      FOR INTERPOLATION PURPOSE.
C
       DIMENSION T1(N),T2(N),X(M),Y(M)
       I=IMAX(Y,M)
       L=I/N
       IF(L.EQ.0) L=1
       J=L/2-L+1
       DO 1 K=1,N
       J=J+L
1      T1(K)=X(J)
       L=(M-I)/N
       IF(L.EQ.0) L=1
       J=I+L/2-L+1
       DO 2 K=1,N
       J=J+L
2      T2(K)=X(J)
       WRITE(6,3)
3      FORMAT(/,5X,'INTERPOLATION STATIONS',/,10X,'X/C')
       WRITE(6,4) T1,T2
4      FORMAT(7X,F6.4)
       RETURN
```

```
      END
      SUBROUTINE PRESS(AE,PH,NPT,S1,S2,S3,RLE,C,S,ETA,
     * CPU,CPL,
     * ALE,TE,YBRK)
C
C     THIS ROUTINE COMPUTES THE WING PRESSURE
C     DISTRIBUTION.
C
      DIMENSION ALE(6),TE(6),YBRK(6)
      DIMENSION S1(NPT),S2(NPT),S3(NPT),CPU(NPT),CPL(NPT)
      SA=SIN(AE)
      CA=COS(AE)
      AN=0.5-PH/3.1415926
      A=PH
      Y=ETA*S
      IF(Y/C.LE.0.5) GO TO 3
      DO 1 I=1,NPT
      PH=PHC2(ALE,TE,YBRK,ETA,S,I,NPT)
      SP=SIN(PH)
      CP=COS(PH)
      X=(COS(3.1415926*FLOAT(I)/FLOAT(NPT))+1.0)/2.0
      IF(I.EQ.NPT) GO TO 2
      T1=CA*(CP+S1(I))
      T2=(SA*(1.0/X-1.0)**0.5)*(1.0+S3(I)/CP)
      T3=1.0+S2(I)*S2(I)/(CP*CP)
      CPU(I)=1.0-CA*CA*SP*SP-(T1+T2)*(T1+T2)/T3
      CPL(I)=1.0-CA*CA*SP*SP-(T1-T2)*(T1-T2)/T3
      GO TO 1
2     T1=SA*(1.0+S3(I)/CP)
      T2=((RLE/ 2.0    )**0.5)/CP
      CPU(I)=1.0-CA*CA*SP*SP-(T1/T2)*(T1/T2)
      CPL(I)=CPU(I)
1     CONTINUE
      PH=A
      RETURN
3     DO 4 I=1,NPT
      PH=PHC2(ALE,TE,YBRK,ETA,S,I,NPT)
      SP=SIN(PH)
      CP=COS(PH)
      FP=ALOG((1.0+SIN(PH))/(1.0-SIN(PH)))/3.1415926
      X=(COS(3.1415926*FLOAT(I)/FLOAT(NPT))+1.0)/2.0
      IF(I.EQ.NPT) GO TO 5
      T1=(1.0+CP*S1(I))/((1.0+S2(I)*S2(I))**0.5)
      T2=FP*CP*S2(I)/(1.0+S2(I)*S2(I))
      T3=SA*CP*(1.0/X-1.0)**AN
      T4=(1.0+S3(I))/((1.0+S2(I)*S2(I))**AN)
      CPU(I)=1.0-((T1-T2)*CA+T3*T4)*((T1-T2)*CA+T3*T4)
      CPL(I)=1.0-((T1-T2)*CA-T3*T4)*((T1-T2)*CA-T3*T4)
      GO TO 4
5     T1=(1.0+S3(I))/((RLE/ 2.0    )**AN)
```

```
      CPU(I)=1.0-SA*SA*CP*CP*T1*T1
      CPL(I)=CPU(I)
4     CONTINUE
      PH=A
      RETURN
      END
      FUNCTION CLOC(A,T,Y,E)
C
C     THIS ROUTINE COMPUTES THE LOCAL WING CHORD.
C
      DIMENSION A(6),Y(6),T(6)
      DO 1 I=1,5
      L=I+1
      IF(E.GT.Y(L)) GO TO 1
      J=I
      GO TO 2
1     CONTINUE
2     PCT=(E-Y(J))/(Y(L)-Y(J))
      DC=T(L)-A(L)-T(J)+A(J)
      CLOC=T(J)-A(J)+DC*PCT
      RETURN
      END
      FUNCTION PHC2(A,T,Y,E,SP,K,NPT)
C
C     THIS ROUTINE COMPUTES THE SWEEP ANGLE OF THE
C     50-PERCENT CHORD LINE.
C
      DIMENSION A(6),T(6),Y(6)
      X=(COS(FLOAT(K)*3.1415926/FLOAT(NPT))+1.0)/2.0
      DO 1 I=2,6
      L=I
      IF(Y(I).GT.E) GO TO 2
1     CONTINUE
2     J=L-1
      PHC2=X*(T(L)-A(L))+A(L)-X*(T(J)-A(J))-A(J)
      PHC2=PHC2/((Y(L)-Y(J))*SP)
      PHC2=ATAN(PHC2)
      RETURN
      END
      SUBROUTINE PLOT(X,Y,XMIN,XMAX,YMMN,YMMX,M,N)
C
C     THIS ROUTINE PLOTS THE PRESSURE DISTRIBUTIONS.
C
      DIMENSION X(50,2),Y(50,2),LINE(73),ISY(5),V(5),H(5)
      DATA IV,      ISY/1HI,         1HA,1HB,1HC,1HD,1HE/
      YMIN=YMMN
      YMAX=YMMX
      IF((XMIN.EQ.0.0).AND.(XMAX.EQ.0.0))
     * CALL MAXMIN(X,Y,XMAX,XMIN,YMAX,YMIN,M,N)
      DX=(XMAX-XMIN)/73.0
```

```
      DY=(YMAX-YMIN)/45.0
      D1=(XMAX-XMIN)/4.0
      D2=(YMAX-YMIN)/4.0
      DO 1 I=1,5
      V(I)=YMAX-FLOAT(I-1)*D2
1     H(I)=XMIN+FLOAT(I-1)*D1
      WRITE(6,3)
3     FORMAT(1H1)
      DO 10 I=1,45
      CALL BLK(LINE)
      IF((I.EQ.1).OR.(I.EQ.12).OR.(I.EQ.23).OR.
     * (I.EQ.34).OR.(I.EQ.45)) GO TO 6
      GO TO 7
6     CALL HOR(LINE)
      IFLAG=I
7     DO 2 J=1,73,18
2     LINE(J)=IV
      DO 4 K=1,N
      DO 4 KK=1,M
      IF(ABS(YMAX-DY/2.0-Y(KK,K)).LE.ABS(DY/2.0))
     * CALL PT(X(KK,K),XMIN,DX,LINE,ISY(K))
4     CONTINUE
      YMAX=YMAX-DY
      IF(IFLAG.EQ.0) GO TO 5
8     IF(IFLAG.LT.12) GO TO 9
      IFLAG=IFLAG-10
      GO TO 8
9     WRITE(6,11) V(IFLAG),LINE
11    FORMAT(5X,1PE12.4,3X,73A1)
      GO TO 10
5     WRITE(6,12) LINE
12    FORMAT(20X,73A1)
10    IFLAG=0
      WRITE(6,13) H
13    FORMAT(/,13X,5(1PE12.4,6X))
      RETURN
      END
      SUBROUTINE HOR(L)
C
C     THIS ROUTINE DRAWS HORIZONTAL GRID LINES WHEN
C     PLOTTING.
C
      INTEGER L(73)
      DATA L2/1H-/
      DO 1 I=1,73
1     L(I)=L2
      RETURN
      END
      SUBROUTINE BLK(L)
C
```

```
C      THIS ROUTINE BLANKS OUT A LINE WHEN PLOTTING.
C
       INTEGER L(73)
       DATA L2/1H /
       DO 1 I=1,73
1      L(I)=L2
       RETURN
       END
       SUBROUTINE PT(X,XMIN,DX,LINE,ISY)
C
C      THIS ROUTINE PLACES A SYMBOL AT A PARTICULAR POINT
C      WITHIN THE PLOT LINE.
C
       INTEGER LINE(73)
       DO 1 I=1,73
       IF((XMIN+FLOAT(I)*DX).GT.X) GO TO 2
1      CONTINUE
       RETURN
2      LINE(I)=ISY
       RETURN
       END
       SUBROUTINE MAXMIN(X,Y,XMAX,XMIN,YMAX,YMIN,M,N)
C
C      THIS ROUTINE PROVIDES AUTO-SCALING FOR THE
C      PLOTS WHEN NECESSARY.
C
       DIMENSION X(M,N),Y(M,N)
       XMAX=X(1,1)
       XMIN=XMAX
       YMAX=Y(1,1)
       YMIN=YMAX
       DO 1 I=1,M
       DO 1 J=1,N
       IF(X(I,J).GT.XMAX) XMAX=X(I,J)
       IF(X(I,J).LT.XMIN) XMIN=X(I,J)
       IF(Y(I,J).GT.YMAX) YMAX=Y(I,J)
       IF(Y(I,J).LT.YMIN) YMIN=Y(I,J)
1      CONTINUE
       RETURN
       END
```

VITA

Phillip L. Yeakley was born in Logansport, Indiana on September 23, 1951. He attended elementary school in New Waverly, Indiana and was graduated from Lewis-Cass High School in June, 1969. The following September he entered Purdue University, and in May, 1974 he received a Bachelor of Science degree in Aeronautical Engineering. In June of 1974 he accepted a position as a project engineer with the Arnold Research Organization, Inc. in Tullahoma, Tennessee. In September of 1974 he entered the Graduate School of the University of Tennessee Space Institute, in Tullahoma. He received his Master of Science degree with a major in Mechanical Engineering in August, 1980.

The author is a member of Delta Sigma Phi. Mr. Yeakley is currently employed by the Lockheed California Company in Burbank, California.

He is married to the former Joanne M. Mulligan of South Bend, Indiana.